



Ph.D. Thesis

# **GNSS Signal Processing and Spatial Diversity Exploitation**

Author:

José Antonio García Molina

Thesis advisor:

Prof. Juan A. Fernández Rubio

Department of Signal Theory and Communications

Universitat Politècnica de Catalunya

Barcelona, February 2020



*A mis padres y hermanos*

*To Tamara*



*“Even in empty space, time and space still exist.”*

Sean M. Carroll

*“Essentially, all models are wrong, but some are useful.”*

George E. P. Box



# Abstract

Global Navigation Satellite Systems (GNSS) signals are broadly used for positioning, navigation and timing (PNT) in many different applications and use cases. Although different PNT technologies are available, GNSS is expected to be a key player in the derivation of positioning and timing for many future applications, including those in the context of the Internet of Things (IoT) or autonomous vehicles, since it has the important advantage of being open access and worldwide available. Indeed, GNSS is performing very well in mild propagation conditions, achieving position and time synchronization accuracies down to the cm and ns levels, respectively. Nevertheless, the exploitation of GNSS in harsh propagation conditions typical of urban and indoor scenarios is very challenging, resulting in position errors of up to tens or even hundreds of meters, and timing accuracies of hundreds of ns.

This thesis deals with the processing of GNSS signals for positioning and timing in harsh propagation conditions. In particular, the focus is on signal processing techniques exploiting the spatial diversities present both at transmission and reception levels when multiple GNSS satellites are in view by multiple receiver antennas, which form a multiple-input multiple-output (MIMO) system. In this context, three problems or research areas open in the GNSS literature are targeted. The first research area is the unambiguous estimation of and positioning with high-order binary offset carrier (BOC) signals. The second research area is the time synchronization in indoor conditions. And the third research area is the positioning with co-located and distributed receiver antennas.

In the first research area, this thesis shows that the robust unambiguous positioning with high-order BOC signals in harsh propagation conditions is possible when jointly exploiting these signals in the position domain and taking advantage of the spatial diversity introduced by arrays of antennas. The proposed estimators introduce an important benefit with respect to single-satellite-based unambiguous techniques (operating at pseudorange level) thanks to the processing gain introduced by the MIMO-GNSS system formed. Indeed, when multiple antennas are featured by the receiver, the proposed approach allows the exploitation of high-order BOC signals even in indoor conditions, achieving positioning accuracies of few meters in propagation conditions for which BPSK(1) signals can only achieve accuracies of tens of meters. Moreover, the proposed solutions are implementable based on state-of-the-art multi-correlator receiver architectures, and allow a drastic reduction of the computational burden with respect to the typical implementation of the so-called direct positioning estimation (DPE) techniques.

In the second research area, this thesis proposes a joint time and channel estimation approach for static indoor GNSS receivers featuring an array of antennas in order to improve the timing

accuracy in indoor propagation conditions. This approach exploits both the structure of the diffuse multipath components of the indoor channel and the MIMO system formed by all the GNSS signals received via an array of antennas. Simulation results with a wideband satellite-to-indoor channel model show that the proposed timing estimators allow an important mitigation of the dominant indoor multipath conditions. Therefore, the joint time and channel estimation approach proposed is considered an appealing solution for indoor applications with tight synchronization requirements, as can be the case in indoor small cells for 5G.

Finally, in the third research area, this thesis proposes the exploitation of co-located and distributed receiver antennas for positioning in harsh propagation conditions. In order to improve the performance achieved with co-located antennas, a distributed array processing approach for collaborative GNSS-based snapshot positioning is proposed in the MIMO-GNSS framework. In this solution, one of the receivers is used as anchor and a distributed array is formed, allowing to transform the positioning problem into an angle estimation problem in order to reduce the computational burden. The exploitation of the spatial diversity introduced by multiple receivers enables the derivation of an improved position solution for receivers in degraded propagation conditions, taking in particular advantage of those in better propagation conditions.

# Acknowledgments

This thesis would not have been possible without the support of many people I'm lucky to be surrounded by.

First of all, I would like to thank Juan for his continuous support and advice, and for accepting to be my thesis advisor back in 2016.

This thesis was certainly influenced by many technical discussions with several colleagues and friends at ESA over the last 9 years. I would like to especially thank Moi and Juanma for the brainstorming on GNSS, high-order BOC processing and propagation channels since 2012, and the collaboration in the years after. Thank you to Gustavo, Josevi and many other colleagues for contributing to better understand the problems faced by GNSS receivers when operating in harsh propagation conditions. Thank you to all those I had the opportunity to discuss different R&D topics, especially David, Sergi, Adria, Vicente and Marco. And finally I would also like to thank Massimo and Riccardo for welcoming and supporting my research.

Por supuesto, gracias en especial a mis padres y hermanos por estar siempre ahí.

And last, but not least, thank you Tamara for your infinite support, advice and patience in these last years. It would have been impossible without you!



# Contents

|   |             |
|---|-------------|
| <b>Abstract</b> .....   | <b>v</b>    |
| <b>Acknowledgments</b> .....  | <b>vii</b>  |
| <b>Notation</b> .....   | <b>xiii</b> |
| <b>Acronyms</b> .....   | <b>xv</b>   |
| <b>1 Introduction</b> .....   | <b>1</b>    |
| 1.1 Motivation and objectives .....   | 2           |
| 1.2 Thesis outline and research contributions .....   | 6           |
| <b>2 Background and State-of-the-Art</b> .....  | <b>11</b>   |
| 2.1 Brief introduction to GNSS .....  | 12          |
| 2.2 GNSS in harsh propagation conditions .....  | 19          |
| <b>3 Unambiguous Positioning with High-Order BOC Signals</b> .....                                | <b>25</b>   |
| 3.1 Background and motivation .....   | 26          |
| 3.2 The DOME approach .....   | 28          |
| 3.2.1 Signal model for the DOME approach .....  | 30          |
| 3.2.2 Dual-optimization multi-correlator-based estimators.....                                    | 32          |
| 3.2.3 Simulation results .....  | 36          |
| 3.3 Unambiguous positioning in the MIMO-GNSS framework .....                                      | 46          |
| 3.3.1 Unambiguous positioning with high-order BOC signals for single-antenna receivers .<br>..... | 47          |

|          |  |           |
|----------|--|-----------|
| 3.3.1.1  | System and signal model .....  | 47        |
| 3.3.1.2  | Unambiguous position estimator: the MISO-MLE solution .....                                | 50        |
| 3.3.1.3  | Implementation aspects of the MISO-MLE solution .....                                      | 52        |
| 3.3.1.4  | Comparison with state-of-the-art techniques.....   | 53        |
| 3.3.2    | Unambiguous positioning with high-order BOC signals for multiple-antenna receivers .....   | 55        |
| 3.3.2.1  | System and signal model .....  | 55        |
| 3.3.2.2  | Unambiguous position estimator: the MIMO-MLE solution .....                                | 58        |
| 3.3.2.3  | Implementation aspects of the MIMO-MLE solution .....                                      | 59        |
| 3.3.3    | Simulation results .....   | 61        |
| 3.4      | Conclusions .....  | 68        |
| <b>4</b> | <b>Indoor Timing.....</b>  | <b>71</b> |
| 4.1      | Background and motivation .....  | 72        |
| 4.2      | System and signal model.....   | 73        |
| 4.3      | Exploiting the spatial diversity.....  | 76        |
| 4.3.1    | Intermediate clock bias estimation .....   | 77        |
| 4.3.2    | Exploiting the indoor channel properties.....  | 79        |
| 4.3.3    | Alternative exploitation of the spatial correlation of the NLOS multipath components ..... | 81        |
| 4.3.4    | Implementation aspects of the proposed indoor timing solutions .....                       | 83        |
| 4.4      | Simulation results.....  | 85        |
| 4.5      | Conclusions .....  | 94        |
| <b>5</b> | <b>From Co-located to Distributed Array Solutions.....</b>                                 | <b>95</b> |
| 5.1      | Background and motivation .....  | 96        |
| 5.2      | The MIMO-GNSS solution indoors.....  | 98        |
| 5.3      | A collaborative solution in the MIMO-GNSS framework (Co-MIMO-GNSS) .....                   | 102       |

|  |  |            |
|--|--|------------|
| 5.3.1  | System and signal model .....                              | 102        |
| 5.3.2  | Formation of the distributed array rigid body .....        | 104        |
| 5.3.3  | Distributed array signal model .....                       | 106        |
| 5.3.4  | MLE of the angle of the distributed array rigid body ..... | 107        |
| 5.3.5  | Hybrid position solution .....                             | 107        |
| 5.3.6  | Implementation aspects of the collaborative solution ..... | 108        |
| 5.3.7  | Simulation results .....                                   | 108        |
| 5.3.8  | Trusted distributed array rigid body .....                 | 111        |
| 5.4  | Conclusions .....  | 113        |
| <br><b>6 Conclusions and Future Research .....</b> |  | <b>117</b> |
| <br><b>List of Publications .....</b>              |  | <b>121</b> |
| <br><b>Bibliography .....</b>                      |  | <b>123</b> |



# Notation

Vectors and matrices are denoted by lower case and upper case bold letters, respectively. Scalars are denoted by italic letters. The superscripts  $T$  and  $H$  denote the transpose and Hermitian transpose operations, respectively.

|  |   |
|--|---|
| $j$  | Imaginary unit ( $j = \sqrt{-1}$ )  |
| $\pi$  | Pi  |
| $\mathbb{R}^{N \times M}, \mathbb{C}^{N \times M}$ | Set of $N \times M$ matrices with real and complex entries, respectively.   |
| $\hat{x}$  | Estimation of the parameter $x$ .   |
| $ x $  | Absolute value of the scalar $x$ .  |
| $\ \mathbf{x}\ $                                   | $\ell^2$ -norm of vector $\mathbf{x}$ , such that $\ \mathbf{x}\ ^2 = \mathbf{x}^H \mathbf{x}$ .                      |
| $[\mathbf{x}]_i$                                   | $i$ -th element of vector $\mathbf{x}$ .  |
| $[\mathbf{X}]_{i,j}$                               | The element of matrix $\mathbf{X}$ in row $i$ and column $j$ .  |
| $\{x_i\}_{i=1}^N$                                  | Set of terms $x_i$ with index from $i = 1$ to $i = N$ .   |
| $\{\mathbf{x}_i\}_{i=1}^N$                         | Set of vectors $\mathbf{x}_i$ with index from $i = 1$ to $i = N$ .  |
| $\mathbf{I}$                                       | Identity matrix.  |
| $\det(\mathbf{X})$                                 | Determinant of $\mathbf{X}$ .   |
| $CN(\boldsymbol{\mu}, \boldsymbol{\Sigma})$        | Complex multivariate Gaussian distribution with mean $\boldsymbol{\mu}$ and covariance matrix $\boldsymbol{\Sigma}$ . |
| $U(a, b)$  | Uniform distribution with $a$ and $b$ as minimum and maximum values, respectively.                                    |
| $\arg \max_x f(x)$                                 | Values of $x$ that maximize the function $f(x)$ .   |
| $\arg \min_x f(x)$                                 | Values of $x$ that minimize the function $f(x)$ .   |
| $\exp(\cdot)$                                      | Exponential function.   |
| $\log_{10}(\cdot)$                                 | Base-10 logarithm.  |

|                         |                                       |
|-------------------------|---------------------------------------|
| $\text{sgn}(\cdot)$     | Signum function.                      |
| $\lfloor \cdot \rfloor$ | Floor function.                       |
| $\dot{f}(t)$            | Derivate of time of function $f(t)$ . |
| $=$                     | Equal to.                             |
| $\triangleq$            | Defined as.                           |
| $\approx$               | Approximately equal to.               |
| $\sim$                  | Distributed according to.             |
| $s. t.$                 | Subject to.                           |

# Acronyms

|              |  |
|--------------|--|
| 3G           | Third Generation mobile networks                     |
| 4G           | Fourth Generation mobile networks                    |
| 5G           | Fifth Generation mobile networks                     |
| ADC          | Analog to Digital Converter                          |
| A-GNSS       | Assisted GNSS  |
| AWGN         | Additive White Gaussian Noise                        |
| BOC          | Binary Offset Carrier                                |
| BPSK         | Binary Phase Shift Keying                            |
| C/A          | Coarse/Acquisition                                   |
| C/No         | Carrier-to-Noise Density Ratio                       |
| Co-MIMO-GNSS | Collaborative MIMO-GNSS                              |
| CRLB         | Cramér-Rao Lower Bound                               |
| DLL          | Delay-Locked Loop                                    |
| DOME         | Double-Optimization Multi-correlator-based Estimator |
| DPE          | Direct Position Estimation                           |
| DSSS         | Direct-Sequence Spread-Spectrum                      |
| DTE          | Direct Time Estimation                               |
| ECEF         | Earth-Centered Earth-Fixed                           |
| ESA          | European Space Agency                                |
| E-L          | Early-Late   |
| FE           | Front-End  |
| FFT          | Fast Fourier Transform                               |
| FLL          | Frequency-Locked Loop                                |

|            |   |
|------------|---|
| GLONASS    | Globalnaya Navigacionnay Sputnikovaya Sistema             |
| GNSS       | Global Navigation Satellite System                        |
| GPS        | Global Positioning System                                 |
| H-DPE      | Hybrid Direct Position Estimation                         |
| HDOP       | Horizontal Dilution Of Precision                          |
| IF         | Intermediate Frequency                                    |
| IIR        | Infinite Impulse Response                                 |
| IoT        | Internet of Things  |
| ITU        | International Telecommunication Union                     |
| ITU-R      | ITU Radiocommunication sector                             |
| LAMBDA     | Least Squares Ambiguity Decorrelation Adjustment method   |
| LOS        | Line-Of-Sight   |
| LS         | Least Squares   |
| LTE        | Long Term Evolution                                       |
| MCE        | Maximum Correlation Estimator                             |
| Mcps       | Megachip per second                                       |
| MIMO       | Multiple-Input Multiple-Output                            |
| MIMO-GNSS  | Multiple-Input Multiple-Output GNSS                       |
| MIMO-JTC   | MIMO Joint Time and Channel estimator                     |
| MIMO-JTCC  | MIMO Joint Time and Channel spatial Correlation estimator |
| MIMO-Radar | Multiple-Input Multiple-Output Radar                      |
| MIMO-SAR   | Multiple-Input Multiple-Output Synthetic Aperture Radar   |
| ML         | Maximum Likelihood  |
| MLE        | Maximum Likelihood Estimator/Estimation                   |

|        |  |
|--------|--|
| MP     | Multipath  |
| NLOS   | Non-Line-Of-Sight  |
| PC-MLE | Post-Correlation MLE   |
| PDF    | Probability Density Function                                     |
| PDOP   | Position Dilution Of Precision                                   |
| PDP    | Power-Delay Profile  |
| PLL    | Phase-Locked Loop  |
| PNT    | Positioning, Navigation and Timing                               |
| PPP    | Precise Point Positioning  |
| PRN    | Pseudorandom Noise   |
| PTP    | Precise Time Protocol  |
| PVT    | Position, Velocity and Time                                      |
| RF     | Radio Frequency  |
| RMSE   | Root-Mean-Square Error   |
| RTK    | Real-Time Kinematic  |
| RTT    | Round-Trip Time  |
| SAGE   | Space-Alternating Generalized Expectation-Maximization Algorithm |
| SDR    | Software-Defined Radio   |
| SNR    | Signal-to-Noise Ratio  |
| SoO    | Signal of Opportunity  |
| TOW    | Time of Week   |
| TTFF   | Time To First Fix  |
| UWB    | Ultra-wideband   |
| V2V    | Vehicle-to-Vehicle   |

V2X

Vehicle-to-everything

WLS

Weighted Least Squares

# 1

## Introduction

**T**HIS thesis deals with the processing of Global Navigation Satellite Systems (GNSS) signals for positioning and timing in harsh propagation conditions. In particular, the focus is on signal processing techniques exploiting the spatial diversities present both at transmission and reception levels when multiple GNSS satellites are in view by multiple receiver antennas, which form a multiple-input multiple-output (MIMO) system. In this context, three problems or research areas open in the GNSS literature are targeted. The first research area is the unambiguous estimation of and positioning with high-order binary offset carrier (BOC) signals. The second research area is the time synchronization in indoor conditions. And the third research area is the positioning with co-located and distributed receiver antennas.

This chapter is organized in two sections. Section 1.1 introduces the motivation and objectives of the thesis. Then, Section 1.2 presents the thesis outline and the research contributions.

## 1.1 Motivation and objectives

GNSS signals are broadly used for positioning, navigation and timing (PNT) in many different applications and use cases, including location-based services (LBS) in smartphones and other devices, road and vehicular applications, agriculture, aviation, or time synchronization of critical infrastructures, just to name a few. Moreover, GNSS is expected to play a key role in applications like the Internet of Things (IoT) or autonomous vehicles. In many of the current applications, the achieved accuracy and availability of the positioning and/or timing solution/s are important parameters. Furthermore, some of the future applications and services are expected to impose increasingly demanding performance requirements in scenarios typically challenging for the exploitation of GNSS signals, like indoors.

GNSS is performing very well in mild propagation conditions (e.g., open-sky conditions), with position and time synchronization accuracies of the order of few meters and tens of ns, respectively, when standard positioning techniques are used; and sub-meter position accuracies are achievable with high-accuracy solutions based on carrier-phase observables, like precise point positioning (PPP) or real-time kinematic (RTK) solutions. Nevertheless, the exploitation of GNSS in harsh propagation conditions typical of urban and indoor scenarios is very challenging. Indeed, in these scenarios, the impact of effects like blockage and multipath can highly degrade the achievable availability and accuracy of both standard and high-accuracy PNT solutions, resulting in position errors of up to tens or even hundreds of meters, and timing accuracies of hundreds of ns.

Other technologies may be exploited together with, or as alternative to, GNSS to improve the availability and accuracy of the final positioning and navigation solution in harsh propagation conditions. Examples of these technologies include very different user sensors like inertial measurement units (accelerometers, gyroscopes), magnetometers, barometers, cameras, radars or lidars, and signals of opportunity (SoO) from terrestrial communication systems like WiFi, Bluetooth, or cellular communication systems like 3G, 4G and 5G. Future positioning and navigation solutions are expected to be based on a fusion or hybridization of different technologies and techniques, including GNSS. These hybrid solutions may exploit additional assistance or support data, including 2D/3D maps or radio and magnetic fingerprint maps based on crowd-sourced data. The set of specific technologies used will highly depend on the specific use case and application, which will impose requirements in terms of accuracy and availability; but also in terms of integrity and authenticity of the solution; and cost, size or power consumption of the receiver or device. In terms of performance, the relative contribution of

GNSS to the hybrid position solution will highly dependent on the technologies and additional support data used, the fusion and estimation techniques exploited, and the propagation conditions of the GNSS signals.

Although different technologies are available, GNSS is expected to be a key player in the derivation of positioning and timing for many future applications since it has the important advantage of being free, open access, worldwide available, no additional infrastructure is needed, and enables the derivation of very accurate solutions in certain environment conditions. Additionally, hybrid solutions are expected in general to target the exploitation of all the technologies and measurements considered in the best way possible to enable ubiquitous positioning with the best achievable accuracy; and in certain use cases the GNSS contribution may drive the final achieved performance. This can be the case in situations where SoOs, assistance data or fingerprinting maps are not available, or do not provide the required accuracy (note that the user may operate in very different and changing conditions); or when the quality of the sensors used by the receiver is not good enough for achieving the required accuracy in a continuous way (accuracy comes at a cost, and this cost may not be compatible with the target application). Moreover, for some applications a GNSS-only solution may be a good option for meeting the target user requirements. Therefore, it is in general not only of interest, but also necessary, to derive estimation techniques enabling the enhanced exploitation of the GNSS signals received for the achievement of the ultimate performance possible.

There are several open GNSS research areas with potential to enable the achievement of future stringent positioning and timing requirements, but at the same time with quite some room for improvement. Among these areas, one can find the unambiguous estimation of high-order BOC signals. These signals allow the achievement of high-precision code-based solutions, but at the cost of introducing an ambiguity in the estimation problem. Indeed, in practice the achievement of accurate and precise positioning solutions in harsh propagation conditions is very challenging with state-of-the-art unambiguous estimation techniques due to the impact of the so-called false locks (resulting in biases of several meters or tens of meters in the position solution). Based on this, the first objective of this thesis is to enable the achievement of robust unambiguous positioning with high-order BOC signals in harsh propagation conditions where the usage of state-of-the-art unambiguous techniques results in biases in the position estimation due to the impact of false locks.

Another research area of high interest is indoor timing. Future applications to come may require accurate and precise timing to operate. An example of this is indoor small cells in 5G, which are expected to have very tight time synchronization requirements of the order of tens of ns. Different current technologies and technical solutions may be considered for this purpose, like the precise time protocol (PTP), or commercial solutions based on satellite signals from low-earth orbits. But these solutions either require additional infrastructure or their usage is not for free. Being able to exploit GNSS signals in indoor small cells or similar future applications would be of high interest to enable a free and open access timing solution independent of additional ad-hoc infrastructure. Nevertheless, the exploitation of GNSS signals indoors is a

challenging topic due to the dominant impact of the non-line-of-sight (NLOS) signal propagation conditions, which limit the achievable timing accuracy. Based on the current limitations and the potential of GNSS for indoor timing applications, the second objective of this thesis is to enable the exploitation of GNSS signals in indoor conditions for timing with accuracies of the order of tens of ns.

Moving back to positioning, many different techniques have been proposed in the literature to improve the exploitation of GNSS signals in scenarios in which the impact of effects like blockage, fading or multipath are dominant. Among them, array processing and cooperative or collaborative positioning are interesting research areas to deal with the harsh propagation conditions typical of urban and indoor scenarios. In the former, the multiple antennas featured by a receiver are typically used to mitigate fading and multipath, as well as other interferences. In the latter, a set of multiple GNSS receivers in a certain location are used together to derive or improve their position solution. For this purpose, the distances or ranges between the receivers considered need to be estimated e.g., based on vehicle-to-vehicle (V2V) or vehicle-to-everything (V2X) communication technologies, ultra-wideband (UWB) or WiFi RTT (round-trip time) solutions. The way different antennas or receivers are exploited for positioning in harsh propagation conditions is an open problem in the literature, and there are alternative implementations still to be investigated. Moreover, the fast evolution of 5G standards and V2V/V2X communications, together with commercial Cloud platforms, could make feasible a broad application of the collaborative positioning concept to enable ubiquitous, accurate and precise positioning in urban and indoor scenarios. Therefore, the third objective of this thesis is to enable the improvement of positioning in harsh propagation conditions based on GNSS signals received with co-located and distributed receiver antennas.

In order to achieve the three main objectives defined above, this thesis focuses on signal processing techniques exploiting spatial diversity. In particular, the thesis proposes to exploit both the spatial transmission and reception diversities available when the GNSS signals transmitted by multiple satellites are received by multiple antennas. In this case, the system formed by the multiple GNSS satellites and the multiple receiver antennas (featured by a single or multiple receivers) can be modeled as a multiple-input multiple-output GNSS system (hereafter referred to as MIMO-GNSS system). Therefore, the positioning and timing problems in harsh propagation conditions can be seen as MIMO-GNSS estimation problems in which the different received versions of each of the signals transmitted by the GNSS satellites in view are jointly exploited. It is to be noticed that the usage of multiple co-located antennas in GNSS receivers may be a suitable solution in applications like autonomous vehicles or critical infrastructures; and for other use cases with stringent cost, size and power consumption requirements, like in the case of IoT and smartphone devices, the exploitation of multiple distributed receivers is still an option.

It is important to remark that the “MIMO” term is typically used in communications when multiple transmission and reception antennas are exploited for improving the capacity of the radio communication link in multipath propagation conditions. The “MIMO-radar” term is

typically used in radar when multiple transmission and reception antennas are exploited for improving the spatial resolution (by creating the so-called “virtual” antenna array), and for fading and interference mitigation. As opposed to MIMO communications, possibly orthogonal transmitted waveforms are used in MIMO-radar. Similarly, the “MIMO-SAR” term is used in the particular case of synthetic aperture radar (SAR). Analogously to the exploitation of the MIMO terminology in communications and radar, we will use the “MIMO-GNSS” term when multiple GNSS satellites and multiple reception antennas are jointly exploited for achieving a ubiquitous, accurate and precise PNT solution in degraded or harsh propagation conditions where this is challenging with state-of-the-art techniques. This will be the case in fading and multipath conditions typical of urban and indoor scenarios; but this framework may be also interesting in scenarios in which GNSS signals are vulnerable, like in the presence of external interferences, or under jamming or spoofing attacks. Note that in this case, similarly to the case of MIMO-radar, (quasi-) orthogonal transmitted waveforms are typically used by GNSS.

The exploitation of the signals from multiple satellites and/or multiple reception antennas in GNSS is not a new topic. Indeed, there has been extensive research on areas like arrays of antennas, cooperative and collaborative positioning, and direct position estimation (DPE) for the exploitation of the spatial diversity in GNSS; and this thesis builds on it. Moreover, the MIMO-GNSS system could just be exploited to derive solutions already available in the literature, so under certain assumptions we may not get any benefit or difference with respect to other estimators. As discussed in the previous paragraphs, the exploitation of GNSS signals in harsh propagation conditions is still very challenging, and there is still room for improving the estimation techniques and processing approaches available in the literature. In particular, some of the assumptions typically assumed in the signal model used in state-of-the-art estimators for exploiting the spatial diversity in GNSS may not be adequate in realistic propagation conditions typical of urban and indoor scenarios. An example of this is the typical assumption of the availability of the line-of-sight (LOS) signals (i.e., the components of interest) and the presence of one or several specular interference components to be mitigated (e.g., multipath ray/s or other interference contributions). Although this type of signal model may allow to derive elegant, accurate and precise estimators performing optimally when the model applies (e.g., in open-sky and controlled scenarios), this may not be the case in more realistic conditions where the exploitation of GNSS signals by state-of-the-art receivers is still challenging (e.g., in NLOS propagation conditions and in the presence of diffuse multipath).

Based on the previous discussion, this thesis focuses on the exploitation of the MIMO-GNSS system based on signal models that are considered “useful” in realistic harsh propagation conditions (i.e., that allow the robust application of the derived estimators in these conditions for achieving an improvement of the positioning or timing performance with respect to state-of-the-art solutions). This will be in general translated in the usage of simplified signal models with respect to the reality, acknowledging that in practice it is very complex (if not unfeasible) to model correctly the actual signal propagation conditions faced by the receiver in urban and indoor scenarios. This is also related to the methodology that is followed in this thesis to assess the performance of the proposed positioning and timing estimators, which is based on the

execution of simulations with controlled and realistic channel models (including ITU-R channels). This approach targets the demonstration of the benefits of the proposed techniques in the propagation conditions in which they are expected to operate and be useful (i.e., in those conditions in which the usage of GNSS currently has important limitations).

## 1.2 Thesis outline and research contributions

This section lays out the structure of this dissertation, which is divided in six chapters, and the research contributions of the thesis. The research performed in this thesis has been published in different journal articles and international conferences, and is partially part of two patents. These research contributions can be separated in three main research areas aligned with the three main objectives of this thesis: a) the unambiguous estimation of and positioning with high-order BOC signals, b) indoor timing, and c) positioning with co-located and distributed array solutions. Each of these research areas are covered in separate chapters, as described below.

**Chapter 1** presents the motivation and objectives of this thesis, and the thesis outline and research contributions presented herein. **Chapter 2** presents a summary of the background and state-of-the-art, briefly introducing GNSS and its exploitation for positioning and timing, as well as the current limitations faced by GNSS receivers in harsh propagation conditions. In particular, the main operational concepts behind GNSS receivers are briefly presented, as well as different technology trends being currently considered for the processing of GNSS signals. Different signal processing techniques that have been addressed in the literature to deal with the estimation of GNSS signals in harsh propagation conditions are briefly reviewed, identifying the limitations when exploiting BPSK and BOC signals.

**Chapter 3** focuses on the unambiguous estimation of and positioning with high-order BOC signals in harsh propagation conditions. The research performed on this topic can be divided in two main research areas: techniques operating at pseudorange or single-satellite level (i.e., following the DOME approach), and techniques operating at positioning level (i.e., in the MIMO-GNSS framework). First, the DOME approach is presented together with the different estimators proposed in this context and the corresponding simulation results. Compared to state-of-the-art techniques, the DOME approach further exploits the time diversity in the unambiguous estimation problem via the usage of multiple integration periods; and relies on a multi-correlator architecture in order to consider in the problem multiple correlation peaks of the cross-correlation function (instead of only the main and secondary peaks). Then, the unambiguous positioning in the MIMO-GNSS framework is introduced, presenting the estimators in the position domain both for the single- and multiple-antenna receiver configurations and the corresponding simulation results. The estimators in the MIMO-GNSS framework build on DPE and array processing techniques in order to introduce an additional processing gain in the unambiguous estimation problem by exploiting the spatial transmission

and reception diversities. The conclusions are presented at the end of the chapter. This chapter is based on the material of the following publications:

- [Gar19a] J. A. Garcia-Molina, and J. A. Fernandez-Rubio, “Collective Unambiguous Positioning with High-Order BOC Signals,” *IEEE Transactions on Aerospace and Electronic Systems*, vol. 55, no. 3, pp. 1461-1473, June 2019. © 2018 IEEE. <https://ieeexplore.ieee.org/document/8477092>
- [Gar16a] J. A. Garcia-Molina, M. Navarro-Gallardo, G. Lopez-Risueño, and M. Crisci, “Robust unambiguous Estimation of High-Order BOC Signals: The DOME approach,” *NAVIGATION, Journal of the Institute of Navigation*, vol. 63, no. 4, pp. 509–518, Winter 2016. © 2016 Institute of Navigation. <https://doi.org/10.1002/navi.162>
- [Gar15a] J. A. Garcia-Molina, “Method and Apparatus for Tracking a Binary Offset Carrier Navigation Signal,” European Patent Application No. EP3104195A1, 10 Jun. 2015.
- [Gar19b] J. A. Garcia-Molina, and J. A. Fernandez-Rubio, “Array Processing and Unambiguous Positioning of Signals with Multi-Peak Correlations,” *ION GNSS+ 2019*, Miami, Florida, Sep. 2019. <https://doi.org/10.33012/2019.17024>
- [Gar17a] J. A. Garcia-Molina, J. A. Fernandez-Rubio, R. Weiler, and M. Crisci, “Snapshot Processing of High-Order BOC Signals in the Cloud: on Sensitivity and Distortion Effects,” *ION GNSS+ 2017*, Portland, Oregon, Sep. 2017. <https://doi.org/10.33012/2017.15245>
- [Gar15b] J. A. Garcia-Molina, M. Navarro-Gallardo, G. Lopez-Risueño, and M. Crisci, “Robust Unambiguous Tracking of High-Order BOC Signals: a Multi-Correlator Approach,” *ION GNSS+ 2015*, Tampa, Florida, Sep. 2015. <https://www.ion.org/publications/abstract.cfm?articleID=13049>

**Chapter 4** focuses on indoor timing based on GNSS signals, targeting the enhancement of the timing accuracy in indoor propagation conditions. In particular, the concept of “composite MIMO channel” is introduced, and a joint time and composite MIMO channel estimation approach for static indoor GNSS receivers featuring an array of antennas is proposed. This approach allows to rely on the coarse timing estimations performed by state-of-the-art techniques (typically based on pseudorange estimations) as *a priori* information; and enables to further mitigate the impact of the indoor channel by exploiting both the structure of the diffuse multipath components and the spatial diversity introduced by the array of antennas. Simulation results in realistic indoor channel conditions are presented at the end of the chapter, followed by the conclusions. This chapter is based on the material of the following publications:

- [Gar18a] J. A. Garcia-Molina, “Method and Apparatus for Performing Joint Channel and Time Estimation in a GNSS Receiver,” International Patent Application No. PCT/EP2018/063660, 2018.
- [Gar18c] J. A. Garcia-Molina, and J. A. Fernandez-Rubio, “Positioning and Timing in the MIMO-GNSS Framework,” *NAVITEC 2018*, Noordwijk, The Netherlands, Dec. 2018. <https://ieeexplore.ieee.org/document/8642703>

**Chapter 5** focuses on positioning in harsh propagation conditions, going from co-located to distributed array solutions. The chapter starts with the exploitation of receivers featuring multiple antennas for positioning in indoor conditions in the MIMO-GNSS framework. This approach builds on DPE and array processing techniques in order to exploit the spatial transmission and reception diversities available. Simulation results in this case are presented. Then, the exploitation of distributed receivers for the formation of distributed arrays of antennas is introduced to further improve the achievable positioning accuracy. In particular, the joint exploitation of all the signals received by a set of receivers as a collaborative positioning problem is proposed. Compared to state-of-the-art cooperative and collaborative solutions, where typically the pseudoranges derived by the receivers are used as baseline in the estimation, the proposed solution exploits directly the signals gathered by all the receivers. Moreover, taking one of the receivers as anchor, the collaborative positioning problem is proposed to be transformed into a collaborative angle estimation problem in order to reduce the computational burden. The simulation results are presented at the end of the chapter, followed by the conclusions. This chapter is based on the material of the following publications:

- [Gar19c] J. A. Garcia-Molina, and J. A. Fernandez-Rubio, “Collaborative Snapshot Positioning via Distributed Array Processing,” *ION GNSS+ 2019*, Miami, Florida, Sep. 2019. <https://doi.org/10.33012/2019.16876>
- [Gar18c] J. A. Garcia-Molina, and J. A. Fernandez-Rubio, “Positioning and Timing in the MIMO-GNSS Framework,” *NAVITEC 2018*, Noordwijk, The Netherlands, Dec. 2018. <https://ieeexplore.ieee.org/document/8642703>
- [Gar18b] J. A. Garcia-Molina, J. A. Fernandez-Rubio, and J. M. Parro, “Exploiting Spatial Diversity for NLOS Indoor Positioning,” *ION GNSS+ 2018*, Miami, Florida, Sep. 2018. <https://doi.org/10.33012/2018.15865>
- [Gar17c] J. A. Garcia-Molina, and J. M. Parro, “Cloud-based GNSS Processing of Distributed Receivers of Opportunity: Techniques, Applications and Data-collection Strategies,” *6th International Colloquium on Scientific and Fundamental Aspects of GNSS/Galileo*, Valencia, Spain, Oct. 2017.

- [Gar17b] J. A. Garcia-Molina, and J. A. Fernandez-Rubio, “Exploiting Spatial Diversity in Low-cost SDR Platforms: the MIMO-GNSS approach,” *6th International Colloquium on Scientific and Fundamental Aspects of GNSS/Galileo*, Valencia, Spain, Oct. 2017.

Finally, **Chapter 6** presents the conclusions of the thesis and the areas for future research.

In summary, the **contributions of this thesis** to the three main research areas covered in Chapters 3, 4, and 5 are the following:

- i. An approach and estimators for the robust unambiguous estimation or tracking of high-order BOC signals based on the solution of a double optimization problem exploiting a multi-correlator architecture and multiple integration periods (dubbed the DOME approach). This enables the enhancement of the SNR conditions under which the identification of the main correlation peak is performed (targeting the reduction of the probability of false lock), and the exploitation of *a priori* known distortions of the cross-correlation function (which may degrade the probability of false lock). (*See Section 3.2.*)
- ii. An approach and estimators for the robust unambiguous positioning with high-order BOC signals directly in the position domain, both in single- and multiple-antenna configurations, achieving enhanced performance with respect to techniques operating at pseudorange or single-satellite level. This enables the exploitation of high-order BOC signals in harsh propagation conditions where the usage of single-satellite level techniques result in a high probability of false lock. (*See Section 3.3.*)
- iii. A framework (dubbed the MIMO-GNSS framework) for positioning and timing exploiting the transmission and reception spatial diversities available in GNSS receivers featuring multiple antennas and operating in harsh propagation conditions where NLOS propagation conditions may be dominant, like urban and indoor environments. (*See Chapter 3, 4, and 5.*)
- iv. The concept of composite MIMO channel in the MIMO-GNSS framework, enabling the achievement of enhanced timing performances in indoor environments thanks to the exploitation of the structure of the diffuse multipath and to the improvement of the equivalent SNR conditions in the MIMO-GNSS system formed. (*See Chapter 4.*)
- v. A joint time and composite MIMO channel estimation approach for static indoor GNSS receivers featuring an array of antennas. This approach enables the achievement of accurate and precise time synchronization in indoor propagation conditions even when NLOS propagation conditions are dominant. Two estimators based on the solution, via Monte Carlo methods, of multi-hypothesis optimization problems in the receiver’s clock bias domain are proposed. Each of the estimators follows a different approach to exploit the spatial correlation of the NLOS multipath components. (*See Chapter 4.*)

- vi. The exploitation of the MIMO-GNSS framework in collaborative positioning, moving from a co-located to a distributed array configuration for improving the positioning solution of receivers in harsh propagation conditions. This enables the joint exploitation of receivers in nearby locations experiencing different propagation conditions. (*See Chapter 5.*)
- vii. A distributed array processing approach for positioning based on a) the formation of a distributed array “rigid body” based on the exploitation of peer-to-peer ranges between receivers and using one of the receivers as anchor, and b) the estimation of a collaborative position as the solution of the angle of the distributed array rigid body, which is used as constraint in the estimation problem. This enables the derivation of a position solution for receivers in highly degraded propagation conditions (or experiencing external interferences) by exploiting other receivers in nominal or less degraded propagation conditions. (*See Chapter 5.*)
- viii. The concept of “trusted” distributed array rigid body as the one composed by the subset of receivers, out of the ones in nearby locations, with “positive” contribution to the collaborative position solution. This targets the exclusion of receivers impacted by strong multipath reflections or spoofing attacks. (*See Chapter 5.*)
- ix. The assessment of the proposed estimators for positioning and timing based on both controlled and realistic channel models. (*See Chapter 3, 4, and 5.*)

# 2

## Background and State-of-the-Art

GNSS signals are currently exploited in the context of many different applications and use cases for positioning and timing purposes. The great success of GNSS-based PNT solutions may be explained by the availability of open access and worldwide available GNSS signals allowing the achievement of positioning and timing accuracies down to the sub-meter and ns levels, respectively. Nevertheless, GNSS signals received on-ground are very weak. Indeed, the achievable accuracy and availability of the GNSS-based PNT solutions is highly dependent on the user environment in which the GNSS signals are received, and on the specific receiver techniques and technologies exploited. This explains the important amount of research performed on GNSS signal processing in the last years to deal with the exploitation of GNSS signals in degraded propagation conditions.

This chapter is organized in two sections. Section 2.1 is briefly introducing the basics of GNSS at conceptual level, and provides references available in the literature going into further

details on general GNSS system, signal and receiver aspects of interest in the context of this thesis. Then Section 2.2 briefly reviews the state-of-the-art on the exploitation of GNSS signals in harsh propagation conditions.

The material presented in this chapter has been partially published by the author in [Gar15a], [Gar15b], [Gar16a], [Gar17a], [Gar17b], [Gar17c], [Gar18a], [Gar18b], [Gar18c], [Gar19a], [Gar19b], and [Gar19c].

## 2.1 Brief introduction to GNSS

Assuming we are outdoors, if we look up in the sky we may have in view a certain number of GNSS satellites, each of them transmitting different GNSS signals potentially targeting different user services. Some of those GNSS signals are open access signals waiting to be exploited worldwide by users and devices that want to know, with a certain accuracy, their current position and/or time. Let us consider a receiver with  $M$  GNSS satellites in view from a certain GNSS system (i.e., a certain GNSS constellation) in ideal LOS signal propagation conditions, as depicted in Fig. 2.1. The processing of a GNSS signal per satellite is assumed (all with the same modulation and transmitted at the same frequency band) such that  $M$  GNSS signals with equivalent modulation are targeted to be tracked for estimating the receiver's position. In ideal LOS conditions, the complex baseband signal received by the GNSS antenna from the  $M$  GNSS satellites in view can be modeled as

$$x(t) = \sum_{m=1}^M a_m(t) g_m(t - \tau_m(t)) \exp\{j2\pi f_m(t)t\} + e(t), \quad (2.1)$$

where  $a_m$ ,  $\tau_m$  and  $f_m$  are the complex amplitude, time-delay and frequency-shift for the LOS signal of the  $m$ -th satellite, respectively,  $e$  is the noise component, and  $g_m$  is the complex baseband model of the direct-sequence spread-spectrum (DSSS) signal transmitted by the  $m$ -th GNSS satellite.

The GNSS signals transmitted by the different satellites of a certain constellation are expected to be time-synchronized (i.e., all the satellites of the constellation are aligned with a common GNSS system time). Based on this, the concept behind GNSS-based positioning is quite straightforward, and is based on the estimation of the so-called “pseudoranges” between the receiver and the set of  $M$  GNSS satellites in view. In general, the pseudoranges are not equivalent to the geometric ranges between receiver and satellites due to the potential time offset between the receiver time and the GNSS system time (this explains the usage of the prefix). Therefore, in practice both the receiver's position and time need to be typically

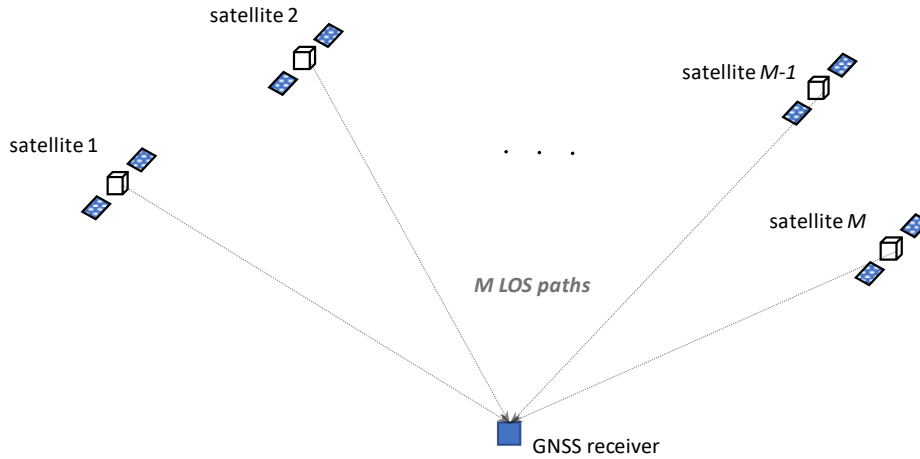


Fig. 2.1: Illustration of the system composed by  $M$  GNSS satellites and a GNSS receiver in open-sky conditions (with the GNSS signals in LOS signal conditions).

estimated, with the derived solution corresponding to that being consistent with the estimated pseudoranges. For a good summary of the conventional positioning process based on the estimated pseudoranges, the reader is referred to [San13].

In the introduction above, a certain GNSS signal from a GNSS system has been considered. Nowadays, there are different GNSS systems being exploited in parallel by mass-market and commercial GNSS receivers, including the ones that can be already found in smartphones: from the American GPS, and the Russian GLONASS systems, to newer systems like the European Galileo and the Chinese Beidou. The availability of multiple GNSS systems is of interest for the receivers from a position availability and accuracy point of view in harsh propagation conditions (where only few areas of the sky may be observed by the receiver, such that a limited number of satellites per constellation can be tracked). Each of the GNSS systems is using its own reference time to which the transmitted DSSS signals are synchronized. These DSSS signals are typically consisting on a pseudorandom noise (PRN) code different for each of the signals/satellites considered (being quasi-orthogonal between them and known *a priori* by the receiver), and the navigation data modulated on it. Other GNSS signals are not containing any navigation data, being only modulated by a secondary or overlay code (typically referred to as pilot signals). Different signal modulations are considered in practice, from legacy BPSK to more complex BOC-based modulations. The exploitation of BPSK signals is typically of interest from the acquisition point of view, while BOC-based signals are being introduced targeting high-accuracy code-based pseudorange estimations. Moreover, current GNSS systems transmit different signals in different frequencies within the L-band (e.g., L1/E1, L5/E5, L2, E6, etc.), offering different services to the users, from open services to governmental and/or military services. This is additionally of interest to the receivers for achieving higher

positioning accuracies thanks to the usage of precise positioning techniques exploiting the carrier-phase pseudorange estimations in multiple GNSS frequencies. A good overview on GNSS systems and signals can be found in [Kap06] and [Teu17].

Looking more into the details of conventional GNSS receivers, the receiver processing is typically divided in two general and separated steps: a first step in which the receiver is performing the code and carrier synchronization of the GNSS signals received (required for the estimation of the pseudorange measurements), and a second step in which the pseudorange measurements for the different satellites in view are used in the positioning solution (process typically referred to as multilateration). Additionally, navigation data is required for deriving the receiver’s position, which can be obtained by demodulating the broadcasted navigation message transmitted in the GNSS signals (typically containing the TOW, clock and orbit data for the satellite, the almanacs of the GNSS constellation, and ionospheric corrections, among others). Alternatively, assisted-GNSS (A-GNSS) may be considered instead, removing the need to demodulate the broadcasted navigation message.

Typical GNSS receivers are featuring a single antenna receiving the GNSS signals, together with noise and potential interferences. After the antenna, the RF front-end is in charge of amplifying, filtering, down-converting and digitizing the signal received. Then, the digitized signal goes through a “baseband” processing stage (note that the processed GNSS signals may not be necessarily in baseband), in which the acquisition and tracking of each of the GNSS signals in view is performed. Both acquisition and tracking stages are based on the cross-correlation of the received signal with the local PRN code replicas of the target GNSS signals to be exploited by the receiver. It is to be noticed that the GNSS signals are received with a certain time delay and frequency offset depending on the position, velocity, time, and time-drift of the receiver and each of the GNSS satellites. Therefore, the estimation of the time delay and frequency offset of the GNSS signal received gives information about the receiver’s position, time, and velocity. Fig. 2.2 illustrates a generic GNSS receiver architecture. A good overview on GNSS receiver architectures can be found in [Kap06] and [Teu17].

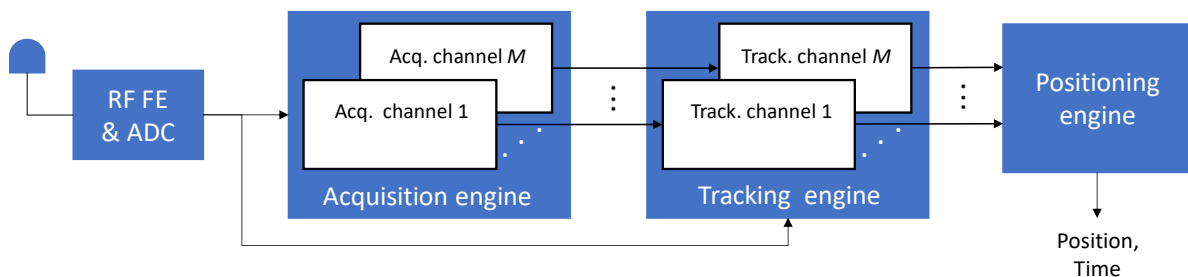


Fig. 2.2: Illustration of a generic GNSS receiver architecture.

The acquisition stage targets the detection of the signals from the GNSS satellites in view and a first coarse estimation of the PRN code phase (i.e., the code delay) and the carrier frequency of each GNSS signal. For this purpose, multi-correlator and/or parallel search approaches (e.g., FFT-based) may be used to scan the code phase and carrier frequency areas in which the signals are expected. These architectures are typically exploited in mass-market receivers in order to allow the acquisition of multiple satellites/signals in parallel, which is beneficial for reducing the time required to derive the first position solution (typically referred to as the time-to-first-fix, TTFF).

One of the key aspects highly impacting the ability of a GNSS receiver to acquire GNSS signals at the beginning of its operation is the initial receiver conditions (i.e., how much *a priori* information is available by the receiver). This limits the ability of the receiver to provide a first position fix in the shortest possible time (i.e., in the shortest TTFF). Basically, the better we know the receiver's state vector (i.e., its position, time, reference frequency, and velocity) and the satellites' state vectors (or the data needed to derive them), the more we can reduce the search space (in the code phase and frequency dimensions) that needs to be scanned by the acquisition engine. This has a direct impact on the resources required to acquire the GNSS signals. Indeed, assistance data is nowadays exploited in mass-market receivers to reduce the TTFF and enable higher acquisition sensitivities with equivalent processing resources. This is, of course, of interest to allow the exploitation of GNSS signals in harsh propagation conditions typical of urban and indoor scenarios. The assistance is typically composed by navigation data, and coarse or fine time, frequency and position information. Also important in harsh propagation conditions, the availability of assistance data allows to reduce the amount of data needed from the broadcasted navigation modulated in the GNSS signals (eventually, no demodulation may be needed). A good overview on A-GNSS can be found in [Dig09].

Once the acquisition is performed, a refinement of the code phase and carrier frequency for each GNSS signal is typically performed by the tracking stage. Additionally, the carrier phase tracking may be also performed (from which carrier-based pseudoranges can be obtained). The tracking stage of conventional receivers is typically based on delay-locked loops (DLL) in charge of the fine alignment of the code phase of the received signal and the local replica; and frequency-locked loops (FLL) and/or phase-locked loops (PLL) aligning the carrier frequency and/or phase, respectively. Conventional DLL, FLL and PLL are based on closed-loops operating at post-correlation level and exploiting up to three correlators (the so-called "early", "prompt", and "late" correlators) uniformly distributed around the main peak of the cross-correlation function between the received signal and the local replica of the target GNSS signal. These up to three correlators are exploited by the "discriminator" used by the DLL (i.e., the code delay error estimator); while the discriminators of the FLL and PLL only exploit the prompt correlator (which, ideally, is aligned with the maximum of the cross-correlation function). Alternatively to the closed-loops, open-loops may be also used in the case very low C/No conditions are targeted (with the objective to be more stable than closed-loops) [Gra09]; and alternatively to the usage of up to three correlators, multi-correlators may be used as well

to derive multiple correlation points of the cross-correlation function (with the objective of having a more robust and/or accurate tracking) [Phe01].

Most of current commercial receivers are based on the so-called narrow-correlators (see [Die92] and [Kap06] for details). The concept behind narrow-correlators consists in reducing the separation between the early and late correlators used by the DLL (i.e., to reduce the so-called early-late spacing) such that: a) the noise contribution of the corresponding correlation samples have a higher correlation between them, and, thus, a lower impact on the code phase estimation performed by the discriminator; and b) the discriminator is less impacted by multipath rays with a delay relatively long with respect to the early-late spacing. Narrow-correlators are typically exploited in steady-state code tracking conditions to enable the derivation of accurate code-based pseudoranges, while “wide-correlators” are typically used right after acquisition (due to the higher code phase uncertainty).

Another important factor impacting the accuracy of the code-based pseudoranges is the modulation used by the GNSS signals, as introduced earlier. For BPSK signals, a higher accuracy is achieved by exploiting a higher chip rate thanks to the sharper correlation peak obtained. In this case, BPSK( $n$ ) typically denotes a BPSK signal with a chip rate of  $R_c = n \cdot f_0$  (with  $f_0 = 1.023$  Mcps). The usage of BOC signals is being introduced in new GNSS generations in order to obtain a sharper correlation peak than with legacy BPSK signals (which is translated in a more accurate code phase estimation), at the cost of side-peaks appearing in the autocorrelation function. The complex baseband model of the BOC-modulated DSSS signal can be modeled as [Kap06]

$$g(t) = v(t)\text{sgn}\{\sin(2\pi f_{sc}t + \varphi)\}, \quad (2.2)$$

where  $v(t)$  is the PRN code,  $f_{sc}$  is the so-called subcarrier frequency of the BOC signal, and  $\varphi$  is the phase angle typically used to define if the BOC signal is sine phased (BOC<sub>sin</sub>, for  $\varphi = 0$ ), or cosine phased (BOC<sub>cos</sub>, for  $\varphi = \pi/2$ ). BOC signals are typically denoted as BOC( $m, n$ ), with the subcarrier frequency  $f_{sc} = m \cdot f_0$ , and the chip rate  $R_c = n \cdot f_0$ . The ratio between  $m$  and  $n$  defines the number of correlation peaks of the autocorrelation function. For the so-called high-order BOC signals (where  $m > n$ , and multiple peaks are present in the autocorrelation function), the identification of the main peak (marking the reference for the code phase estimation) can be very challenging, even in additive white Gaussian noise (AWGN conditions [Gar16a]). Fig. 2.3 depicts an example of the cross-correlation functions in the case of a BPSK signal (with a triangular-like correlation) and of a high-order BOC signal (with multiple correlation peaks) with respect to the chip period  $T_c = 1/R_c$ . It is to be noticed that the cross-correlation functions in this example consider the filtering of the received signals, resulting in a smoothing of the correlation peaks. In general the lower the filter bandwidth, the lower the code phase estimation accuracy due to the reduced sharpness of the main correlation peak.

In order to improve the signal-to-noise ratio (SNR) conditions in which the GNSS estimators operate at post-correlation level (i.e., the equivalent SNR conditions observed) for the coarse

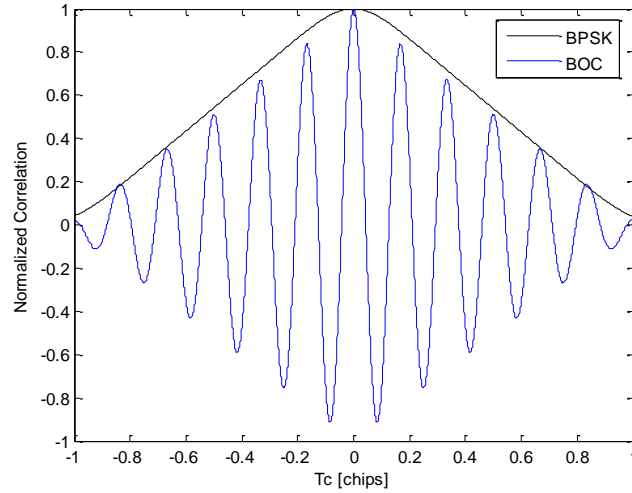


Fig. 2.3: Illustration of the cross-correlation function for BPSK and BOC signals.

or fine estimation of the GNSS signals' time delay and frequency offset (at acquisition or tracking level), longer integration times are typically considered when performing the correlation with the local code replicas. In particular in the acquisition of the GNSS signals, both coherent and non-coherent integrations may be considered to achieve a certain acquisition sensitivity linked to a given probability of detection and false alarm. Typically, the coherent integration time is limited by the data modulation of the GNSS signal (unless a pilot signal is available, or the data is wiped off), the receiver's clock quality, and the user's dynamics. After this point, non-coherent integrations (insensitive to the previous limitations) are used to further improve the SNR conditions, but at the cost of the so-called squaring losses (reducing the SNR gain introduced with respect to the coherent integration case). A good overview on this topic can be found in [Pan09]. It is to be noticed that, in this thesis, in many occasions results refer to certain SNR conditions instead of  $C/N_0$  conditions. The reason for this is that, in practice, the receiver's RF FE, the processing architecture and the integration time exploited is impacting the SNR conditions observed by the estimators. Thus, for equivalent  $C/N_0$  conditions at GNSS antenna or baseband level, different SNR conditions may be obtained at post-correlation level. Using as reference the SNR conditions at post-correlation level allows to unambiguously define the conditions in which the estimators are assessed, independently of the actual receiver architecture and integration time used. Moreover, when indicating  $C/N_0$  values in this thesis they will typically refer to the equivalent  $C/N_0$  values available at post-correlation level (i.e., independent of the implementation losses introduced by a specific receiver architecture).

The PRN code phase estimated by the tracking stage marks the so-called "fractional" pseudorange, defined within a PRN code length. This can be later translated into the pseudorange used in the positioning solution based on the time marks provided in the navigation

message modulated on the GNSS signals, e.g., the time of week (TOW); or by solving the transmission time as an additional unknown in the positioning problem (see [Dig09]). Once enough satellites are tracked and the corresponding pseudoranges are derived (at least 4 satellites are required for deriving 3D position and time, assuming the receiver is located on-ground), a position fix can be derived. After the first fix, the receiver may continue operating in continuous mode (as done in conventional receivers) or applying a certain duty-cycling in order to save power (i.e., being the receiver engine active only a portion of the time). In the former, both code- and carrier-based pseudoranges may be targeted to be exploited in the positioning solution, eventually using PPP and/or RTK carrier-based solutions for achieving a high-accuracy position estimation when precise products are made available to the receiver (see [San13] for an introduction to carrier-based positioning). In the latter, signal snapshots with a certain period and duty cycle are exploited to achieve the target position accuracy (typically, a lower accuracy than the continuous mode may be expected), while maintaining the power consumption as low as possible. In both cases, additional user sensors may be exploited to improve the accuracy and/or availability of the positioning solution. Also in both cases, the processing is typically performed locally in the GNSS chipset. An alternative to this is the application of the Cloud-GNSS processing approach [Luc16], [Gar17c], in which part of, or all, the GNSS processing is offloaded from the GNSS chipset to the Cloud (i.e., the signal snapshots can be processed directly in the Cloud). This might be of interest for the application of advanced signal processing techniques not feasible to be implemented in the GNSS chipset due to the high computational resources and/or power consumption required with respect to conventional techniques. Moreover, not only advanced assistance information may be available for exploitation in the Cloud (e.g., 3D maps, radio or magnetic fingerprint maps, etc.), but also the signal snapshots from receivers in nearby locations allowing the cooperative or collaborative processing for positioning purposes [Gar17c].

In practice, the processing architectures and techniques applied in GNSS receivers are highly dependent on the target application and use case, where different design drivers may apply. In some cases, achieving a high accuracy is the main target; in other cases, the driver is low power consumption, cost and size of the GNSS chipset, even if at the cost of degraded performance; some applications are targeting open-sky conditions, while others are operating in urban or indoor conditions; some receivers may be connected to a network, while others may not; and additional user sensors and/or signals or sources of opportunity may be used in the positioning solution. So, in reality, the general GNSS receiver operations introduced above should be considered only as illustrative of what may be happening in the receiver we are using.

Besides the receiver architecture and techniques exploited, and the signals used, a key factor impacting the achievable accuracy and availability of the positioning and timing solution is the channel propagation conditions. Indeed, GNSS systems are originally designed for their exploitation outdoors, where LOS signals are available with enough received power. This explains the amount of research performed by the GNSS and signal processing community for enabling the usage of GNSS signals in harsh conditions where the receiver has to be able to process very weak signals and deal with effects like blockage, fading and multipath.

## 2.2 GNSS in harsh propagation conditions

The exploitation of GNSS signals in harsh propagation conditions is very challenging, limiting the availability of the GNSS-based PNT solution, as well as the achievable accuracy. Multiple processing approaches and techniques have been proposed and studied in the literature to deal with the presence of fading and multipath conditions, as well as other interference conditions (see in particular [Pan09], [Bro11a], [Sah08], [Won12], [Clo07], [Clo08], [Clo09], [Axe11], [Bha17], [Sec05], and [Fer16]). In general, the modeling of the channel conditions can be very complex (in particular, in urban and indoor scenarios), and some of the techniques proposed may be highly sensitive to the signal models exploited in their derivation (making them work in controlled and/or mild conditions, but being potentially not applicable, or not robust, in realistic conditions). Indeed, some of the techniques broadly applied in practice in harsh propagation conditions (like narrow-correlators [Die92]) do not rely on highly complex signal models, being robust and relatively low-complexity solutions adaptable to different user and environment conditions. Nevertheless, there is still room for improvement of the GNSS-based solutions (or of the contribution of GNSS in the overall PNT solution, potentially based on different technologies/signals).

In urban and indoor conditions, effects like blockage, fading and multipath impact both the ability of the receiver to derive its position and the achievable accuracy of the PNT estimation for both standard and high-accuracy solutions. This results in position errors of up to tens or even hundreds of meters, and timing accuracies of hundreds of ns. Therefore, in practice, when targeting ubiquitous positioning in this type of scenarios, the GNSS receivers or the devices embedding them might rely on other sources and/or systems to be able to continuously derive the receiver's position in those harsh propagation conditions (in some cases, at the cost of a degraded performance).

In general, in harsh propagation conditions the signal received by the GNSS antenna from the  $M$  GNSS satellites in view can be modeled in a simplified way as

$$x(t) = \sum_{m=1}^M x_m^{LOS}(t) + \sum_{m=1}^M x_m^{NLOS}(t) + e(t), \quad (2.3)$$

where  $x_m^{LOS}(t)$  is the LOS contribution for the  $m$ -th satellite (i.e., the desirable GNSS signal component), and  $x_m^{NLOS}(t)$  embeds the contribution of the NLOS multipath components for the  $m$ -th satellite (i.e., the undesired GNSS signal components). In practice,  $x_m^{NLOS}$  may contain multiple components (from few specular components to diffuse multipath) [Sec12], [Ste03], [Hei08], [Jos14]. Moreover, it is to be noticed that in propagation conditions typical of indoor scenarios, the LOS signals can be highly degraded, or even missing, so NLOS propagation conditions may be dominant (i.e., the receiver operates in “NLOS conditions”).

Fig. 2.4 illustrates, in a simplified way, the propagation conditions in the case of an urban scenario, where both LOS and NLOS multipath components may be received by the GNSS receiver. Fig. 2.5 illustrates the impact of a harsh propagation channel on the cross-correlation function of a BPSK signal (the land mobile multipath channel in [ITU09] is considered) compared to the ideal case in absence of noise, and in the case of AWGN conditions. As can be observed, the cross-correlation function is distorted by the propagation channel, inducing a bias of its maximum. Thus, this would be translated in a bias of the code phase estimation performed based on this cross-correlation function.

The main limitation in terms of signal and position availability in a GNSS receiver is the low SNR (or C/No) conditions in which the GNSS receiver needs to operate to derive the synchronization parameters of the individual GNSS signals. In order to increase the observed SNR per satellite signal, longer coherent and non-coherent integration periods are typically considered in the literature, as discussed in the previous section, but receiver, environment and user constraints limit in practice the maximum integration periods that can be applied in commercial receivers. Additionally, open-loop architectures may be exploited, trying to perform a more stable estimation or tracking of the GNSS signals at low SNR conditions with respect to the conventional closed-loop architectures [Phe01]. Other receiver architectures have been proposed in the literature in order to make the estimation of the GNSS signals more robust. Some of those techniques are based on the application of vector tracking loops (VTL) [Las09]

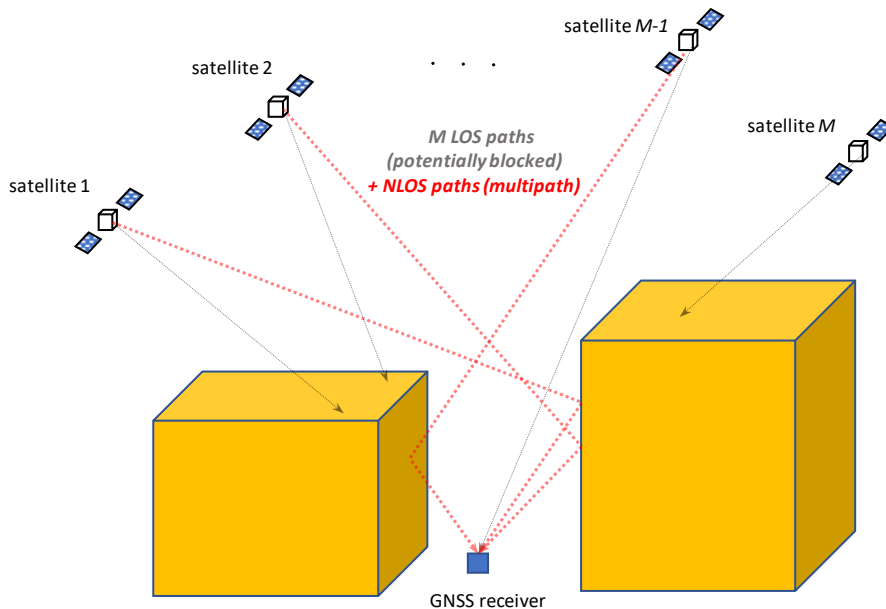


Fig. 2.4: Simplified illustration of the propagation conditions in an urban scenario (note that in reality several NLOS multipath components may be received).

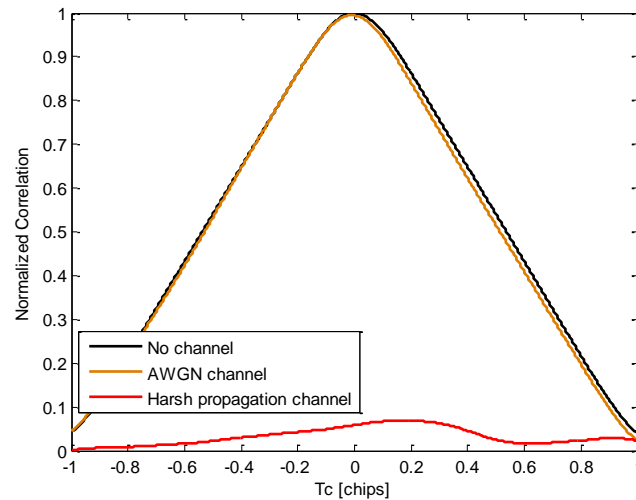


Fig. 2.5: Illustration of the impact of the propagation channel on the cross-correlation function (example for a BPSK signal).

in which the position estimation is exploited to assist or help the tracking loops of the receiver (in order to support the tracking of weak signals). Following a similar approach, collective detection and estimation, and direct position estimation approaches have also been proposed for the joint exploitation of the received GNSS signals in order to enable the operation at low SNR conditions (see [DiE07], [Clo07], [Clo09b], [Clo09a]).

In terms of accuracy, many research lines have targeted the mitigation of the multipath impact on the estimation or tracking of GNSS signals, including the estimation of the multipath components via maximum likelihood (ML) based solutions, like in [Sah08], or solutions based on the usage of Bayesian-like estimators, like in [Clo08]. In general, multipath estimation techniques are performing well in mild or controlled scenarios (e.g., open-sky scenarios, or controlled multipath conditions) but are actually not performing well in realistic conditions (where signals are buried in noise, multipath cannot be modeled with one or few components, and the channel conditions are rapidly changing in time). DPE solutions have also been proposed to mitigate, to some extent, the impact of multipath without the need to estimate it (see [Clo07], [Clo09b]). In practice, most of the current commercial receivers are based on narrow-correlators for achieving good accuracies and multipath rejection, being, so far, the most robust and simple technique for that purpose (see [Die92] and [Kap06] for details). Moreover, it is to be noticed that carrier-based positioning can be applied without the need to estimate the multipath in the mild propagation conditions in which some of the multipath estimation techniques available in the literature can perform well.

Additionally, array signal processing techniques have also been extensively proposed in the literature for the detection and mitigation of multipath and interference (see in particular [Sec05], [Fer06], [Fer09a], [Fer09b], [Clo09a], and [Fer16]). In general, state-of-the-art techniques have focused on mild propagation conditions where LOS signals are considered to be present, and the target is the mitigation (i.e., rejection) of other undesired multipath reflections and/or interference signals. Nevertheless, the exploitation of spatial diversity in realistic propagation conditions typical of urban and indoor conditions, where LOS signals can be highly degraded, or even missing, and NLOS propagation conditions may be dominant, has not been dealt with in detail in the GNSS literature. In these conditions, distinguishing between the desired and undesired components is far from being trivial due to the low C/No conditions and the important multipath reflections received from different directions of arrival (not anymore few specular components, but diffuse multipath, may be received). Fig. 2.6 illustrates an example of a system with a GNSS receiver featuring a uniform linear array with  $N$  antenna elements.

Another approach to take advantage of spatial diversity at reception level, in this case in a distributed way, is the application of cooperative and collaborative techniques exploiting the GNSS observables or signals from different receivers in nearby locations, together with the information about the distances between those receivers (see [Gare12a], [Gare12b], [Sol13], and [And18]). Fig. 2.7 illustrates the cooperative/collaborative positioning configuration for the case of three receivers. The distances or ranges between each pair of receivers or peers (i.e., the peer-to-peer ranges) can be obtained by exploiting different communication systems that may

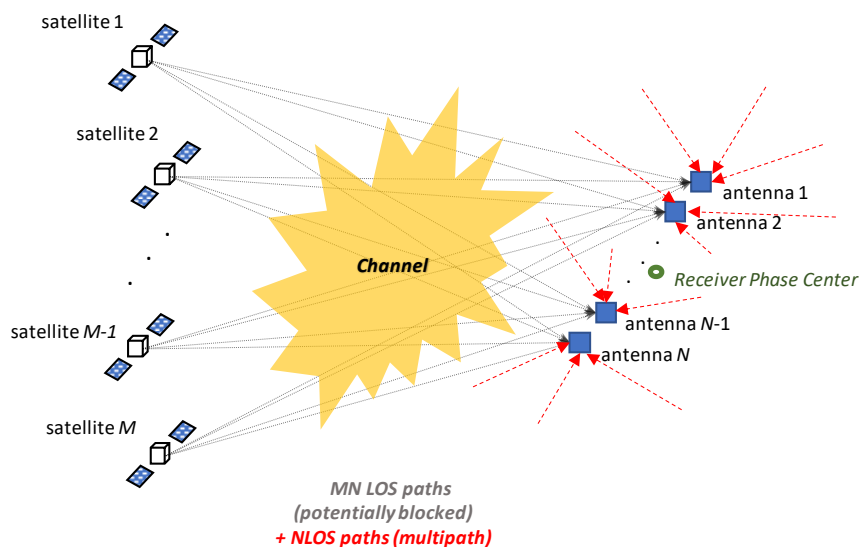


Fig. 2.6: Illustration of a system with a GNSS receiver featuring an array of antennas.

be available in the receivers (e.g., UWB-based and Wi-Fi RTT range estimation solutions [Guv18], [Au16]). Thus, collaborative positioning can be considered a hybrid positioning approach since different technologies are exploited. This has been shown to be an interesting approach for enabling the derivation of a PNT solution for receivers in highly degraded propagation conditions (for which otherwise it would be very difficult to achieve a position fix, or it would be achieved with a very poor performance), thanks to other receivers in nearby locations operating in better propagation conditions.

The usage of GNSS signals in harsh propagation conditions is challenging in general for any GNSS signal considered, but in particular for high-order BOC signals, as shown in [Gar16a], [Gar19b]. In this case, the cross-correlation function observed by the receiver presents multiple correlation peaks, so the receiver needs to resolve the ambiguity (i.e., identify the main peak of the cross-correlation function) such that the resulting pseudorange measurement is not biased (and no biases are present in the final position estimation). This task is in particular challenging for low SNR conditions (since the relative power between main and side peaks can be below 1 dB). Additionally, receiver front-end distortions can modify the actual cross-correlation function observed by the receiver, so some calibration and/or correction might be additionally needed in some cases.

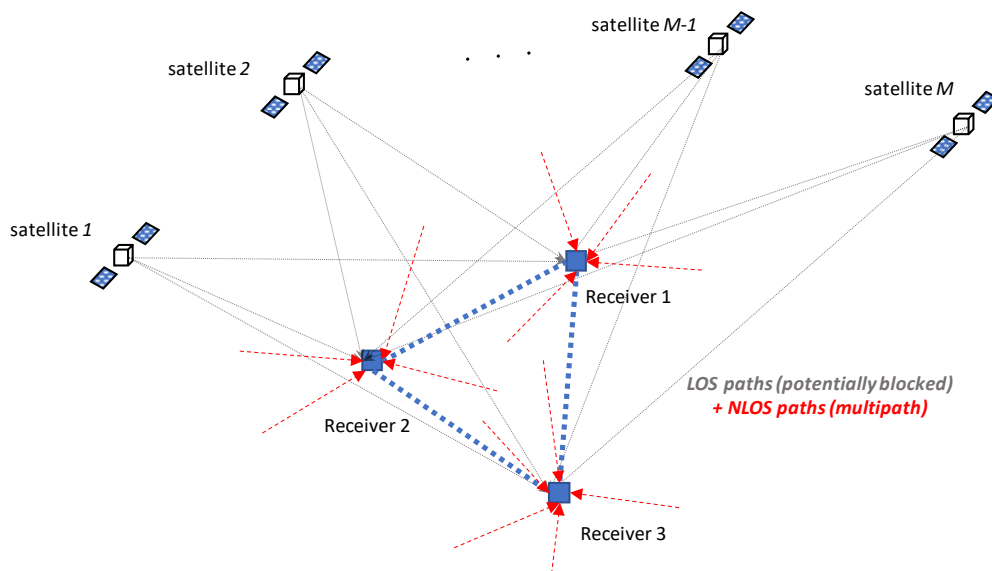


Fig. 2.7: Illustration of cooperative/collaborative positioning configuration.



# 3

## Unambiguous Positioning with High-Order BOC Signals

**T**HE unambiguous estimation of high-order BOC signals, and the later positioning based on these, remains an open problem in the literature. Although extensive research has been published on the topic, this is a very challenging problem when the receiver is operating in harsh propagation conditions where fading and multipath effects are dominant, resulting in potentially biased pseudorange and/or position estimations. The estimation techniques available in the literature are typically able to provide accurate and precise code-based estimations in mild propagation conditions. Nevertheless, these techniques start being unstable or not accurate (i.e., not applicable in practice) in propagation conditions typical of urban or indoor environments where it is difficult to identify correctly the main correlation peak out of the

multiple peaks of the cross-correlation function. This imposes an important limitation in the exploitation of this type of signals in harsh propagation environments.

This thesis proposes to overcome the limitations observed in state-of-the-art unambiguous estimation techniques based on two different estimation approaches. The first approach proposed operates at pseudorange or single-satellite level, and targets the robust unambiguous estimation of high-order BOC signals based on the solution of a double optimization problem exploiting a multi-correlator architecture (dubbed the DOME approach). The second approach proposed operates in the position domain, targeting an enhanced robustness with respect to techniques operating at single-satellite level (including the DOME approach). In this case, both single- and multiple-antenna configurations are considered (i.e., the unambiguous estimation in the MIMO-GNSS framework is considered), jointly exploiting the available spatial diversities in each case for improving the robustness of the unambiguous position solution based on high-order BOC signals.

This chapter is organized as follows. Section 3.1 discusses the background and motivation. Section 3.2 describes the DOME approach, the signal model exploited and the resulting estimators, and the simulation results obtained. Section 3.3 describes the unambiguous positioning in the MIMO-GNSS framework, the signal model exploited and the resulting estimators for single- and multiple-antenna configurations, and the corresponding simulation results. Finally, Section 3.4 presents the conclusions.

The material presented in this chapter has been published by the author in [Gar15a], [Gar15b], [Gar16a], [Gar17a], [Gar19a], and [Gar19b].

### 3.1 Background and motivation

The exploitation of BOC signals in GNSS enables the achievement of higher code-based pseudorange accuracies than legacy BPSK signals, at the cost of new correlation peaks appearing in the autocorrelation function. Therefore, there is a certain risk that the receiver estimates, or locks onto, a side peak of the cross-correlation function instead of the main peak, resulting in a bias in the pseudorange estimation and, consequently, in the estimated receiver's position when this happens. The probability to estimate, or lock onto, the wrong correlation peak (i.e., to have a “false lock”, as referred to throughout the thesis) can be in particular important when considering high-order BOC signals in harsh propagation conditions [Gar16a], [Gar19a]. In this case, main and side correlation peaks can have very similar powers and be only few meters away from each other, making the unambiguous estimation challenging due to the low C/No conditions during fading periods and to the additional impact of multipath.

The unambiguous estimation problem has been extensively discussed in the literature, resulting in the proposal of many different techniques and processing approaches to deal with

the ambiguity problem [Loh17]. Some of these techniques focus on getting rid of the ambiguity problem either by estimating and/or tracking the equivalent BPSK envelope of the BOC signal [Mar03], resulting in the non-exploitation of the original accuracy provided by the BOC signal structure; or by trying to cancel the side peaks of the BOC's cross-correlation function via the application of so-called un-matched filters [Kim07], which in practice results in a loss of the equivalent SNR observed at post-correlation level, in particular at low SNR conditions [Nav12]. Other techniques focus on solving the ambiguity problem by identifying the main peak out of the multiple peaks present in the cross-correlation function, preserving the original accuracy of the BOC signal, but resulting in a risk to lock onto a false lock. In this group, we can find techniques like the Bump Jumping [Fin99], the Double Estimator [Hod07], the Code-Subcarrier Smoothing [Nav13], or the Astrium Correlator [Sch13], just to name a few. In general, these techniques are well suited for mild propagation conditions typical of open-sky scenarios, but start having limitations or become unstable in urban scenarios where low  $C/N_0$  conditions (typically below around 30 dB-Hz) are experienced by the receiver [Gar14]. Indeed, it is important to highlight that just AWGN channel conditions, without the need of additional multipath components, are enough to trigger the appearance of false locks given the autocorrelation properties of the high-order BOC signals [Gar16a], [Gus16a].

The unambiguous estimation problem has also been proposed to be solved using the LAMBDA method [Wen14], tackling the problem as a carrier phase ambiguity one. In this case the ambiguity is solved at position level based on the code and subcarrier observables previously estimated for all the BOC signals being tracked. This approach has shown a higher robustness than other subcarrier-based tracking methods operating at pseudorange level when operating in the presence of multipath in nominal  $C/N_0$  conditions [Wen14]. Nevertheless, the robustness of the LAMBDA method in harsh propagation conditions has not been demonstrated in the literature.

In summary, most of the techniques available in the literature may not be applicable in practice in urban scenarios in which the receiver needs to operate at low  $C/N_0$  conditions and in the presence of multipath. The problem is even more challenging when moving to light-indoor or indoor conditions where NLOS propagation conditions may be dominant. Therefore, there is a need to derive robust estimators enabling the unambiguous exploitation of high-order BOC signals in harsh propagation conditions. This is of high interest in order to extend the operational region in which GNSS receivers can exploit in practice the high code-based accuracies provided by high-order BOC signals. For this purpose, this thesis discusses two different solutions, as introduced earlier: the DOME approach originally proposed in [Gar15a], [Gar15b] and [Gar16a], operating at single-satellite level (Section 3.2); and the unambiguous positioning based on the MIMO-GNSS approach originally proposed in [Gar19a], operating in the position domain (Section 3.3).

## 3.2 The DOME approach

Most of the current unambiguous estimation techniques are based on legacy GNSS receiver architectures exploiting few correlators (e.g., 5 correlators, including the so-called very-early and very-late correlators on top of the nominal early, prompt and late correlators) and a closed-loop tracking architecture. In order to overcome the problems encountered on the estimation of high-order BOC signals in harsh environments, a possible alternative approach is the usage of a multi-correlator architecture for the partial or complete sampling of the cross-correlation function and the application of open-loop estimation techniques allowing for the unambiguous estimation of high-order BOC signals even at low  $C/N_0$  conditions. A further knowledge of the cross-correlation function, including not only the main peak but also some or all the side peaks, may provide useful information for estimating the code delay unambiguously. This idea is already partially applied in techniques like Bump Jumping [Fin99], where a single sample of the secondary peaks of the cross-correlation function is used for detecting false locks. We can extend the estimation problem to the case in which multiple samples of the cross-correlation function (i.e., multiple cross-correlation samples) are available and the target is to perform an unbiased code delay estimation considering the full set of samples while maintaining the original BOC accuracy. This approach will allow to perform a direct recovery from a false lock beyond the secondary peaks in case more than two side peaks are observed.

A multi-correlator-based approach for the unambiguous estimation of high-order BOC signals is presented in this section. In particular, the ambiguity problem is proposed to be solved at post-correlation level via the solution of two parallel and dependent optimization problems in which multiple cross-correlation samples are exploited, as originally presented in [Gar15a], [Gar15b] and [Gar16a]. The proposed approach can be applied in both open- and closed-loop architectures, being therefore suitable for application in both snapshot-based and continuous-tracking-based GNSS receivers. This approach is dubbed the DOME (Double Optimization Multi-correlator-based Estimation) approach.

The two optimization problems considered are defined as follows. On the one hand, the first optimization problem targets the accurate and precise estimation of the code delay of the main correlation peak, for which, in general, a subset of the multiple cross-correlation samples available (e.g., the ones corresponding to the main correlation peak) are exploited in order to reduce the impact of noise and multipath on the estimation (i.e., resembling the narrow-correlator estimation approach [Die92]). This optimization problem is subject to a constraint (the unambiguous estimation of the main peak) which is defined based on the solution of the second optimization problem. On the other hand, the second optimization problem targets the identification of the main correlation peak (constraint imposed to the first optimization problem), for which, in general, the full set of cross-correlation samples available are exploited, covering not only the main correlation peak but two or more side peaks. The high-level description of the DOME approach is summarized in Fig. 3.1.

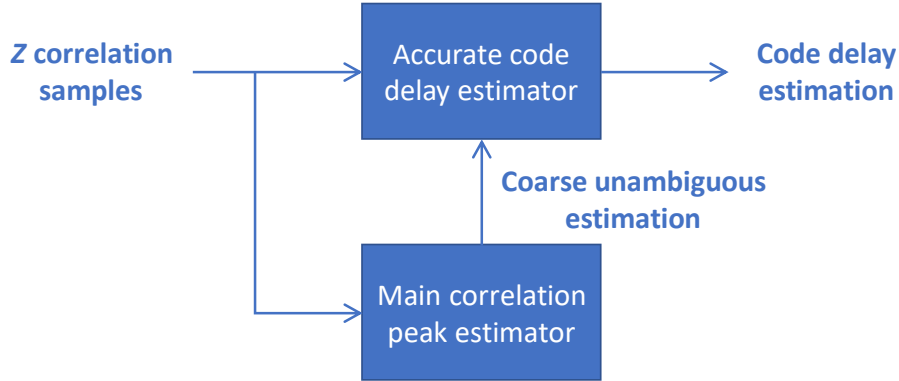


Fig. 3.1: High-level description of the DOME approach [Gar15a], [Gar15b], [Gar16a].

In the definition of the optimization problems used by the DOME approach, several integration periods may be considered in order to improve the SNR conditions in which the estimations are performed (i.e., the equivalent SNR conditions observed by the estimator), with the final target to operate in the linear region of the estimators. This is of interest in the first optimization problem of the DOME approach in order for the code delay estimator to attain the Cramér-Rao Lower Bound (CRLB) even at low  $C/N_0$  conditions. In this way, the variance of the estimations is reduced and, consequently, also the probability to lock onto a false lock during the tracking of the BOC signal in harsh propagation conditions. And it is of course also of interest in the second optimization of the DOME approach in order to maximize the probability to identify correctly the main peak out of the multiple peaks of the cross-correlation function.

In case important distortions are introduced in the cross-correlation function by the receiver (e.g., distortions induced by the RF front-end filtering stages), this may have an important impact on the ability to unambiguously track the BOC signals. In particular, the probability of false lock in this case may increase due to the introduced asymmetries in the cross-correlation function (e.g., increasing the relative power of some of the side peaks with respect to the main peak). In this case, a model of the expected cross-correlation function can be considered in the estimation problem in order to account for any filtering or *a priori* known distortion introduced by the receiver, targeting to mitigate the impact on the probability of false lock. The model of the expected cross-correlation function may also be of interest to make the approach applicable to any BOC signal or receiver configuration (e.g., in terms of the correlator spacing used). Nevertheless, this has the important drawback to increase the computational burden of the resulting solution.

In the following, Section 3.2.1 presents the signal model exploited, Section 3.2.2 presents the DOME approach, and Section 3.2.3 presents the simulation results obtained.

### 3.2.1 Signal model for the DOME approach

Let us consider a system consisting of a GNSS satellite transmitting a high-order BOC signal with a given PRN code which is then received by the antenna of a GNSS receiver. The PRN code is assumed to be known *a priori* by the receiver, and it is considered that the acquisition of the high-order BOC signal has been already performed and the receiver is in the tracking stage. A multi-correlator matched filter is applied by the GNSS receiver based on the coherent integration period corresponding to the time instant  $i$  for the generation of a sampled version of the cross-correlation function  $\hat{R}_{xb,i}(\tau)$  between the sampled versions of the received signal  $x(t)$  and the local signal replica  $b(t)$  around the code delay  $\hat{\tau}_c$  estimated by the tracking loop.

Let us define the complex vector  $\mathbf{r}_i \triangleq \mathbf{r}_i(\tau) \in \mathbb{C}^{Z \times 1}$  containing the set of  $Z = 2F + 1$  complex cross-correlation samples at the output of the multi-correlator matched filter for the time instant  $i$  as

$$\mathbf{r}_i = [r_{i,1} \ r_{i,2} \ \dots \ r_{i,Z}]^T, \quad (3.1)$$

with  $r_{i,z}$  the complex cross-correlation sample for the  $z$ -th correlator, which can be defined as [Gar17a]

$$r_{i,z} = \hat{R}_{xb,i}(\hat{\tau}_c - (F - z + 1)\delta), \quad (3.2)$$

where  $\delta$  is the correlator spacing used. In order to define a signal model for  $\mathbf{r}_i$ , let us define the expected cross-correlation vector  $\mathbf{s}(\tau) \in \mathbb{C}^{Z \times 1}$  for a given code delay  $\tau$  as

$$\mathbf{s}(\tau) = [s_1(\tau) \ \dots \ s_Z(\tau)]^T, \quad (3.3)$$

where the correlation samples are defined as

$$s_z(\tau) = R_f(\hat{\tau}_c - \tau - (F - z + 1)\delta), \quad (3.4)$$

with  $R_f(\rho)$  the reference filtered cross-correlation function (with  $\rho = 0$  corresponding to the expected maximum of the main lobe of the cross-correlation function for the high-order BOC signal), which includes the impact introduced by the GNSS receiver's RF front-end.

It is to be noticed that the correlation samples observed by the receiver are impacted by the multipath and noise components, as well as other interference components that might be present in the scenario in which the receiver operates. Therefore, in general we can model the complex cross-correlation vector as

$$\mathbf{r}_i = \sum_{d=0}^D a_{i,d} \mathbf{s}(\tau_{i,d}) + \mathbf{e}_i, \quad (3.5)$$

where the  $0$ -th component in the summation models the LOS signal,  $D$  is the number of multipath rays present during the coherent integration time,  $a_{i,d}$  and  $\tau_{i,d}$  are the complex amplitude and delay at time instant  $i$  of the  $d$ -th multipath ray, respectively, and  $\mathbf{e}_i \in \mathbb{C}^{Z \times 1}$  is a complex colored Gaussian noise vector with covariance matrix  $\mathbf{C}$ , i.e.,  $\mathbf{e}_i \sim \mathcal{CN}(\mathbf{0}, \mathbf{C})$ .

In the following, the knowledge and, therefore, the estimation, of the multipath rays is not considered in the problem since multipath estimation in realistic harsh propagation conditions is a difficult problem still open in the literature. This is mainly due to the difficulties to model the multipath with a set of specular rays (in the best case, the number of specular rays and their properties are still unknown), and to the fact that multipath components are typically buried in noise (making very challenging, or unfeasible, to distinguish between LOS, multipath and noise components). The focus, therefore, is on the unambiguous tracking of the LOS signal delay (i.e., the tracking of the main correlation peak) without considering the multipath rays in the signal model (resulting eventually in a biased estimation due to multipath). Based on this, we can model the cross-correlation vector  $\mathbf{r}_i$  as

$$\mathbf{r}_i \approx a_i \mathbf{s}(\tau_i) + \mathbf{e}_i, \quad (3.6)$$

where  $a_i$  and  $\tau_i$  are the complex amplitude and delay of the LOS signal for time instant  $i$ . Taking into account that under this assumption  $\mathbf{r}_i \sim \mathcal{CN}(a_i \mathbf{s}(\tau_i), \mathbf{C})$ , the complex multivariate probability density function (PDF) of  $\mathbf{r}_i$  with  $a_i$  and  $\tau_i$  as parameters can be defined as

$$p(\mathbf{r}_i; \tau_i, a_i) = \frac{1}{\pi^K \det(\mathbf{C})} \exp[-(\mathbf{r}_i - a_i \mathbf{s}(\tau_i))^H \mathbf{C}^{-1} (\mathbf{r}_i - a_i \mathbf{s}(\tau_i))]. \quad (3.7)$$

### 3.2.2 Dual-optimization multi-correlator-based estimators

Let us start considering the case in which the cross-correlation function  $\hat{R}_{xb,i}(\tau)$  is a symmetric filtered version of the ideal autocorrelation function, such that no distortions or asymmetries are introduced in the cross-correlation function by the receiver RF front-end. Moreover, the correlator spacing  $\delta$  used in the generation of the cross-correlation vector  $\mathbf{r}_i$  is such that the main peak can be identified with a residual impact of the correlation sampling process. Under these assumptions, the maximum likelihood estimator (MLE) of  $\tau_i$  corresponds to the delay that maximizes the cross-correlation function, such that it can be derived as  $\hat{\tau}_i = \hat{\tau}_c - (F - \hat{z}_i + 1)\delta$ , where

$$\hat{z}_i = \arg \max_z |[\mathbf{r}_i]_z|, \quad (3.8)$$

with  $z = \{1, \dots, Z\}$ . In the case  $Z$  and  $\delta$  are such that  $\mathbf{r}_i$  allows to sample the complete cross-correlation function (i.e., the main and side peaks of the high-order BOC signal), the estimator in (3.8) allows us to directly derive an unambiguous estimation of the code delay. Nevertheless, it is to be noticed that the accuracy of the code delay obtained in (3.8) is limited by  $\delta$ . Therefore, a refinement process is needed in order to fully exploit the accuracy provided by the high-order BOC signal. This may be done in different ways. One option is to perform a fine estimation, equivalent to the fine acquisition typically done in snapshot receivers [Sec12]. For doing this, we can exploit the signal model defined for  $\mathbf{r}_i$ , in which a model of the expected cross-correlation function  $\mathbf{s}(\tau)$  is considered. This allows us not to be limited by the correlator spacing. In this case, the MLE at post-correlation level (i.e., based on  $\mathbf{r}_i$  and  $\mathbf{s}(\tau)$ ) is found by minimizing the cost function [Gar15a]

$$\Lambda_i(\tau_i, a_i) = (\mathbf{r}_i - a_i \mathbf{s}(\tau_i))^H \mathbf{C}^{-1} (\mathbf{r}_i - a_i \mathbf{s}(\tau_i)). \quad (3.9)$$

Another alternative is to apply a standard code tracking loop based on a DLL with a discriminator exploiting the 3 correlators around the main correlation peak. In this case, the usage of a narrow-correlator will allow us to fully exploit the accuracy of the high-order BOC signal, attaining the CRLB for nominal-to-high C/No conditions (at least, in ideal AWGN channel conditions).

In order to derive an unambiguous code estimation, while fully exploiting the code accuracy of high-order BOC signals, we may apply a dual-optimization or dual-estimation approach. In this configuration, one of the estimators is in charge of resolving the code ambiguity (i.e., estimate the main correlation peak out of the multiple peaks in the cross-correlation function),

for which in general the exploitation of the  $Z$  correlation samples available are of interest; and the other estimator is in charge of performing a fine estimation of the main peak, for which in general the exploitation of the correlation samples of the main correlation peak are of interest for mitigating the impact of noise and multipath. Additionally, in order to allow a robust unambiguous estimation, we may exploit several integration periods, targeting the operation of the estimators in their linear region. Thus, in the following it is considered that a set of the last  $R$  complex cross-correlation vectors from instant  $i - R + 1$  to instant  $i$  are available, i.e.,  $\{\mathbf{r}_{i-j}\}_{j=0}^{R-1} = \{\mathbf{r}_i, \dots, \mathbf{r}_{i-R+1}\}$ . Based on this, we can define the unambiguous code delay estimation  $\hat{\tau}_i$  (i.e., a code delay estimation based on the main correlation peak of the BOC's cross-correlation function) at time instant  $i$  as the solution of the non-linear minimization problem subject to a constraint [Gar15a]

$$\begin{aligned} \hat{\tau}_i = \arg \min_{\tau} \sum_{j=0}^{Q-1} (\mathbf{r}_{i-j} - \hat{a}_{i-j,1} \mathbf{s}(\tau))^H (\mathbf{W}_1 \mathbf{C}^{-l}) (\mathbf{r}_{i-j} - \hat{a}_{i-j,1} \mathbf{s}(\tau)) \\ \text{s.t. } |\tau - \hat{\tau}_{ref_i}| < \theta, \end{aligned} \quad (3.10)$$

where  $\theta$  is a design parameter –which is BOC modulation dependent– defining the maximum allowed difference between the estimated code delay  $\hat{\tau}_i$  and a reference estimation  $\hat{\tau}_{ref_i} = \hat{\tau}_c - (F - \hat{z}_{ref_i} + 1)\delta$ , where  $\hat{z}_{ref_i}$  is defined as the solution of the maximization problem

$$\begin{aligned} \hat{z}_{ref_i} = \arg \max_z \sum_{j=0}^{P-1} |[\mathbf{r}_{i-j}]_z| \\ \text{s.t. } 1 + \lfloor (Z - Z_t)/2 \rfloor \leq z \leq Z - \lfloor (Z - Z_t)/2 \rfloor, \end{aligned} \quad (3.11)$$

with  $Z_t \leq Z$ . The estimators in (3.10) and (3.11) are a possible implementation of the first and second optimization problems in the DOME approach, respectively. In the following, the estimator (3.11) is referred to as the maximum correlation estimator (MCE). It is to be noticed that the exploitation of several integration periods in (3.10) is performed via the summation of several cost functions (defined based on the MLE approach), instead of applying the typical non-coherent (or differential) integrations directly to the set of complex cross-correlation vectors  $\{\mathbf{r}_{i-j}\}_{j=0}^{Q-1}$ . This approach is followed in order to be able to apply the MLE as baseline since the complex multivariate PDF of the non-coherent integrations of  $\{\mathbf{r}_{i-j}\}_{j=0}^{Q-1}$  does not follow anymore a Gaussian distribution. Nevertheless, this results in a high computational

burden, so alternative approaches may be exploited in practice (e.g., applying the non-coherent integrations to the complex correlation vectors before the cost function is generated).

The estimators in (3.10) and (3.11) are defined in an open and flexible way via the usage of the selection matrix  $\mathbf{W}_1$  and  $Z_t$ . This allows for the selection of the number of correlation samples to be considered in both optimization problems and to be able to choose between the exploitation or not of the covariance matrix  $\mathbf{C}$ . The definition of the covariance matrix  $\mathbf{C}$ , the selection matrix  $\mathbf{W}_1$  and  $Z_t$ , the complex amplitudes  $\hat{a}_{i-j,1}$ , and the number of integration periods  $Q$  and  $P$  used in (3.10) and (3.11), respectively, are discussed in the following paragraphs.

The covariance matrix  $\mathbf{C}$  of the complex colored noise present at post-correlation level is defined as a  $Z \times Z$  non-diagonal matrix and it depends on the BOC signal to be tracked. Therefore, in practice it is not needed to be computed since the expected value is known *a priori*. The selection matrix  $\mathbf{W}_1$  will be in general defined such that a subset of the  $Z$  available samples are in practice exploited in the minimization problem; while  $Z_t$  will be in general equal to  $Z$  in order to exploit all the available samples of the cross-correlation function. It is to be noticed that  $\mathbf{W}_1$  can be defined as a  $Z \times Z$  diagonal positive definite matrix (used as weighting matrix), although it could be defined in any other different way, e.g., as  $\mathbf{W}_1 = \mathbf{A}_1 \mathbf{C}$ , with  $\mathbf{A}_1$  an  $Z \times Z$  diagonal positive definite weighting matrix, resulting in  $\mathbf{W}_1 \mathbf{C}^{-1} = \mathbf{A}_1 \mathbf{C} \mathbf{C}^{-1} = \mathbf{A}_1$ , being therefore in this case the minimization in (3.10) not dependent on  $\mathbf{C}$  (thus, following a non-linear least squares approach). Taking into account that the noise component in the cross-correlation function is correlated and overlapped in the frequency domain with the BOC signal component (which is a normal consequence of the matched filter applied in the correlation and dump process typically applied by the receiver), the exploitation of the covariance matrix will not bring the noise filtering benefits that would be obtained in the case in which noise and signal components follow different covariance matrices (i.e., are not overlapped in the frequency domain). Therefore, the main benefit of the implementation of the DOME approach based on the estimators in (3.10) and (3.11) is to enable the adaptation of the number of correlators used and of the integration periods exploited to make each of the estimators work in its linear region.

The complex amplitudes  $\hat{a}_{i-j,1}$  for every summand  $j$  (corresponding to the coherent integration performed for time instant  $i - j$ ) in the minimization problem in (3.10) can be estimated following the well-known least squares (LS) solution [Kay13]

$$\hat{a}_{i-j,1} = (\mathbf{s}^T(\tau)(\mathbf{W}_1 \mathbf{C}^{-1})\mathbf{s}(\tau))^{-1} \mathbf{s}^T(\tau)(\mathbf{W}_1 \mathbf{C}^{-1})\mathbf{r}_{i-j}. \quad (3.12)$$

$Q$  and  $P$  are integer numbers defining the number of integration periods that are considered in the minimization problems in (3.10) and (3.11), respectively, in order to increase the unambiguous estimation sensitivity (note  $Q, P \leq R$ ). It has to be noticed that this process is analogous to the non-coherent integration typically performed in GNSS receivers operating in

harsh propagation conditions.  $Q$  and  $P$  can be defined adaptively depending on the propagation environment under which the code tracking is performed. In general,  $Q$  will be set such that the estimator of the code delay based on the main correlation peak attains the CRLB (i.e., the code delay estimator works in its linear region) while minimizing the response time to the signal dynamics. This way, a good definition of  $Q$  will minimize the probability of false locks during tracking conditions. And  $P$  will be set such that the unambiguous identification of the main peak can be performed with a given probability of false lock, while minimizing the time to detect eventual false locks. It is to be noticed that for high-order BOC signals the equivalent integration period required might be in the order of one second to keep the false detection probability low at low C/No conditions (i.e., below around 30 dB-Hz). And for very low C/No conditions (i.e., below around 20 dB-Hz) low false detection probabilities might be difficult to be maintained, being therefore of interest to disable the false lock detection/correction until better C/No conditions are achieved.

The DOME approach is compatible with both open- and closed-loop receiver architectures. In the former, the estimator can be applied per signal snapshot to provide the current unambiguous code delay estimation, being therefore applicable in snapshot-based receivers or in the fine acquisition stage of typical continuous-tracking receivers. In the latter, it can be used as a non-coherent discriminator, providing the code phase error based on the set of  $Z$  samples available, or just as detector and corrector of eventual false locks, working then in parallel to the closed tracking loop. In both cases an additional low-pass filter can be applied to the code delay estimation in (3.10) in order to decrease the code estimation variance. And, as for any typical GNSS receiver, carrier phase and/or frequency estimations can be considered as aiding in the tracking of the user dynamics, which will allow for a higher flexibility in the definition of  $Q$  in the first optimization problem of the DOME approach.

It is to be noticed that a closed form expression cannot be found for the proposed estimator in (3.10). Therefore, the optimization problem has to be solved iteratively (e.g., following the Newton-Raphson method) or via the application of grid-search approaches [Kay13]. In order to reduce the computation burden, a possible implementation of the DOME approach can be based on the usage of a typical DLL-based receiver architecture. In this case, a narrow-correlator DLL can be used to replace the estimator in (3.10), which is then “aided” by an open-loop estimator implementing (3.11), in charge of identifying the correct peak. This approach, depicted in Fig. 3.2, allows the straightforward implementation in state-of-the-art closed-loop-based receivers.

Let us consider now the case in which the cross-correlation function  $\hat{R}_{xb,i}(\tau)$  is impacted by the RF front-end filtering stage, such that it is not anymore symmetric, being the original relative power of the side peaks with respect to that of the main peak altered. This may result in an important impact on the ability to identify the main peak of the cross-correlation function, and, thus, in a degraded probability of false lock. In order to tackle this issue, one possible solution is to exploit the model of the expected cross-correlation function  $\mathbf{s}(\tau)$  in the second optimization problem of the DOME approach in order to account for *a priori* known distortions introduced by the receiver. This, of course, has the important drawback to increase the

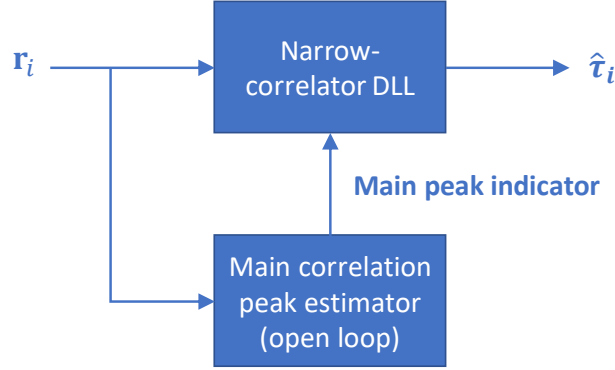


Fig. 3.2: Application of the DOME concept to a DLL-based architecture [Gar15a], [Gar15b], [Gar16a].

computational burden of the resulting solution. In this case the reference code delay marking the main correlation peak can be defined as [Gar15a]

$$\hat{\tau}_{ref_i} = \arg \min_{\tau} \sum_{j=0}^{P-1} (\mathbf{r}_{i-j} - \hat{\mathbf{a}}_{i-j,2} \mathbf{s}(\tau))^H (\mathbf{W}_2 \mathbf{C}^{-1}) (\mathbf{r}_{i-j} - \hat{\mathbf{a}}_{i-j,2} \mathbf{s}(\tau)), \quad (3.13)$$

where  $\mathbf{W}_2$  and  $\hat{\mathbf{a}}_{i-j,2}$  are defined similarly to  $\mathbf{W}_1$  and  $\hat{\mathbf{a}}_{i-j,1}$ , but in this case  $\mathbf{W}_2$  is such that, in general, the  $Z$  samples of the cross-correlation vector will be exploited to identify the main correlation peak out of the multiple side correlation peaks. In the following, the estimator (3.13) is referred to as the post-correlation MLE (PC-MLE).

### 3.2.3 Simulation results

The DOME approach has been implemented in a baseband software receiver in order to assess its performance via simulation in both controlled and realistic scenarios when tracking high-order BOC signals, as originally presented in [Gar15a], [Gar15b] and [Gar16a]. A  $\text{BOC}_{\cos}(15, 2.5)$  signal is considered herein as a representative case of high-order BOC signal. The DOME configuration used for the derivation of the performance results presented in the following subsections is summarized in Table 3.1.

As discussed in the previous section, the variance of the code delay estimation is driven by the first optimization problem of the DOME approach, defined in (3.10). The performance of

| Parameter                 | Value                        |
|---------------------------|------------------------------|
| Modulation                | BOC <sub>cos</sub> (15, 2.5) |
| Receiver bandwidth        | 40 MHz                       |
| Coherent integration time | 10 ms                        |
| Correlator spacing        | 0.031 chips                  |
| $Z$                       | 33                           |
| $Q, P$                    | Variable                     |
| $\mathbf{W}_m$            | Variable                     |
| Low-pass filter bandwidth | 1 Hz                         |

Table 3.1. Simulation configuration for the DOME approach [Gar15a], [Gar15b], [Gar16a].

the code delay estimation in AWGN conditions has been assessed when the number of integrations periods considered is  $Q = 10$ , three correlation samples are effectively exploited (via the matrix  $\mathbf{W}_1$ ), and a low-pass filter with a bandwidth of 1 Hz is used in order to smooth the estimations. Additionally,  $\mathbf{W}_1$  is such that the noise covariance matrix  $\mathbf{C}$  is in practice not exploited in the estimation. As expected, and based on the fact that (3.10) is a non-coherent estimator using the ML approach as baseline, the variance of the code delay estimation in AWGN conditions attains the CRLB (derived based on [Wei03]) when the equivalent SNR observed by the estimator is relatively high (equivalent to post-correlation C/No values above around 25 dB-Hz when considering the configuration in Table 3.1 for  $Q = 10$ ), while for low equivalent SNRs the variance is notably higher than the CRLB. This can be observed in the code delay error ( $1\sigma$ ) depicted in Fig. 3.3, where the  $\sqrt{\text{CRLB}}$  is included for comparison, and the SNR per coherent integration period is indicated (note that a processing gain of up to 10 dB is introduced for  $Q = 10$ ). Moreover, it is important to remark that the usage of  $Q > 1$  is of interest in order to make the estimator work in its linear region at low SNR conditions per coherent integration period, reducing also in this way the probability to go to a false lock during tracking conditions.

The ability to identify the main correlation peak for ensuring the unambiguous code delay estimation of high-order BOC signals is driven by the second optimization problem in the DOME approach. The target in this case is to allow for a low probability of false lock (i.e., a low probability to have a biased pseudorange estimation). This can be in particular challenging for low C/No conditions (for which the equivalent SNRs observed by the estimators are low). Assuming that the receiver is in tracking conditions and no distortions are introduced in the cross-correlation function by the filtering stage, Fig. 3.4 shows the probability of false lock in AWGN conditions for the MCE estimator in (3.11) with  $P$  equal to 1, 10 and 100, and the configuration in Table 3.1 (note that the full set of correlation samples available are exploited, corresponding to half of the correlation span, i.e.,  $\pm 0.5$  chips). The impact of the number of integration periods  $P$  exploited can be clearly observed in the results, enabling to improve the equivalent SNR conditions observed by the estimator. For  $P = 10$ , the MCE estimator shows a

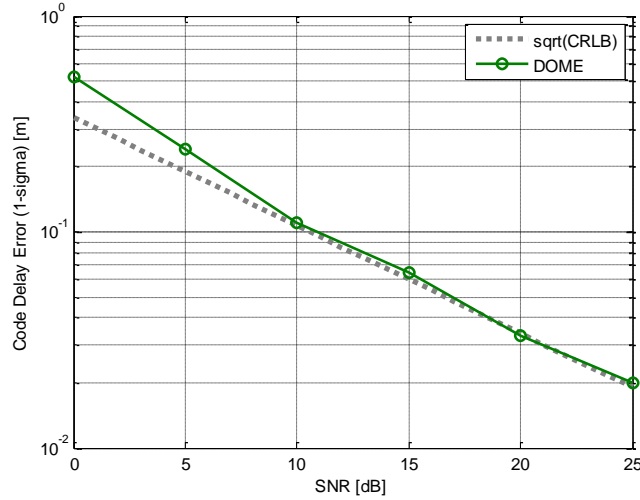


Fig. 3.3: Code delay error ( $1\sigma$ ) in AWGN conditions for a  $\text{BOC}_{\cos}(15, 2.5)$  and the receiver configuration in Table 3.1 for  $Q = 10$ . Note that the SNR per coherent integration period is indicated [Gar15b], [Gar16a].

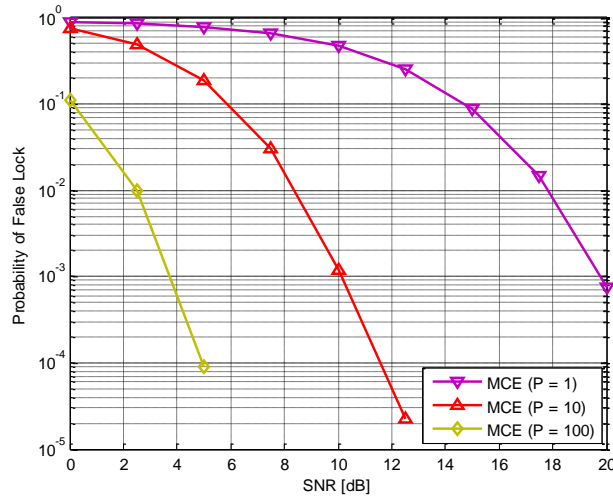


Fig. 3.4: Probability of false lock in AWGN conditions when considering the MCE estimator in tracking conditions and the receiver configuration in Table 3.1 for  $P$  equal to 1, 10 and 100. Note that the SNR per coherent integration period is indicated [Gar16a].

probability of false lock below  $10^{-3}$  for SNR values per coherent integration period above around 10 dB. This is equivalent to a probability of false lock below around  $10^{-3}$  for post-correlation

$C/N_0$  values (not considering implementation losses) above around 30 dB-Hz. Even when using  $P = 100$  (equivalent to a total integration period of 1 second), achieving a relative low probability of false lock down to 20 dB-Hz is still challenging (indeed, this is considered the lowest  $C/N_0$  conditions that can be achieved with reasonable integration periods). It is to be noticed that the MCE estimator is equivalent to the MLE when considering the application of a perfect match filter in the correlation process. Therefore, in this case the application of (3.11) in the DOME approach is of interest, being both desirable in terms of computational burden and probability of false lock achieved.

The unambiguous estimation can be also challenging when certain correlation spacings are used by the receiver and no previous code delay estimations have been performed (e.g., when performing a single snapshot processing or, equivalently, when performing a fine estimation of the code delay in the acquisition stage of high-order BOC signals). In order to illustrate this, Fig. 3.5 shows the probability of false lock obtained when the DOME approach is applied to the processing of signal snapshots (with several coherent integration periods within each signal snapshot), and considering two different estimators for resolving the ambiguity (second optimization problem in the DOME approach): the MCE estimator, and the PC-MLE estimator defined in (3.13). For the PC-MLE estimator,  $\mathbf{W}_2$  in (3.13) is such that the noise covariance matrix  $\mathbf{C}$  is in practice not exploited in the estimation (therefore, showing the benefit introduced by the usage of the expected cross-correlation function). In both cases, ten integration periods are considered in order to improve the equivalent SNR conditions observed by the estimators (i.e.,  $P = 10$ ) and the full set of correlation samples available are exploited in the estimations (i.e.,  $Z = 33$ ).

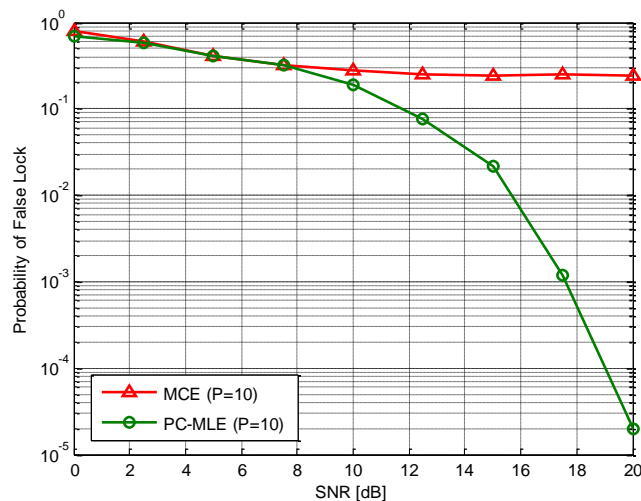


Fig. 3.5: Probability of false lock in AWGN conditions when considering a signal snapshot processing for the receiver configuration in Table 3.1 and  $P = 10$  for the MCE and PC-MLE estimators. Note that the SNR per coherent integration period is indicated [Gar15b], [Gar16a].

As can be observed in Fig. 3.5, when the expected cross-correlation function is exploited in the problem (PC-MLE), the probability of false lock decreases for higher SNR conditions, as expected. Nevertheless, when the maximum of the correlation samples is used to identify the main peak (MCE), there is a saturation effect, resulting in high probabilities of false lock even for high SNR conditions. Indeed, the limiting factor in this case is the correlator spacing used by the receiver in the processing of a signal snapshot when no *a priori* information about the expected position of the main peak is considered. The reason for this saturation of the probability of false lock comes from the fact that, in some cases, independently of the SNR conditions, the main peak of the cross-correlation function cannot be properly sampled (even for relatively low correlator spacing values in terms of code tracking), inducing that the maximum of the received correlation samples corresponds to a side peak. This “distortion” effect of the sampled cross-correlation function that the receiver observes is illustrated in Fig. 3.6. It is to be noticed that the correlator spacing considered in the simulation presented is such that an optimum fine code delay estimation can be obtained (i.e., representative narrow-correlator spacing values are used). The results shown demonstrate the benefit, in terms of performance, of exploiting the expected cross-correlation function in (3.13) under the conditions considered in this simulation. Nevertheless, it is important to remark that the application of the PC-MLE instead of the MCE introduces an important computational burden. Moreover, comparing the results in Fig. 3.4 and 3.5, the best performance is obtained by the MCE estimator in tracking conditions (i.e., when no sampling resolution issues are observed). A possible way to get rid of this sampling resolution issue in snapshot processing mode is the usage of lower correlator spacing values, at the cost of a higher number of correlators needed to cover the same number of correlation peaks (see [Gus16b]).

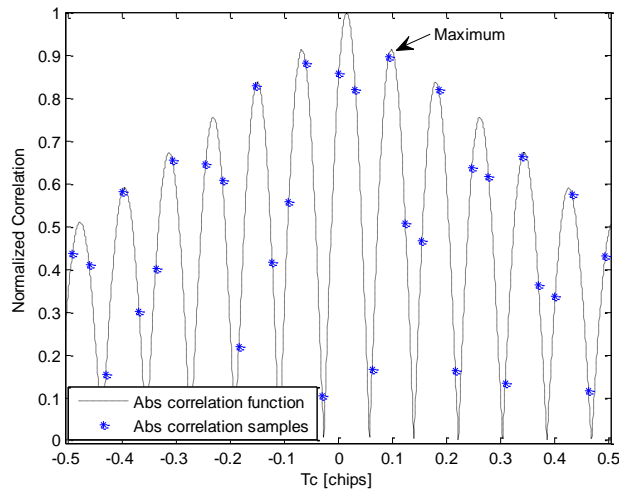


Fig. 3.6: Illustration of the sampling impact when processing a signal snapshot and no *a priori* information about the expected position of the main correlation peak is considered [Gar16a].

In order to illustrate how the DOME approach behaves in case of a false lock for nominal and low  $C/N_0$  conditions, a controlled scenario is used, inducing the tracking of the secondary peak of a  $\text{BOC}_{\cos}(15, 2.5)$  signal, which is at around 10 m from the main peak. In this controlled scenario (an illustration of this controlled scenario can be found in [Nav14]), at instant  $t = 0$  s the LOS signal is highly attenuated (-30 dB) and a strong multipath ray appears. The delay of this multipath ray increases linearly from 0 to around 10 m (achieved at  $t = 5$  s, inducing this equivalent bias in the code delay tracking). Immediately after, the LOS signal is back to nominal power conditions and the multipath ray disappears. At this point the secondary peak is being tracked. From then on, the DOME approach is used to detect and recover from the false lock. Fig. 3.7 shows an example of the DOME results obtained for the controlled scenario when the post-correlation  $C/N_0$  considered is 40 and 20 dB-Hz (representative of nominal and low  $C/N_0$  conditions, respectively – and equivalent to SNR values per coherent integration period of 20 and 0 dB for the configuration in Table 3.1). In this case,  $\mathbf{W}_1$  is such that three correlation samples are used in the fine estimation and the noise covariance matrix  $\mathbf{C}$  is in practice not exploited, and  $Q = 10$ . The PC-MLE estimator is used and  $\mathbf{W}_2$  is defined as an identity matrix. As can be observed, the DOME is able to detect and correct the false lock successfully even at low  $C/N_0$  conditions. For  $C/N_0$  conditions below around 20 dB-Hz it is in practice very difficult to keep a relatively low probability of false lock for reasonable integration periods, as shown earlier. It is to be noticed that the time to detect and correct the false lock (i.e., the latency of the ambiguity resolution) depends on the  $P$  parameter used in the second optimization problem, whose selection is a design trade-off between the probability of false lock to be achieved and the latency to detect and correct eventual false locks. In the example shown,  $P$  is set to 10 and

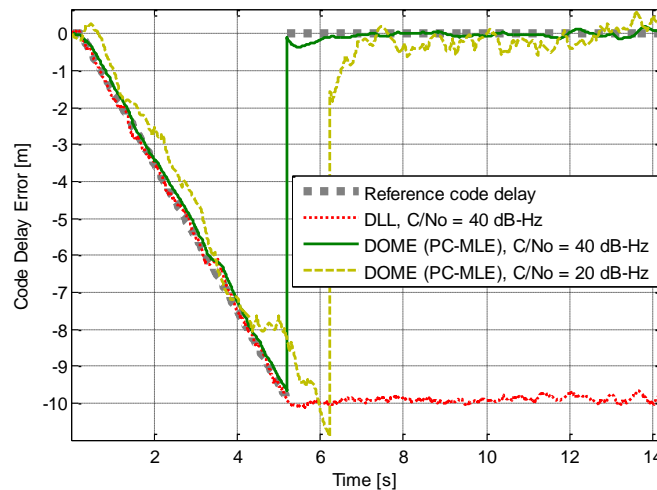


Fig. 3.7: Comparison of the code delay estimation error for a  $\text{BOC}_{\cos}(15, 2.5)$  signal in a controlled scenario in which the false lock is induced for different  $C/N_0$  conditions [Gar15a], [Gar15b], [Gar16a].

100 when the simulated  $C/N_0$  is 40 and 20 dB-Hz, respectively, which explains the different latencies in the correction of the false lock. It is to be noticed that in the configurations presented the false lock probability achieved will not be the same.  $P$  is actually limited to 100 in order to consider realistic integration periods in the simulation (equivalent to a total integration period of 1 s), although higher values would be in practice needed to ensure a relatively low probability of false lock. The code delay error obtained for a typical DLL (without any false detection engine being implemented) is included for completeness, showing a code delay bias of around 10 m that remains until the end of the simulation (as expected). Results in similar simulation conditions for state-of-the-art techniques can be found in [Gar14], where it can be observed that the assessed techniques (including Bump Jumping [Fin99], Double Estimator [Hod07], and Code-Subcarrier Smoothing [Nav13]) start being unstable at 30 dB-Hz.

The ITU-R P.681-7 land mobile multipath channel [ITU09] is considered for the assessment of the DOME approach in realistic propagation conditions typical of an urban environment. In particular, a scenario in which a vehicular user is tracking a satellite at low elevation in the presence of some fading events is considered as example of harsh propagation conditions. Fig. 3.8 shows the channel fading conditions for the simulation period discussed in the following. Note that a nominal SNR of 10 dB per coherent integration period for the LOS signal has been simulated (equivalent to a post-correlation  $C/N_0$  of 30 dB-Hz), therefore being the actual  $C/N_0$  observed by the estimators below 15-20 dB-Hz for some instants. Fig. 3.9 shows the code tracking error results obtained for the DOME in the simulated scenario. In this case the DOME is configured with  $Q = 10$ ,  $P = 100$ , and  $\mathbf{W}_1$  is such that three correlation samples are used in

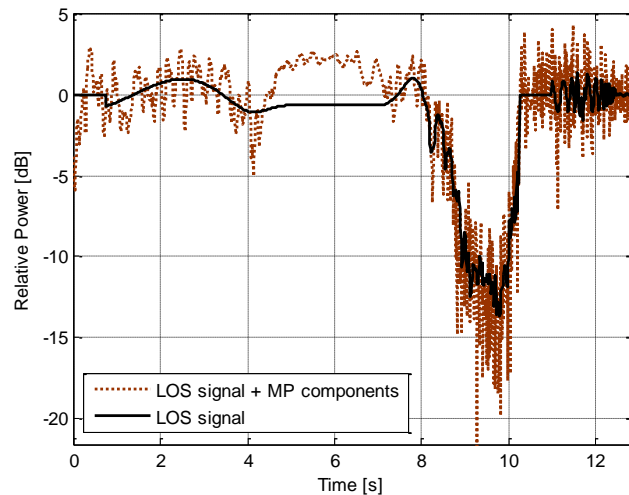


Fig. 3.8: Example of fading conditions in an urban environment realisation as simulated with the ITU-R P.681-7 land mobile multipath channel [Gar15b], [Gar16a].

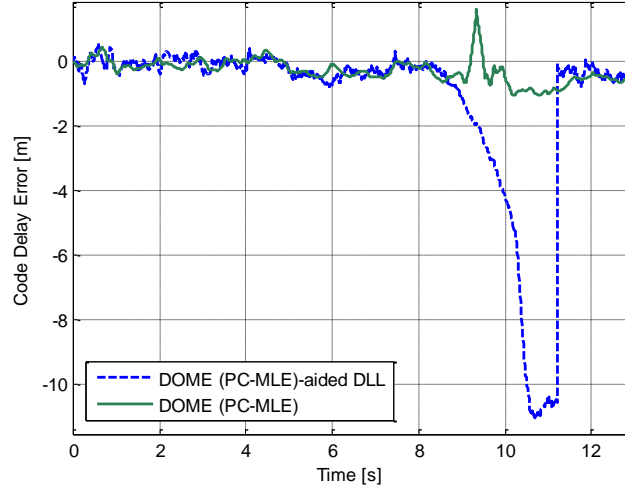


Fig. 3.9: Example of code delay error for the DOME (exploiting the PC-MLE) and a narrow-correlator DLL-based DOME implementation in harsh propagation conditions (corresponding to fading conditions in Fig. 3.8) [Gar15b], [Gar16a].

the fine estimation and the noise covariance matrix  $\mathbf{C}$  is in practice not exploited. The PC-MLE estimator is used and  $\mathbf{W}_2$  is defined as an identity matrix. As can be observed, the DOME approach is able to deal with the appearance of the fading events and keeps tracking the signal even when the  $C/N_0$  is below 20 dB-Hz. It is to be noticed that in a real application it would be recommended to disable the ambiguity resolution for very low  $C/N_0$  conditions (at least, below around 20 dB-Hz) since a low probability of false lock for the ambiguity resolution in the DOME will not be achievable for reasonable values of  $P$ . During the deep fading period between seconds 8 and 10, some peak errors are obtained due to the higher noise and multipath impact (as expected), but in this example the DOME is able to deal with it thanks to the usage of  $Q = 10$  (i.e., making the fine code delay estimator work in its linear region thanks to the improvement of the equivalent SNR). Additionally, the results obtained for a narrow-correlator DLL-based DOME implementation (following the architecture depicted in Fig. 3.2) are presented. In this case it can be observed that a false lock happens during the deep fading period, which is detected and corrected afterwards by the open-loop ambiguity solution (implemented in this case as a false lock detector/corrector). The latency in the detection and correction of the false lock is explained by the usage of  $P = 100$ , equivalent to a total integration time of 1 s (the usage of a lower  $P$  would decrease the latency, but at the cost of increasing the probability of false lock in the ambiguity resolution). It is to be noticed that in the DLL implementation the code loop noise bandwidth is 1 Hz and only coherent integrations (of 10 ms) are considered (i.e., improved configurations could still be applied).

To complete the performance assessment for the DOME approach, Fig. 3.10 shows an example of the impact of the distortions induced by the RF front-end filtering stages on the cross-correlation function obtained for a  $\text{BOC}_{\cos}(15, 2.5)$  signal when considering two different infinite impulse response (IIR) filters: a 9<sup>th</sup> order Butterworth filter, and a 6<sup>th</sup> order Chebyshev filter (with a 5 dB ripple in the passband as a worst-case scenario). In both cases a bandwidth of 40 MHz is considered such that the two main frequency lobes of the  $\text{BOC}_{\cos}(15, 2.5)$  signal can be used. As can be observed, when considering a bad filtering stage an important asymmetry is introduced, making it more difficult to identify the main peak of the cross-correlation function. Fig. 3.11 shows the results obtained when the MCE estimator in (3.11) and the PC-MLE in (3.13) are used to identify the main correlation peak in snapshot mode when considering the IIR filters defined above. In particular, a signal snapshot of 10 ms in AWGN channel conditions is considered (i.e.,  $P = 1$ ). Note that the correlator spacing  $\delta$  considered in this case is around 0.016 chips (i.e., half of the correlator spacing used in the previous simulations; required for avoiding sampling resolution issues in the unambiguous estimation of the maximum of the cross-correlation function, as discussed earlier). The number of correlation samples of the complex vector is  $Z = 129$ , covering the full correlation span (i.e.,  $\pm 1$  chip), unless the opposite is indicated. As can be observed, the impact of the false locks is very important at low-to-nominal SNR conditions for both estimators, even when considering nominal filtering conditions. For higher SNR conditions, it is observed that the probability of false lock for the MCE estimator decreases substantially in nominal filtering conditions (as expected), while remains high in the worst-case filtering scenario. In the worst-case filtering scenario, the benefit introduced by the exploitation of the *a priori* knowledge of the cross-correlation distortion in the PC-MLE is very clear. The probability of false lock obtained by the PC-MLE is in line with the one obtained by

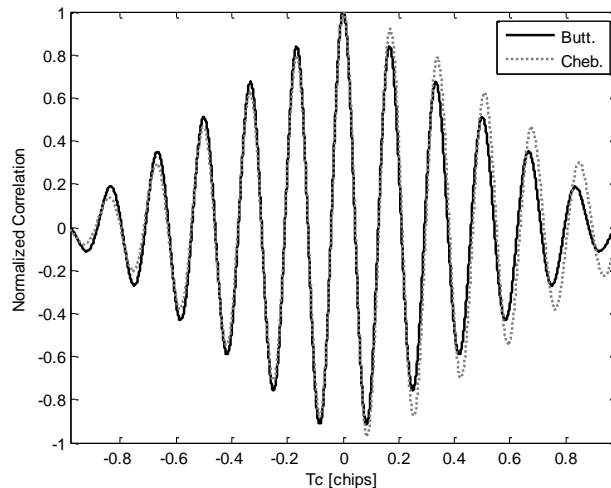


Fig. 3.10. Illustration of the impact of non-linear phase filtering on the cross-correlation function of a  $\text{BOC}_{\cos}(15, 2.5)$  signal [Gar17a].

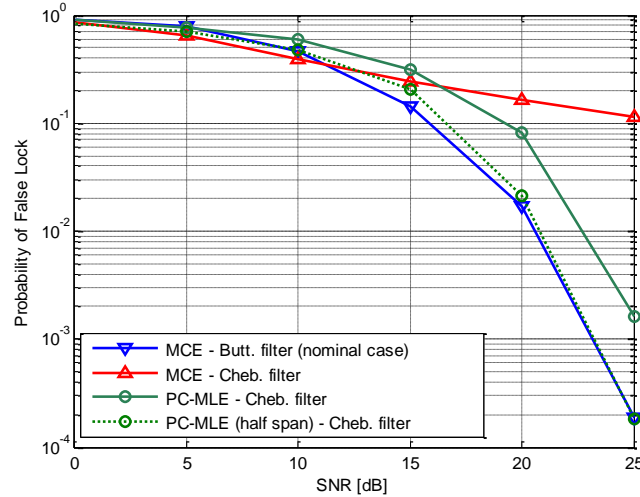


Fig. 3.11. Probability of false lock obtained for the simulated scenario with the MCE and PC-MLE estimators for a  $\text{BOC}_{\cos}(15, 2.5)$  signal [Gar17a].

the MCE in nominal filtering conditions when considering half of the correlation span (i.e.,  $\pm 0.5$  chips). Indeed, the exploitation of the full correlation span in the PC-MLE, instead of half of the span, is not beneficial in terms of probability of false lock due to the higher impact of the noise component in the estimator (as also observed in [Gus16b]).

Based on the simulation results in controlled and urban conditions, it can be concluded that the DOME approach fully exploits the BOC signal accuracy while being robust at low  $C/N_0$  conditions (down to around 20 dB-Hz) and in the presence of fading and multipath. Nevertheless, for very low  $C/N_0$  conditions (below around 20 dB-Hz) the equivalent SNR observed by the estimator remains also low and the probability of false lock is still important. In the absence of distortion or sampling resolution issues degrading the cross-correlation function observed by the estimators (achievable with a proper receiver design), the exploitation of the MCE estimator in the second optimization problem of the DOME is of interest both from a performance and computational burden point of view. Moreover, the first optimization problem of the DOME can be based on a standard DLL exploiting as discriminator the estimator in (3.10) or state-of-the-art solutions. In any case, other advanced solutions are needed to allow the exploitation of high-order BOC signals in harsh propagation conditions typical of urban or indoor conditions. A potential approach is to move the unambiguous estimation problem from the single-satellite level to the position domain, as is discussed in Section 3.3.

### 3.3 Unambiguous positioning in the MIMO-GNSS framework

As has been observed in Section 3.2 for the DOME approach, longer coherent and non-coherent integration periods can be considered in order to increase the SNR observed by the unambiguous estimators (reducing the probability of false lock). Nevertheless, the maximum number of integration periods that can be applied in practice are limited by receiver, user and environment constraints [Sec12], [Pan09], [Bro11a], such that for very low C/No conditions (below around 20 dB-Hz) the equivalent SNR observed by the estimator remains also low and the probability of false lock is still important.

This section proposes to overcome the limitations observed in state-of-the-art unambiguous estimation techniques (including the DOME approach) by introducing an additional processing gain in the unambiguous estimation problem in two spatial dimensions, as originally presented in [Gar19a]. The first dimension is the spatial transmission diversity introduced by the multiple GNSS satellites in view to the receiver. The second dimension is the spatial reception diversity introduced when the receiver features an array of antennas. These two spatial dimensions, and the corresponding spatial processing gains, are proposed to be efficiently exploited in the receiver's position domain, tackling the unambiguous estimation problem at position level instead of at pseudorange level. Working directly in the position domain (collectively exploiting multiple satellites' signals) has shown advantages in the detection and estimation of legacy GNSS signals in terms of sensitivity at low SNR conditions [DiE07], [Clo07], [Clo09b], [Axe11], [Bra10], [Est14], [Nar14], at the cost of a very high complexity of the resulting solution. Nevertheless, the unambiguous positioning problem can be considered as a fine estimation problem in which an *a priori* coarse position solution has been already estimated by the receiver (which can be derived based on e.g., the potentially ambiguous pseudoranges estimated with any conventional tracking technique, or the noisier pseudoranges estimated via the tracking of the BPSK envelope of the BOC signals [Mar03]). Therefore, in practice, the range of positions of interest in the unambiguous positioning problem is bounded. This is drastically reducing the complexity of the implementation with respect to the so-called direct positioning and collective detection techniques [DiE07], [Clo07], [Clo09b], [Axe11], [Bra10], [Est14], [Nar14], since the solution can be based on state-of-the-art receiver architectures.

The main target of the proposed approach is to efficiently exploit the spatial dimensions for enabling the robust unambiguous positioning with high-order BOC signals in the presence of deep fading and at very low SNR conditions (per satellite's signal) for which state-of-the-art single-satellite level unambiguous estimation techniques are already unstable. In the case of the single-antenna receiver configuration, this is achieved by treating the unambiguous estimation of the receiver's position as a multiple-input single-output (MISO) estimation problem in which the multiple transmitted high-order BOC signals are jointly exploited. And when an array of

antennas is featured by the receiver, this is achieved by jointly exploiting both transmission and reception diversities in the resulting multiple-input multiple-output (MIMO) GNSS system.

For both MISO- and MIMO-GNSS systems, the MLE of the receiver's position is used as baseline in the proposed solutions. In both cases, the signal model used in the derivation of the solution is defined such that the focus is kept on efficiently improving the equivalent SNR conditions observed by the estimator, while mitigating the multipath impact taking advantage of the spatial diversities available. In the particular case of the MIMO-GNSS system, a generalist unstructured array signal model not relying on the typical narrowband array assumption used in the GNSS literature [Fer09b] is considered due to the structure of the high-order BOC signals. The proposed array signal model will additionally allow to keep the problem open to the eventual exploitation of unknown spatial GNSS signal structures with directions of arrival different to those of the expected LOS signals. It is to be noticed that this can be of high interest (and a need) in urban and indoor conditions, where only highly attenuated refracted, diffracted and/or reflected multipath components (i.e., NLOS components) might be received [Sec12], [Ste03], [Hei08], [Jos14] (i.e., when the receiver operates in NLOS conditions). Therefore, the proposed approach differs from the typical application of arrays of antennas in the GNSS literature [Fer09a], [Fer09b], [Fer16], [Sec05], where the LOS signal is considered to be always available and the spatial reception diversity is exploited to get rid of multipath components and/or interferences disturbing the estimation of the LOS signal.

In the following, Section 3.3.1 discusses the unambiguous estimation problem in the position domain for a single-antenna configuration, and Section 3.3.2 extends the problem to a multiple-antenna configuration when considering a generalist unstructured array model. Then, Section 3.3.3 presents the simulation results for both single- and multiple-antenna configurations.

### **3.3.1 Unambiguous positioning with high-order BOC signals for single-antenna receivers**

#### **3.3.1.1 System and signal model**

Let us consider a system consisting of  $M$  GNSS satellites, each of them transmitting a high-order BOC signal at a given frequency band with a PRN code orthogonal to the other satellites. The  $M$  BOC signals are then received by a GNSS receiver equipped with a single antenna. It is considered that a coarse estimation of the receiver's position has been already performed by the receiver without unambiguously exploiting the accuracy of the high-order BOC signals. Moreover, it is considered that other parameters needed in practice for the derivation of the fine receiver's position solution (like the GNSS satellites' navigation data or the receiver's clock bias, just to mention some) are known or estimated by other means by the GNSS receiver. The target now is to perform a fine estimation of the receiver's position by fully exploiting, in an unambiguous way, the accuracy of the high-order BOC signals received.

In general, in harsh propagation conditions typical of urban or indoor scenarios the complex baseband signal received by the GNSS antenna from the  $M$  GNSS satellites in view can be modeled as

$$\begin{aligned}
 x_{MP}(t) = & \sum_{m=1}^M a_{m,0}(t) g_m(t - \tau_{m,0}(t)) \exp\{j2\pi f_{m,0}(t)t\} \\
 & + \sum_{m=1}^M \sum_{d=1}^{D_m-1} a_{m,d}(t) g_m(t - \tau_{m,d}(t)) \exp\{j2\pi f_{m,d}(t)t\} + e(t),
 \end{aligned} \tag{3.14}$$

where one LOS signal and  $D_m - 1$  NLOS multipath rays for the  $m$ -th satellite are considered,  $a_{m,d}$ ,  $\tau_{m,d}$  and  $f_{m,d}$  are the complex amplitude, time-delay and frequency-shift for the  $d$ -th signal propagation ray (with  $d=0$  for the LOS signal) of the  $m$ -th satellite, respectively, and  $e$  is the noise component, which is modeled as a complex, circularly-symmetric, zero-mean and temporally-white Gaussian process. The Doppler effect is considered to be modeled not only in the frequency-shift, but also in the time-delay for each signal propagation ray.  $g_m$  is the complex baseband model of the BOC-modulated DSSS signal transmitted by the  $m$ -th GNSS satellite, which can be modeled as in (2.2) in Section 2.1. It is to be noticed that the complex amplitudes  $a_{m,d}$  model both the changes introduced by the data modulated onto the BOC signal and any complex amplitude change introduced by the propagation channel for each of the propagation rays.

In the following, the NLOS multipath components appearing in reality in harsh propagation conditions are not considered in the signal model used as baseline for the derivation of the proposed unambiguous position estimator. The reason is twofold. On the one hand, the joint exploitation of the received signals in the unambiguous estimation of the receiver's position (taking advantage of the different satellites' propagation conditions and geometries), is not only a way to improve the SNR conditions observed by the estimator, but also to mitigate the impact of multipath on the ambiguity resolution, as will be shown later on in the simulation results. Thus, multipath mitigation can be achieved, to some extent, without the need of estimating the multipath components (as shown for legacy GNSS signals in [Clo07], [Clo09b]), which would increase the complexity of the estimator. And, on the other hand, in realistic harsh propagation conditions it is difficult to estimate those multipath components. In practice, the received multipath components are typically buried in noise (making very challenging, or unfeasible, to distinguish between LOS, NLOS and noise components), it is difficult to model them with a set of specular rays (in the best case scenario, the number of rays is still unknown), and their properties (in terms of delay and complex amplitude) are changing continuously in time as fast as the environment surrounding the user does (in particular for mobile users) [Sec12], [Ste03], [Hei08], [Jos14].

Based on the previous considerations, the complex baseband signal received by the GNSS antenna is modeled based on the LOS contributions of the  $M$  GNSS satellites in view as

$$x(t) = \sum_{m=1}^M a_m(t) g_m(t - \tau_m(t)) \exp\{j2\pi f_m(t)t\} + e(t), \quad (3.15)$$

where the 0-th sub-index used in (3.14) for the LOS signals is omitted for simplicity (i.e.,  $a_m \triangleq a_{m,0}$ ,  $\tau_m \triangleq \tau_{m,0}$  and  $f_m \triangleq f_{m,0}$ ). The time-delay  $\tau_m(t)$  and frequency-shift  $f_m(t)$  parameters observed by the receiver for each satellite at time  $t$  are dependent on the receiver position, such that  $\tau_m(t) \triangleq \tau_m(t, \mathbf{p})$  and  $f_m(t) \triangleq f_m(t, \mathbf{p})$ , with  $\mathbf{p} \triangleq \mathbf{p}(t) \in \mathbb{R}^{3 \times 1}$  the position vector in the ECEF coordinate system at time  $t$ . This trivial fact can be exploited to derive the receiver's position directly in the position domain, as already proposed in the literature for legacy signals [DiE07], [Clo07], [Clo09b], [Axe11], [Bra10], [Est14], [Nar14], or, equivalently, for solving the unambiguous estimation problem in the position domain when using high-order BOC signals. Based on this dependence and (3.15), we can define a basis function  $b_m$  for the  $m$ -th satellite as

$$b_m(t, \mathbf{p}) = g_m(t - \tau_m(t, \mathbf{p})) \exp\{j2\pi f_m(t, \mathbf{p})t\}, \quad (3.16)$$

where the dependence of the position vector  $\mathbf{p}$  with the time is omitted for simplicity. Let us consider now the vector  $\mathbf{x} = [x(t_0) \dots x(t_{0+K-1})]^T \in \mathbb{C}^{K \times 1}$  containing a snapshot of  $K$  samples of the signal received by the GNSS antenna with sampling period  $T_s = t_K - t_{K-1}$ . Assuming that  $a_m$ ,  $\tau_m$  and  $f_m$  parameters are constant during the observation time  $T_s K$  (being therefore the position  $\mathbf{p}$  considered constant during the observation time), the vector  $\mathbf{x}$  can be modeled as

$$\mathbf{x} \approx \mathbf{B}(\mathbf{p})\mathbf{a} + \mathbf{e}, \quad (3.17)$$

where  $\mathbf{a} = [a_1 \dots a_M]^T \in \mathbb{C}^{M \times 1}$  gathers the complex amplitudes for the  $M$  LOS contributions,  $\mathbf{e} \in \mathbb{C}^{K \times 1}$  is the complex noise vector (with  $\mathbf{e} \sim \mathcal{CN}(\mathbf{0}, \sigma^2 \mathbf{I})$ ), and  $\mathbf{B}(\mathbf{p}) = [\mathbf{b}_1(\mathbf{p}) \dots \mathbf{b}_M(\mathbf{p})] \in \mathbb{C}^{K \times M}$  is the basis function matrix, which is composed by the basis function vectors for each satellite  $\mathbf{b}_m = [b_m(t_0, \mathbf{p}) \dots b_m(t_{0+K-1}, \mathbf{p})]^T \in \mathbb{C}^{K \times 1}$ .

### 3.3.1.2 Unambiguous position estimator: the MISO-MLE solution

Based on the signal model defined in (3.17), and neglecting irrelevant additive and multiplicative constants, the MLE of the position can be obtained by minimizing the cost function [Kay13]

$$\Lambda_1(\mathbf{p}, \mathbf{a}) = \|\mathbf{x} - \mathbf{B}(\mathbf{p})\mathbf{a}\|^2. \quad (3.18)$$

In the following, an *a priori* coarse position estimation  $\hat{\mathbf{p}}_c$  is considered in the optimization problem, which will drastically simplify in practice the implementation of the proposed ML-based solution. Exploiting this *a priori* coarse position, we can define the unambiguous positioning problem as the ML-based optimization problem [Gar19a]

$$\begin{aligned} \hat{\mathbf{p}}, \hat{\mathbf{a}} &= \arg \min_{\mathbf{p}, \mathbf{a}} \Lambda_1(\mathbf{p}, \mathbf{a}) \\ &s. t. \|\mathbf{p} - \hat{\mathbf{p}}_c\| < \psi, \end{aligned} \quad (3.19)$$

where  $\psi$  defines the search area around the coarse position estimation. In order to derive the ML-based solution at post-correlation level, let us define the correlations  $\hat{\mathbf{r}}_{xx} = \mathbf{x}^H \mathbf{x}$ ,  $\hat{\mathbf{r}}_{xb}(\mathbf{p}) = \mathbf{B}^H(\mathbf{p})\mathbf{x}$ , and  $\hat{\mathbf{R}}_{bb}(\mathbf{p}) = \mathbf{B}^H(\mathbf{p})\mathbf{B}(\mathbf{p})$ . Based on these definitions, the vector of complex amplitudes  $\mathbf{a}$  minimizing  $\Lambda_1$  corresponds to the well-known LS estimator [Kay13]

$$\hat{\mathbf{a}} = \hat{\mathbf{R}}_{bb}^{-1}(\mathbf{p})\hat{\mathbf{r}}_{xb}(\mathbf{p}). \quad (3.20)$$

Substituting now (3.20) into (3.18), a cost function only dependent on  $\mathbf{p}$  is obtained,

$$\Lambda_2(\mathbf{p}) = \hat{\mathbf{r}}_{xx} - \hat{\mathbf{r}}_{xb}^H(\mathbf{p})\hat{\mathbf{R}}_{bb}^{-1}(\mathbf{p})\hat{\mathbf{r}}_{xb}(\mathbf{p}), \quad (3.21)$$

which is equivalent to the cost function exploited in the DPE solution for legacy GNSS signals [Clo07]. Therefore, the unambiguous ML-based estimator of the position can be defined as [Gar19a]

$$\hat{\mathbf{p}} = \arg \max_{\mathbf{p}} \left\{ \hat{\mathbf{r}}_{xb}^H(\mathbf{p}) \hat{\mathbf{R}}_{bb}^{-1}(\mathbf{p}) \hat{\mathbf{r}}_{xb}(\mathbf{p}) \right\} \quad (3.22)$$

$$s. t. \|\mathbf{p} - \hat{\mathbf{p}}_c\| < \psi.$$

In the following, the estimator in (3.22) is referred to as the MISO-MLE solution.

Fig. 3.12 shows an example of the cost function to be maximized in (3.22) (shown for illustrative purposes only with respect to the horizontal position plane) when considering the transmission of a  $\text{BOC}_{\cos}(15, 2.5)$  signal by eleven satellites in view by the receiver at good SNR conditions, and with an horizontal dilution of precision (HDOP) equal to one. As can be observed in this example, the multiple correlation peaks of the  $\text{BOC}_{\cos}(15, 2.5)$  signals (see Fig. 2.3 in Section 2.1) induce the appearance of multiple peaks also in the position domain. In particular, the maximum at the  $[0,0]$  position corresponds to the actual position of the receiver, while the rest of local peaks (i.e., “false” position peaks) correspond to the contributions of the side peaks in the horizontal position plane.

In case low SNR conditions are observed for the signals of all or most of the satellites in view, it might be challenging to unambiguously derive the receiver’s position for high-order BOC signals, even when considering the exploitation of the transmission diversity in the position domain, as proposed herein, resulting in biased position solutions with a non-negligible probability. In this situation, different alternatives might be followed. One possibility is to

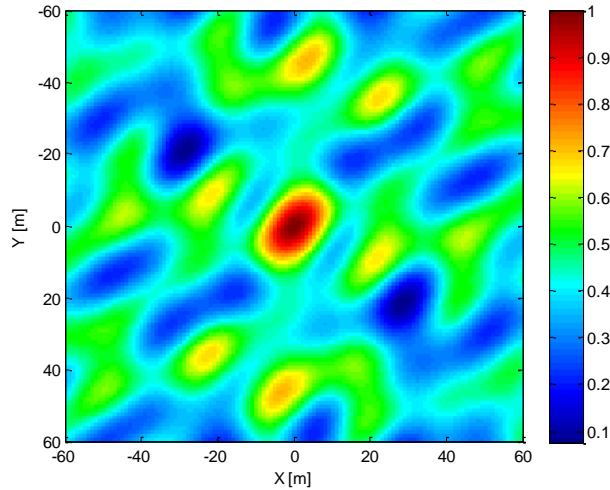


Fig. 3.12. Illustration of the normalized cost function in the horizontal position plane for a scenario with eleven satellites (with an equivalent HDOP equal to 1.0) transmitting  $\text{BOC}_{\cos}(15, 2.5)$  signals when considering high SNR conditions for all the satellites [Gar19a].

derive only a coarse position estimation based on the BPSK envelopes of the high-order BOC signals in view, losing the higher accuracy provided by the BOC signals, but avoiding the ambiguity problem. Another option is to filter the obtained position solutions in the time domain (e.g., applying a Kalman filter or other filtering approaches) such that the biased positions (i.e., the outliers in the position domain) are filtered out. This solution might be applicable at SNR conditions for which the probability to derive biased positions is still relatively low. For worse conditions, we can also consider the non-coherent integration (or other integration approaches) of  $R$  consecutive signal snapshots in order to increase the equivalent SNR conditions under which the position estimator will operate. Last, but not least, we could consider the exploitation of an array of antennas in order to introduce an additional processing gain, as will be proposed later on.

### 3.3.1.3 Implementation aspects of the MISO-MLE solution

The non-linear optimization problem in (3.22) is bounded by the constraint imposed, limiting the search space around the *a priori* coarse position solution available by the receiver before the fine unambiguous position estimation is performed. Taking into account that the error of the coarse position can be in practice in the order of several meters or tens of meters (being  $\psi$  in (3.22) defined accordingly), and that the optimization problem is non-convex (as shown in the example of Fig. 3.12), the direct application of a grid search approach [Kay13] is considered feasible and of interest. The resolution of the grid should be enough to detect unambiguously the maximum of the cost function corresponding to the actual receiver's position (typically, sub-meter grid resolution may be needed).

In case a multi-correlator architecture is considered by the receiver (i.e., a partial or complete sampling, with enough resolution, of the cross-correlation function for each of the satellites in view is already estimated by the receiver), the cross-correlation samples  $\hat{\mathbf{r}}_{xb}$  for each evaluated position  $\mathbf{p}$  in the grid search (as per (3.22)) can be derived from the available multi-correlation samples. Let us assume that in this case the prompt correlation sample (derived from the prompt correlator) for all the satellites in view is driven by the *a priori* coarse position estimation  $\hat{\mathbf{p}}_c$  (which is just a possible implementation scenario). Additionally, let us consider that each sampled cross-correlation function is interpolated in order to derive a continuous version of the estimated cross-correlation function  $\hat{r}_m(\delta)$ , with  $\hat{r}_m(0)$  corresponding to the prompt correlation sample for the  $m$ -th satellite. Based on this, the cross-correlation samples in  $\hat{\mathbf{r}}_{xb}(\mathbf{p})$  can be derived as [Gar19a]

$$\hat{\mathbf{r}}_{xb}(\mathbf{p}) = [\hat{r}_1(\delta_1) \dots \hat{r}_M(\delta_M)]^T \in \mathbb{C}^{M \times 1}, \quad (3.23)$$

where  $\delta_m \triangleq \delta_m(\mathbf{p}, \hat{\mathbf{p}}_c)$  is the expected difference in the  $m$ -th satellite's pseudorange introduced by the change in position from the coarse position estimation  $\hat{\mathbf{p}}_c$  to the evaluated position  $\mathbf{p}$ . This makes the proposed approach fully compatible with state-of-the-art multi-correlator receiver architectures and single-satellite-based acquisition and tracking engines. The resulting unambiguous GNSS receiver can be based on the high-level architecture depicted in Fig. 3.13.

Finally, the derivation of the cost function in (3.22) can be simplified by approximating  $\hat{\mathbf{R}}_{bb}(\mathbf{p})$  as an identity matrix when the cross-correlations between the DSSS signals  $g_m$  of the different GNSS satellites can be considered approximately null (as considered in some practical implementations of collective detection and direct positioning techniques [Axe11], [Est14], [Nar14]). This simplification is exploited in the simulations performed with the MISO-MLE in Section 3.3.3.

### 3.3.1.4 Comparison with state-of-the-art techniques

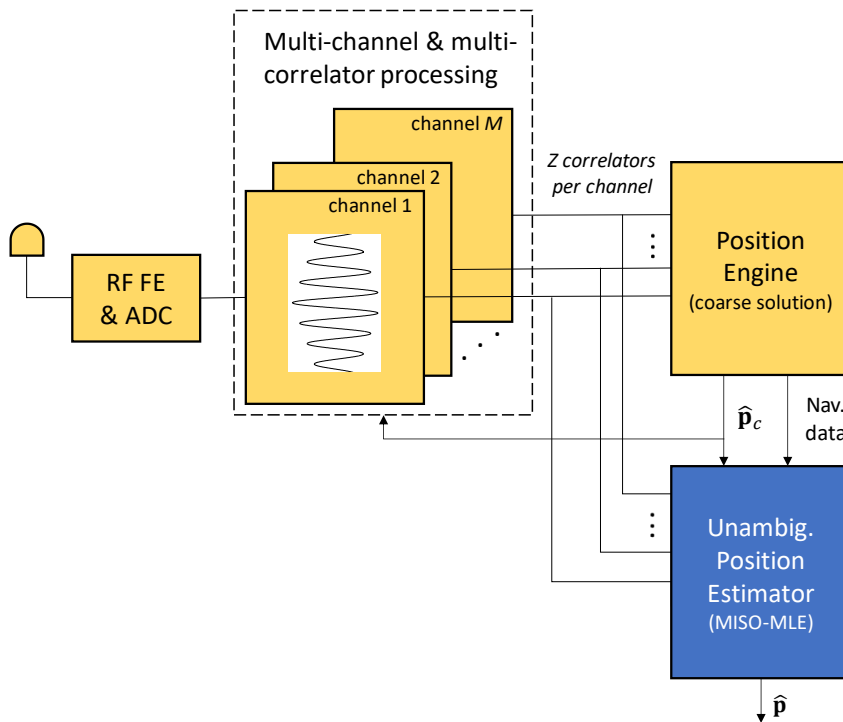


Fig. 3.13. High-level block diagram of a multi-correlator-based GNSS receiver applying the MISO-MLE solution [Gar19a].

In terms of performance, the main advantage of the proposed single-antenna unambiguous position estimator with respect to the unambiguous state-of-the-art techniques operating at pseudorange level is the higher robustness solving the ambiguity problem at low C/No conditions and in the presence of severe multipath. In terms of computational complexity, the proposed approach requires a higher number of correlators per tracked signal (in the order of tens or hundreds, depending on the BOC signal being considered) than state-of-the-art unambiguous techniques, where typically five correlators are used to solve the ambiguity. Nevertheless, it is to be noticed that multi-correlator architectures are nowadays broadly used in mass-market receivers, in particular when targeting the operation in harsh propagation conditions, so their real-time implementation is not considered a problem. On the other hand, the computational burden of solving the unambiguous optimization problem in (3.22) based on the output of the multiple correlators is considerably higher than that of the discriminators used in state-of-the-art single-satellite-based unambiguous tracking techniques. Taking into account that the proposed unambiguous position estimator can be applied in parallel to a conventional positioning engine, as proposed in the block diagram depicted in Fig. 3.13, the solution of (3.22) can be derived with a lower rate (typically, down to 1 Hz) than the update rate of the single-satellite tracking loops, such that the computational burden can be adjusted in order to allow the real-time implementation in conventional receiver architectures.

Comparing now the proposed unambiguous estimator to direct positioning and collective detection and acquisition techniques applied to legacy signals [DiE07], [Clo07], [Clo09b], [Axe11], [Bra10], [Est14], [Nar14], it is to be noticed that the main target in this section is not to allow the exploitation of signals that otherwise could not be acquired or tracked (as achieved with the application of collective acquisition techniques), but to solve in a robust way the ambiguity problem appearing when tracking high-order BOC signals. This allows the application of the proposed unambiguous estimator based on conventional acquisition, tracking and positioning engines, relying directly on the output of the correlators and a potentially ambiguous position solution, as shown in Fig. 3.13. In this way, the computational burden of the overall receiver can be reduced with respect to conventional direct positioning and collective techniques, at the cost of not achieving an improved acquisition and tracking sensitivity.

Last but not least, it is worth to briefly compare the single-antenna unambiguous position estimator to the LAMBDA-based method proposed in [Wen14]. Both techniques solve the ambiguity problem in the position domain. The main difference is that while the estimator proposed in this section exploits directly the complex samples obtained from the multiple correlators for each BOC signal being tracked, the LAMBDA-based method exploits the code and sub-carrier measurements previously estimated for each of the BOC signals (i.e., an estimation process has been already applied for each BOC signal before solving the ambiguity in the position domain). The direct exploitation of the output of the correlators (i.e., the sampled cross-correlation functions for each BOC signal being tracked) is expected to provide the optimum performance in terms of ambiguity resolution. Indeed, this will allow to solve the ambiguity problem even when most of the BOC signals being tracked are highly affected by

low  $C/N_0$  conditions and severe multipath. Moreover, this approach will allow the full exploitation of the spatial reception diversity in the multi-antenna configuration discussed in Section 3.3.2.

### 3.3.2 Unambiguous positioning with high-order BOC signals for multiple-antenna receivers

#### 3.3.2.1 System and signal model

Let us consider the same system model used in Section 3.3.1, but exploiting now an array of  $N$  antennas in the GNSS receiver, as depicted in Fig. 3.14. In this array of antennas, the distribution of the antennas is arbitrary, and the relative position of each of the antennas with respect to the receiver phase center is *a priori* known by the receiver and does not change with time. Therefore, the position  $\mathbf{p}_n$  for each antenna can be defined based on the position  $\mathbf{p}_0$  of the receiver phase center, i.e.,  $\mathbf{p}_n = \mathbf{p}_0 - \Delta\mathbf{p}_j$ , being  $\mathbf{p}_0$  the position to be unambiguously estimated in this case. Moreover, all the signals received by the  $N$  antennas are considered to be referenced to the same receiver clock. As for the single-antenna case, it is assumed that the receiver has already performed a coarse estimation of the receiver's position without

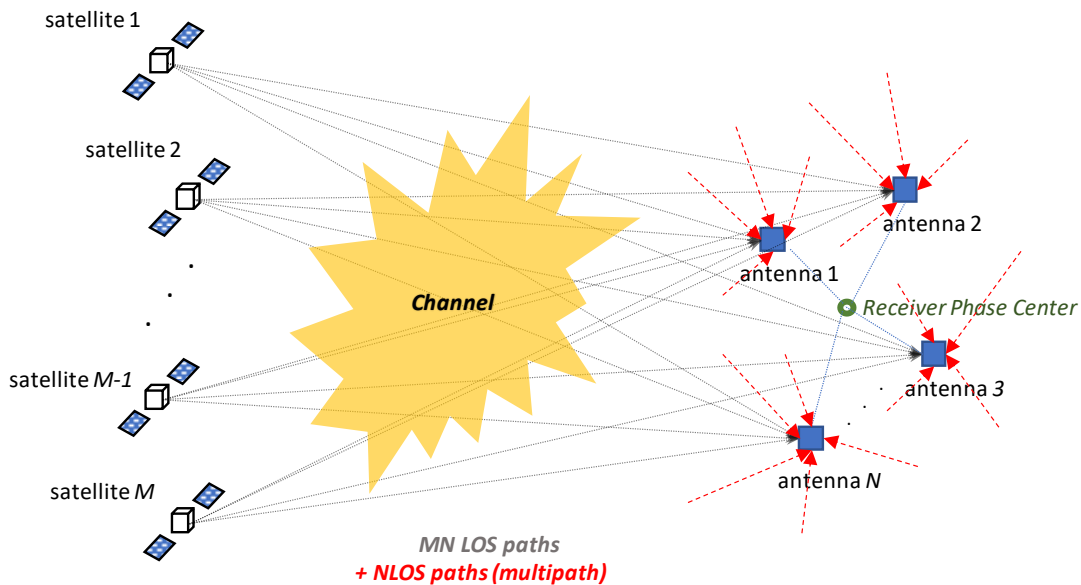


Fig. 3.14. Illustration of the MIMO-GNSS system.

unambiguously exploiting the accuracy of the high-order BOC signals. Thus, the target in this section is to perform a fine estimation of the receiver's phase center position by fully exploiting, in an unambiguous way, the accuracy of the high-order BOC signals received with the array of antennas and jointly exploiting both transmission and reception diversities.

In order to build now the complete signal model for the  $N$  receiver's antennas with an arbitrary distribution, a generalist unstructured antenna array model is considered, not relying on the typical narrowband array assumption exploited in the GNSS literature [Fer09a], [Fer09b], [Fer16], [Sec05], and with an arbitrary structure of the complex amplitudes of the  $MN$  LOS signal contributions received. The narrowband array model is proposed not to be applied herein given the high accuracy provided by the high-order BOC signals, which is in the order of few cm for nominal  $C/N_0$  conditions [Gar16a] (i.e., in the order, or below, the distance between the receiver's antennas). Thus, modeling the propagation delays between the receiver's antennas as phase shifts is not realistic, and could result in additional biases in the estimation of the high-order BOC signals. Therefore, the different propagation delays on the received high-order BOC signals for each antenna need to be modeled. On the other hand, the unstructured array model is an interesting and desired feature for several reasons. First of all, this model is beneficial in order for the proposed solution to be independent of the quality of the phase calibration of the array of antennas, being applicable to un-calibrated arrays and/or low-end array solutions. Moreover, this makes the solution also independent of the phases of the transmitted signals, so it can be applied when unknown data is modulated on the BOC signals. And last, but not least, this will make the resulting array estimator robust to additional phase distortions introduced by the propagation channel.

Temporally and spatially white Gaussian noise is considered in the array signal model. Therefore, the noise component is not meant to model unknown spatial signal structures created by multipath and/or interference sources, as typically considered in the GNSS literature [Fer09a], [Fer09b], [Fer16], [Sec05] (where the LOS signals are assumed to be always available and the spatially colored noise is filtered out to mitigate the impact of those multipath and/or interference sources). The presence of the LOS signal components in harsh propagation conditions typical of urban or indoor environments is not always ensured due to the blockage and shadowing effects. So, trying to spatially filter out the NLOS multipath components received with directions of arrival different to those of the originally expected LOS signals, might not be necessarily beneficial in this type of environment. Indeed, those NLOS signal components might be needed to be exploited for enabling the derivation of an unambiguous position solution in the absence of most or all of the LOS signal components. Therefore, instead of mitigating the impact of multipath on the ambiguity resolution by filtering out the spatially colored noise components (which would additionally increase the computational burden of the estimator), it is proposed to do so by jointly exploiting the different satellites' propagation geometries together with the spatial diversity provided by the array of antennas (being the multipath mitigation tackled without the need of modeling or estimating the multipath components, as will be shown later on).

Based on the previous considerations, the complex baseband signal received by the  $n$ -th GNSS antenna from the LOS contributions of the  $M$  GNSS satellites in view is modeled as

$$x_n(t) = \sum_{m=1}^M a_{m,n}(t) g_m(t - \tau_{m,n}(t)) \exp\{j2\pi f_{m,n}(t)t\} + e_n(t), \quad (3.24)$$

where  $a_{m,n}$ ,  $\tau_{m,n}$  and  $f_{m,n}$  are the complex amplitude, the time-delay and the frequency-shift of the BOC signal from the  $m$ -th satellite received by the  $n$ -th antenna, respectively, and  $e_n$  is the complex noise observed by the  $n$ -th antenna. Following the same approach used for the single-antenna case in (3.16) and (3.17), we can define the vector  $\mathbf{x}_n = [x_n(t_0) \dots x_n(t_{K-1})]^T \in \mathbb{C}^{K \times 1}$  containing a signal snapshot of  $K$  samples received by the  $n$ -th antenna, which is modeled as  $\mathbf{x}_n \approx \mathbf{B}(\mathbf{p}_n)\mathbf{a}_n + \mathbf{e}_n$ , with  $\mathbf{B}(\mathbf{p}_n)$  the basis function matrix for the  $n$ -th antenna.

Since the narrowband antenna array model should not be considered when targeting cm-level accuracies with high-order BOC signals, as discussed earlier, the different propagation delays of the signals received by each antenna need to be modeled. Thus, a basis function  $\mathbf{B}(\mathbf{p}_n)$  for each antenna needs to be considered in the signal model. Exploiting now the temporally and spatially white Gaussian noise assumption, we can simplify the array model representation by defining a multi-antenna basis function matrix  $\mathbf{S}(\mathbf{p}_0)$  based on the single-antenna basis function matrices  $\mathbf{B}(\mathbf{p}_n) \triangleq \mathbf{B}(\mathbf{p}_0 - \Delta\mathbf{p}_n)$  as [Gar19a]

$$\mathbf{S}(\mathbf{p}_0) = \begin{bmatrix} \mathbf{B}(\mathbf{p}_0 - \Delta\mathbf{p}_1) & \mathbf{0} & \dots & \mathbf{0} \\ \mathbf{0} & \mathbf{B}(\mathbf{p}_0 - \Delta\mathbf{p}_2) & \dots & \mathbf{0} \\ \vdots & \vdots & \ddots & \vdots \\ \mathbf{0} & \mathbf{0} & \dots & \mathbf{B}(\mathbf{p}_0 - \Delta\mathbf{p}_N) \end{bmatrix}, \quad (3.25)$$

such that the signal snapshots observed by the  $N$  antennas can be gathered in the vector  $\mathbf{y} = [\mathbf{x}_1^T \dots \mathbf{x}_N^T]^T \in \mathbb{C}^{NK \times 1}$ , which can then be modeled as

$$\mathbf{y} \approx \mathbf{S}(\mathbf{p}_0)\mathbf{c} + \mathbf{i}, \quad (3.26)$$

with the vector  $\mathbf{c} = [\mathbf{a}_1^T \dots \mathbf{a}_N^T]^T \in \mathbb{C}^{MN \times 1}$  containing all the complex amplitudes of the expected  $MN$  LOS contributions, and  $\mathbf{i} = [\mathbf{e}_1^T \dots \mathbf{e}_N^T]^T \in \mathbb{C}^{NK \times 1}$  gathering the noise

components of the  $N$  antennas, being the noise considered to be normalized between antennas, with  $\mathbf{i} \sim \mathcal{CN}(\mathbf{0}, \sigma^2 \mathbf{I})$ , and therefore  $\mathbf{y} \sim \mathcal{CN}(\mathbf{S}(\mathbf{p}_0)\mathbf{c}, \sigma^2 \mathbf{I})$ . It is to be noticed that the signal model in (3.26) differs from the typical matrixial representation of a MIMO signal model based on a MIMO channel matrix (i.e., typically the MIMO channel matrix is defined as  $\mathbf{H} = [\mathbf{a}_1 \dots \mathbf{a}_N] \in \mathbb{C}^{M \times N}$ ). Nevertheless, the representation used simplifies the later derivation of the proposed ML-based estimator and is in line with the assumptions considered.

### 3.3.2.2 Unambiguous position estimator: the MIMO-MLE solution

Based on the MIMO-GNSS signal model in (3.26), the complex multivariate Gaussian PDF of  $\mathbf{y}$  with  $\mathbf{p}_0$  as parameter can be defined as [Kay13]

$$p(\mathbf{y}; \mathbf{p}_0) = \frac{1}{\pi^{NK} \sigma^{2NK}} \exp \left[ -\frac{\|\mathbf{y} - \mathbf{S}(\mathbf{p}_0)\mathbf{c}\|^2}{\sigma^2} \right]. \quad (3.27)$$

Therefore, neglecting irrelevant additive and multiplicative constants, the MIMO-MLE of the receiver's phase center position can be obtained by minimizing the cost function

$$\Lambda_3(\mathbf{p}_0, \mathbf{c}) = \|\mathbf{y} - \mathbf{S}(\mathbf{p}_0)\mathbf{c}\|^2. \quad (3.28)$$

Exploiting now the vector of complex amplitudes  $\mathbf{c}$  minimizing  $\Lambda_3$ , which corresponds to the LS estimator

$$\hat{\mathbf{c}} = \hat{\mathbf{R}}_{ss}^{-1}(\mathbf{p}_0) \hat{\mathbf{r}}_{ys}(\mathbf{p}_0), \quad (3.29)$$

where  $\hat{\mathbf{r}}_{ys}(\mathbf{p}_0) = \mathbf{S}^H(\mathbf{p}_0)\mathbf{y}$  and  $\hat{\mathbf{R}}_{ss}(\mathbf{p}_0) = \mathbf{S}^H(\mathbf{p}_0)\mathbf{S}(\mathbf{p}_0)$ , it can be shown that the minimization of the cost function in (3.28) is equivalent to maximizing the cost function [Gar19a]

$$\Lambda_4(\mathbf{p}_0) = \sum_{n=1}^N \hat{\mathbf{r}}_{x_nb}^H(\mathbf{p}_0 - \Delta\mathbf{p}_n) \hat{\mathbf{R}}_{bb}^{-1}(\mathbf{p}_0 - \Delta\mathbf{p}_n) \hat{\mathbf{r}}_{x_nb}(\mathbf{p}_0 - \Delta\mathbf{p}_n), \quad (3.30)$$

where the cross-correlations for each of the receiver's antennas are defined as  $\hat{\mathbf{r}}_{x_nb}(\mathbf{p}_0 - \Delta\mathbf{p}_n) \triangleq \hat{\mathbf{r}}_{x_nb}(\mathbf{p}_n) = \mathbf{B}^H(\mathbf{p}_0 - \Delta\mathbf{p}_n) \mathbf{x}_n$ , and  $\hat{\mathbf{R}}_{bb}(\mathbf{p}_0 - \Delta\mathbf{p}_n) \triangleq \hat{\mathbf{R}}_{bb}(\mathbf{p}_n) = \mathbf{B}^H(\mathbf{p}_0 - \Delta\mathbf{p}_n) \mathbf{B}(\mathbf{p}_0 - \Delta\mathbf{p}_n)$ . Considering now the availability of an *a priori* coarse position estimation  $\hat{\mathbf{p}}_c$ , we can define the unambiguous positioning problem as the ML-based optimization problem [Gar19a]

$$\begin{aligned} \hat{\mathbf{p}}_0 &= \arg \max_{\mathbf{p}_0} \Lambda_4(\mathbf{p}_0) \\ &s. t. \|\mathbf{p}_0 - \hat{\mathbf{p}}_c\| < \psi, \end{aligned} \quad (3.31)$$

where  $\psi$  is defined as for the single-antenna case in (3.22). In the following, the estimator in (3.32) is referred to as the MIMO-MLE solution.

### 3.3.2.3 Implementation aspects of the MIMO-MLE solution

The non-linear optimization problem subject to a constraint in (3.31) can be solved via the direct application of a grid search approach, given the bounded search space in the position domain. Moreover, considering the implementation of a multi-correlator architecture by the receiver for each of the receiver's antennas (with all the correlators driven by  $\hat{\mathbf{p}}_c$ ), the cross-correlation samples  $\hat{\mathbf{r}}_{x_nb}(\mathbf{p}_0 - \Delta\mathbf{p}_n)$  for each evaluated position  $\mathbf{p}_0$  can be derived from the available multi-correlation samples, as in (3.23) for the single-antenna configuration, but in this case accounting for the relative position of each of the antennas with respect to the receiver's phase center, i.e., [Gar19a]

$$\hat{\mathbf{r}}_{x_nb}(\mathbf{p}_0 - \Delta\mathbf{p}_n) = [\hat{r}_{1,n}(\delta_{1,n}) \dots \hat{r}_{M,n}(\delta_{M,n})]^T, \quad (3.32)$$

with  $\hat{r}_{m,n}(\delta)$  the continuous interpolated version of the estimated cross-correlation function for the  $m$ -th satellite and  $n$ -th antenna, and  $\delta_{m,n} \triangleq \delta_{m,n}(\mathbf{p}_0, \hat{\mathbf{p}}_c)$  the expected pseudorange difference for the  $m$ -th satellite and  $n$ -th antenna introduced by the change in position from the

coarse position estimation  $\hat{\mathbf{p}}_c$  to  $\mathbf{p}_0 - \Delta\mathbf{p}_n$ , with  $\mathbf{p}_0$  the current evaluated position. The resulting multi-antenna unambiguous GNSS receiver can be based on the high-level architecture depicted in Fig. 3.15.

As for the single-antenna configuration, in the MIMO-MLE solution the derivation of the cost function in (3.30) can be simplified by approximating  $\hat{\mathbf{R}}_{bb}(\mathbf{p})$  as an identity matrix when the cross-correlations between the different GNSS signals can be considered approximately null. This simplification is exploited in the simulations performed with the MIMO-MLE in Section 3.3.3.

As an alternative approach for the exploitation of the multiple antennas, these could be used in the unambiguous positioning solution only when required (i.e., during harsh propagation conditions), using by the default only one of the antennas (for which a high-accuracy solution can be derived in mild propagation conditions). Additionally, if only meter-level (or above) positioning accuracies are expected to be achievable with the MIMO-MLE solution (e.g., indoors), and considering relatively short baselines between antennas (e.g., of the order of tens of cm), the cost function in (3.30) may be also simplified by approximating  $\Delta\mathbf{p}_n$  as a zero vector. This simplification removes the need to know the baselines between antennas.

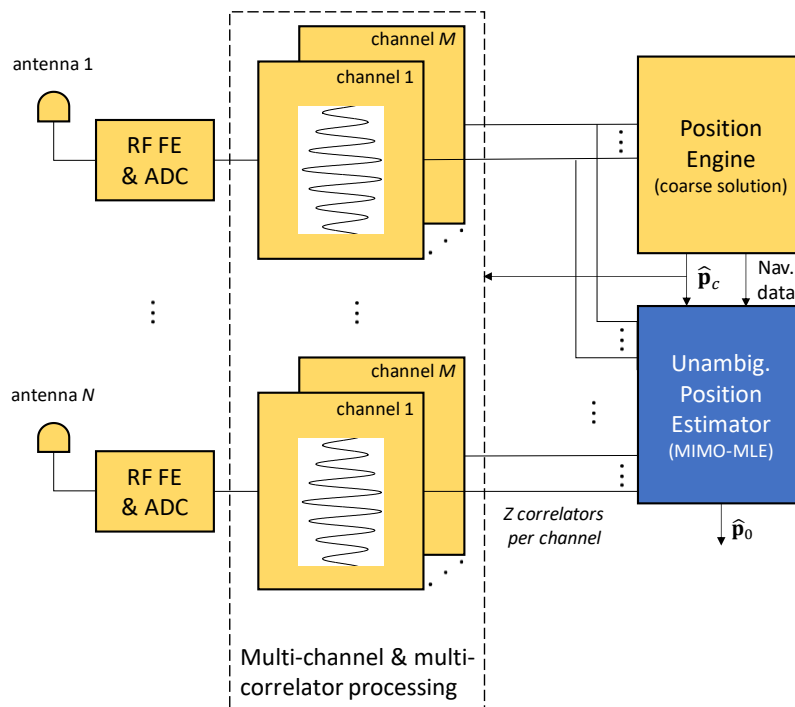


Fig. 3.15. High-level block diagram of a multi-antenna and multi-correlator-based GNSS receiver applying the MIMO-MLE solution [Gar19a].

### 3.3.3 Simulation results

The unambiguous positioning with high-order BOC signals based on the MISO- and MIMO-MLE solutions (for single- and multiple-antenna receiver configurations, respectively) have been simulated via a semi-analytical approach at post-correlation level when considering  $\text{BOC}_{\cos}(15, 2.5)$  signals being transmitted by the GNSS satellites, as originally presented in [Gar19a]. In order to focus on the BOC ambiguity resolution problem at low SNR conditions (which is already a very challenging task), other effects that could degrade further the ability of the receiver to identify unambiguously the main correlation peak are not considered herein since can be tackled by other means as part of the GNSS receiver front-end design (e.g., the application of non-linear phase filters in the receiver front-end highly distorting the cross-correlation function of the BOC signal, or eventual under-sampling or quantization issues impacting the recovery of the original BOC autocorrelation function [Gar16a], [Gar17a], as discussed in Section 3.2). Therefore, it is considered that, for high SNR conditions (where the noise impact is negligible) and in the absence of multipath, the receiver should be able to recover a symmetric filtered version of the autocorrelation function. A bandwidth of 40 MHz is used, allowing the reception of the two main frequency lobes of the  $\text{BOC}_{\cos}(15, 2.5)$  signal.

The usage of  $\text{BOC}_{\cos}(15, 2.5)$  signals is considered herein as a representative case of high-order BOC signal. The probability of false lock (i.e., the probability to have a biased pseudorange estimation) when estimating the maximum of the  $\text{BOC}_{\cos}(15, 2.5)$  cross-correlation function computed from a signal snapshot in AWGN conditions is relatively important for medium-to-low SNR conditions [Gar16a], as discussed in Section 3.2. As shown in Section 3.2.3, a probability of false lock above around  $10^{-3}$  is obtained by the MCE estimator when exploiting 10 integration periods for SNR values per coherent integration period below around 10 dB (which corresponds to a post-correlation  $C/N_0$  of 30 dB-Hz for a coherent integration period of 10 ms). This results in a non-negligible probability of having biased position solutions when using the conventional two-steps positioning approach [Clo09b] based on single-satellite unambiguous estimation techniques, used in the following as reference. In the conventional two-steps approach considered in this section the position solution is computed per signal snapshot based on the application of a weighted least squares (WLS) solution to the individual pseudorange measurements derived from the estimation of the maximum of the cross-correlation function of the BOC signal for each satellite, which corresponds to the MCE estimator in the DOME approach (equivalent to the MLE of the pseudorange in the absence of correlation distortions or when considering the application of a perfect match filter in the correlation process). Note that a correlation span of  $\pm 1$  chip is considered in the MCE estimator (see Table 3.2 for further details).

The first simulated scenario considers eleven satellites in view by a static receiver in a representative geometric configuration for which the HDOP is equal to one. An AWGN channel

| Parameter                    | Value   |
|------------------------------|---|
| Modulation                   | BOC <sub>cos</sub> (15, 2.5)  |
| Receiver BW                  | 40 MHz  |
| Correlator spacing           | 0.031 chips   |
| Correlation Span             | $\pm 1$ chip  |
| Number of satellites ( $M$ ) | 11  |
| Number of antennas ( $N$ )   | [1, 4, 8]   |
| Noise                        | AWGN  |
| Fading and multipath         | Controlled (2 <sup>nd</sup> scenario) and light-indoor (3 <sup>rd</sup> scenario) |

Table 3.2. Simulation parameters used for the assessment of the MISO- and MIMO-MLE solutions [Gar19a].

(spatially white for the array of antennas) is considered in this scenario for simplicity since, at medium-to-low SNR conditions, a simple AWGN is sufficient for inducing the ambiguity problem (as proved in Section 3.2.3). The same SNR conditions are considered for all the received signals, and additional system errors (e.g., satellites' clock and orbit errors) and ionospheric and tropospheric errors are not included in the simulations. For the MIMO system configuration, 4 antennas in an arbitrary distribution are simulated in the array of antennas, whose attitude and relative position with respect to the receiver phase center is considered to be known *a priori*, and with all the antennas' signals considered to be referenced to the same receiver clock. The phase of the simulated correlation functions at post-correlation level per satellite and antenna is random and independent between satellites and antennas. Therefore, no phase calibration is considered in the array of antennas.

The second simulated scenario is equivalent to the first scenario, but controlled fading and multipath are introduced for some of the simulated propagation paths. In particular, out of the eleven satellites in view by the receiver, the LOS signals of the five satellites with the lowest elevations (which correspond to the satellites in view with an elevation below around 30 degrees) are received with an attenuation of 30 dB with respect to the previous scenario (i.e., a constant fading of 30 dB is introduced to the LOS signals of those satellites). For the remaining six satellites, an additional constant attenuation of the LOS signal of 30 dB and a multipath ray with a relative delay of 10 m and a relative power of -10 dB with respect to the original LOS signal are introduced in the simulation in an incremental way (i.e., added to one more satellite

for each new simulation). It is to be noticed that, for the satellites in which controlled fading and multipath are introduced, the multipath ray component is dominant, with 20 dB more power than the attenuated LOS signal. Moreover, the relative delay of the multipath ray with respect to the LOS signal (i.e., 10 m) corresponds approximately to the relative delay of the secondary peak of the autocorrelation function of the  $\text{BOC}_{\cos}(15, 2.5)$  with respect to the main peak (see Fig. 2.3 in Section 2.1). Thus, the second scenario is considered a worst-case scenario for the pseudorange ambiguity resolution since it is inducing that the maximum of the resulting cross-correlation function is approximately located where the secondary peak of the original autocorrelation function is expected (i.e., biased pseudorange estimations are induced when the MLE of the pseudorange is used). This scenario has been used in order to assess the robustness of the proposed estimators in controlled fading and multipath conditions highly impacting the ambiguity resolution per satellite for a different number of satellites. In the case of the array of antennas, the same fading and multipath conditions are considered for all the antennas for simplicity. Although the simulated fading and multipath conditions are simplified with respect to those observed in real urban or indoor propagation scenarios (where multiple refracted, diffracted and/or reflected multipath components are actually received, as assessed in the third scenario), it is of interest to perform the assessment of the MISO- and MIMO-MLE solutions emulating in a controlled way the harsh propagation conditions that are in practice triggering the main problems that the estimators are expected to be facing when operating in reality (i.e., with an important fading of the LOS signal for many of the satellites in view, and an additional impact of the NLOS multipath rays).

Finally, a third simulated scenario in light-indoor conditions is considered. For this purpose, the realistic wideband satellite-to-indoor channel model in the Recommendation ITU-R P.681 [ITU17] has been used. In particular, the propagation conditions for a room with windows are simulated (for further details, see Section 4.4). In this scenario, a receiver featuring 1, 4 and 8 antennas is considered. An 8-antenna configuration is also considered in this third simulated scenario in order to further understand the benefit introduced by the spatial diversity in realistic propagation conditions. It is to be noticed that the spatial correlations between the signals received for each antenna are considered by the indoor channel model used. Therefore, the actual processing gain introduced by the exploitation of arrays of antennas in indoor propagation conditions is assessed in a realistic way. The simulation parameters used in the simulated scenarios presented above are summarized in Table 3.2. The reference SNR at post-correlation level per satellite LOS signal (when not considering yet the channel) is 35 dB for all the satellites (equivalent to a post-correlation C/No of 45 dB-Hz for a coherent integration period of 100 ms).

The MISO- and MIMO-MLE estimators are used to unambiguously estimate the horizontal 2D position of the receiver. The conventional two-steps approach (applied to the single-antenna configuration) exploiting a WLS solution is used as reference in order to understand the benefit of jointly exploiting the spatial diversity in the proposed estimators. In the MISO- and MIMO-MLE estimators, the solution is derived considering a search space in the horizontal 2D position domain limited to a square of 100 by 100 m around the truth receiver position, which is a

realistic search space considering the availability of an *a priori* coarse position estimation (e.g., based on the position solution obtained from the unambiguous, but noisier, BPSK-envelope of the BOC signal). Based on the assumption of an *a priori* coarse position estimation, other parameters like e.g., the receiver’s clock bias, are also considered *a priori* known in the problem, since can be estimated by other means as part of the coarse position estimation. For the first and second scenarios, 1000 Monte Carlo independent runs are considered per receiver configuration and evaluated SNR value for the derivation of the results.

The root-mean-square error (RMSE) of the horizontal position solution obtained for the proposed MISO- and MIMO-ML estimators for the first simulated scenario is shown in Fig. 3.16 with respect to the SNR per satellite signal at post-correlation level, together with the results obtained for the reference WLS solution. Additionally, the lower bound (LB) of the horizontal position error is also included for both single- and multiple-antenna configurations. This LB is computed based on the CRLB in AWGN conditions of the pseudorange estimation per satellite (based on [Wei03] without considering the potentially biased estimations), and the HDOP for the single-antenna configuration (i.e.,  $LB=HDOP\sqrt{CRLB}$ ); and, for the multiple-antenna configuration, also the maximum gain expected to be introduced by the array of antennas (i.e.,  $10\log_{10}(N)$ , with  $N$  equal to four in the simulated case).

As can be observed, the reference WLS solution is impacted by the occurrence of false locks at pseudorange level (i.e., biased pseudorange estimations) for SNR values (at post-correlation level) below around 22.5 dB, and only above this value attains the single-antenna LB (which is

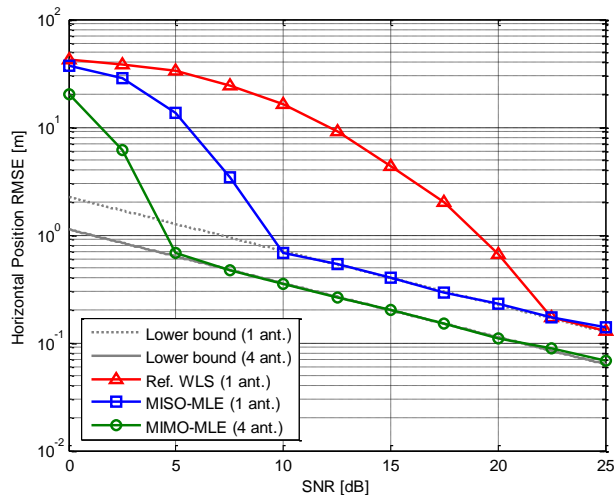


Fig. 3.16. RMSE of the horizontal position estimated with the MISO- and MIMO-ML estimators and the conventional two-steps approach based on a WLS solution in an AWGN channel. Note that the SNR per satellite signal at post-correlation level is indicated [Gar19a].

in line with the results obtained in Section 3.2.3, where a probability of false lock below around  $10^{-3}$  is achieved for an SNR per coherent integration period of 20 dB). The MISO-MLE (equivalent to DPE) is able to attain the single-antenna LB for lower SNR conditions than the reference WLS solution, down to around 10 dB (or an equivalent post-correlation  $C/N_0$  level of 20 dB-Hz for a coherent integration period of 100 ms). This important improvement in the unambiguous estimation of the position is introduced by the joint exploitation of the  $M$  satellites'  $\text{BOC}_{\cos}(15, 2.5)$  signals in the position domain, which enables an improvement of the equivalent SNR conditions observed by the MISO-MLE in the position domain with respect to the one observed per satellite's signal. In this first simulated scenario, where the same SNR conditions are considered for all the received signals, the observed improvement is of up to  $10\log_{10}(M)$  dB. This makes the MISO-MLE in the position domain more robust solving the ambiguity problem than the conventional two-steps approach, in which the ambiguity is solved at pseudorange level and the position solution is derived based on a WLS solution. Moving to the multi-antenna configuration, it is observed that the MIMO-MLE solution attains the multi-antenna LB even at lower SNR conditions than the MISO-MLE (from around 10 dB down to 5 dB) thanks to the additional processing gain introduced by the array of antennas, of up to  $10\log_{10}(N)$  dB (i.e., 6 dB for the four antennas considered in the simulation).

In order to complete the comparison between the different receiver configurations assessed in the first simulation scenario, Fig. 3.17 shows the 95-percentile of the horizontal position errors instead of the RMSE shown in Fig. 3.16. The RMSE is already impacted even when the probability to obtain biased positioning solutions is relatively low, so the 95-percentile figure might be actually more interesting to really understand, from a practical point of view, the

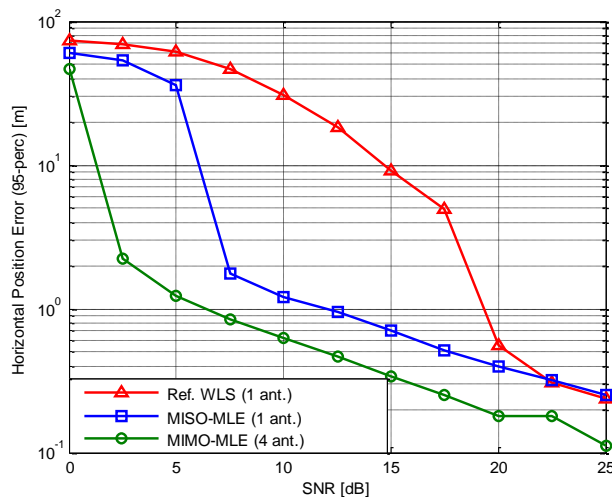


Fig. 3.17. Horizontal position error (95-perc) for the results shown in Fig. 3.16 [Gar19a].

robustness of the proposed solution (i.e., for which SNR conditions can we reasonably trust the position solution). In practice, in a typical receiver implementation we might actually filter the position solutions obtained per time epoch (e.g., with a Kalman filter) in order to smooth the final positioning solution and remove potential outliers. In some cases, this process might be also aided by other sources like e.g., inertial sensors. Therefore, it might be reasonable to think that the receiver should be able to handle biased positioning solutions appearing from time to time (e.g., below 5% of the time). Based on this, and assuming the same AWGN conditions for each of the eleven satellites simulated, the conventional two-steps approach can be considered in practice robust for SNR values down to around 20 dB, while the MISO- and MIMO-MLE solutions can be considered robust for SNR values down to around 7.5 and 2.5 dB, respectively.

Regarding the second simulated scenario, Fig. 3.18 shows the results obtained for the different receiver configurations assessed in terms of the 95-percentile of the horizontal position errors with respect to the number of satellites impacted by the simulated fading and multipath (as described earlier in this section). Two nominal SNR conditions are considered (with an SNR equal to 15 and 20 dB for the satellites not impacted by fading). As can be observed, the conventional two-step approach based on a WLS solution is highly impacted by the simulated fading and multipath conditions. On the other hand, the MISO- and MIMO-MLE solutions are robust to the strong fading and multipath conditions simulated. In particular, the MIMO-MLE shows horizontal errors (95-perc) below the meter, even with four satellites impacted by a multipath bias of 10 m and only two satellites in LOS conditions (for the worst case in which the nominal SNR is set to 15 dB, the horizontal error (95-perc) for the MIMO-MLE solution is

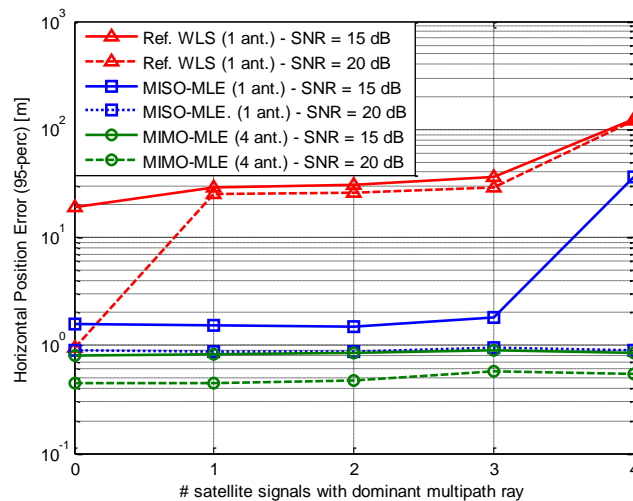


Fig. 3.18. Horizontal position error (95-perc) for the second simulated scenario with SNR set to 15 and 20 dB for the nominal LOS signals [Gar19a].

0.86 m, with respect to around 36 m for the MISO-MLE solution, and around 125 m for the conventional two-steps approach based on the WLS solution).

Moving to the third simulated scenario in light-indoor conditions, Fig. 3.19 shows the RMSE results obtained for the MIMO-MLE with 1, 4 and 8 antennas [Gar19b]; and Fig. 3.20 shows the corresponding horizontal position solutions. In this scenario, 200 independent Monte Carlo runs are considered per receiver configuration. As can be observed from Fig. 3.19 and 3.20, a clear benefit is introduced by the exploitation of the MIMO-MLE solution when the number of antennas increases. Indeed, for the single-antenna configuration (MISO-MLE) the positioning results are highly impacted by false locks, resulting in horizontal errors of several tens of meters. This slightly improves for the 4-antenna configuration, but only with an 8-antenna configuration the impact of false locks is effectively mitigated thanks to the higher processing gain and the spatial diversity introduced by the multiple antennas. This allows to achieve accuracies of few meters indoors, which is far better than what can be achieved with BPSK(1) signals in the same conditions (as will be shown in Section 5.2). Therefore, the proposed estimators in the MIMO-GNSS framework are a promising approach to enable the unambiguous positioning of high-order BOC signals in harsh propagation conditions typical of urban and indoor environments (with  $C/N_0$  levels below 20 dB-Hz), while being implementable based on state-of-the-art multi-correlator receiver architectures.

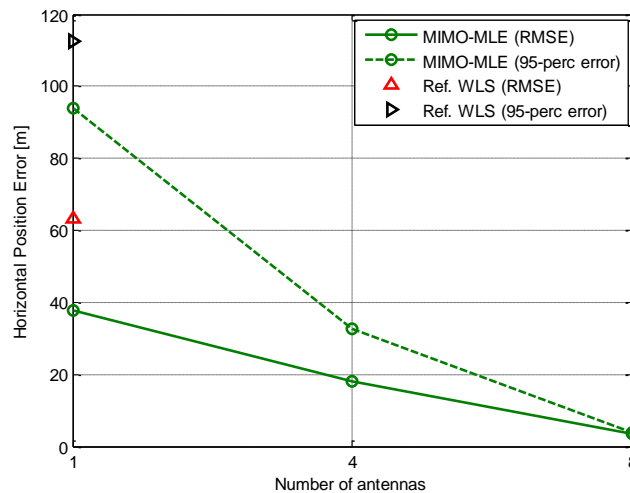


Fig. 3.19. RMSE and 95-percentile errors for the third simulated scenario in light-indoor conditions [Gar19b].

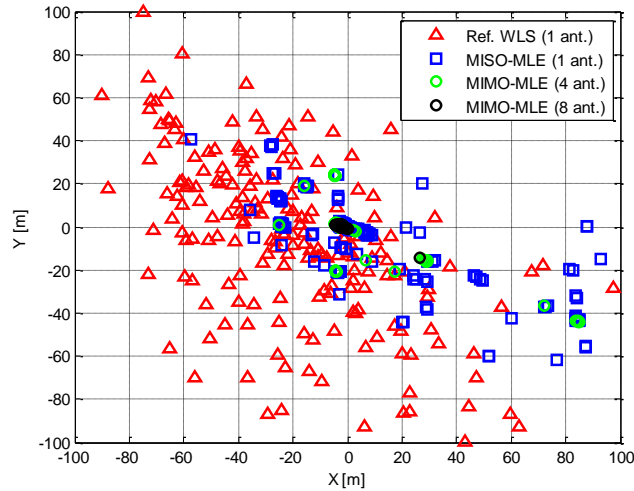


Fig. 3.20. Horizontal position results in the third simulated scenario in light-indoor conditions [Gar19b].

### 3.4 Conclusions

This chapter has started presenting the DOME approach in Section 3.2, focusing on the robust unambiguous code delay estimation of high-order BOC signals at single-satellite level. The proposed approach exploits the time diversity in the unambiguous estimation problem via the usage of multiple integration periods, and relies on a multi-correlator architecture in order to consider multiple correlation peaks of the cross-correlation function. This additionally allows the exploitation of a model of the expected cross-correlation function, which may include *a priori* known distortions introduced by the GNSS receiver. Performance results in both controlled and realistic simulated scenarios have been presented when considering a  $\text{BOC}_{\cos}(15, 2.5)$  signal. The results obtained have shown that the DOME approach fully exploits the BOC signal accuracy while being robust at low  $C/N_0$  conditions (down to around 20 dB-Hz) and in the presence of fading and multipath.

The DOME approach allows the adaptation to different BOC signals, receiver and filtering configurations, and propagation environments. In the absence of distortion or sampling effects degrading the cross-correlation function observed by the estimators (achievable with a proper receiver design), the exploitation of the MCE estimator in the second optimization problem of the DOME is of interest both from a performance and computational burden point of view. Moreover, the first optimization problem of the DOME can be based on a standard DLL. The

exploitation of several integration periods is considered by the DOME approach in order to improve the observed SNR conditions in which the estimations are performed. Nevertheless, since the integration periods that can be applied in practice are limited by receiver, user and environment constraints, for very low  $C/N_0$  conditions (below around 20 dB-Hz) the equivalent SNR observed by the estimator remains also low and the probability of false lock is still important. Therefore, other advanced solutions are needed in order to allow the exploitation of high-order BOC signals in harsh propagation conditions typical of urban or indoor scenarios.

Section 3.3 has presented the unambiguous positioning problem with high-order BOC signals in the MIMO-GNSS framework in order to overcome the limitations observed in state-of-the-art unambiguous estimation techniques operating at single-satellite level (including the DOME approach). In particular, it has been proposed to tackle the ambiguity resolution problem directly in the position domain, enabling the joint exploitation of all the BOC signals received by the GNSS receiver. For this purpose, the MISO- and MIMO-MLE solutions exploiting one or multiple antennas, respectively, have been derived. The processing gain introduced in the unambiguous estimation problem by the spatial transmission and reception diversities allows to improve the equivalent SNR conditions in which the estimator operates and, thus, a reduction of the impact of false locks.

The simulation results obtained show that the proposed MISO-MLE solution outperforms the conventional two-steps positioning approach in both AWGN and fading conditions, being more robust in the unambiguous positioning with high-order BOC signals, and resulting in a lower occurrence of biases in the position solution. Indeed, the joint exploitation of the high-order BOC signals received from all the satellites in view allows the MISO-MLE to attain the lower bound of the position estimation for lower SNR values per satellite signal thanks to the transmission diversity gain. For the MIMO-MLE, an additional improvement of the position performance is obtained thanks to the processing gain introduced by the array of antennas. The MIMO-MLE attains the lower bound even at relatively low SNR conditions, and the position estimator is robust even when the signals from multiple satellites are impacted by severe fading and multipath conditions. Moreover, when several receiver antennas are available, the proposed estimator allows the exploitation of high-order BOC signals even in indoor conditions. This enables to achieve accuracies of few meters indoors, which is far better than what can be achieved with BPSK(1) signals in the same conditions, as will be discussed in Chapter 5. Therefore, the proposed estimators in the MIMO-GNSS framework are a promising approach to enable the unambiguous positioning with high-order BOC signals in harsh propagation conditions typical of urban and indoor environments (with  $C/N_0$  levels below 20 dB-Hz), while being implementable based on state-of-the-art multi-correlator receiver architectures.



# 4

## Indoor Timing

**T**HE exploitation of GNSS signals in indoor scenarios is a challenging topic due to the dominant impact of the indoor propagation conditions. In the particular case of indoor timing applications, this results in an important degradation of the achievable timing accuracy due to the impact of the NLOS multipath signal components. This limits the usage of current GNSS receivers in applications with time synchronization requirements in the order of tens of ns.

This thesis proposes a joint time and composite MIMO channel estimation approach for static indoor GNSS receivers featuring an array of antennas in order to improve the timing accuracy in indoor conditions. This approach exploits both the structure of the diffuse multipath components of the indoor channel and the MIMO system formed by all the GNSS signals received via an array of antennas. The concept of composite MIMO channel is introduced for enabling a robust mitigation of the dominant diffuse multipath in indoor timing applications.

Multiple hypotheses on the structure of the composite MIMO channel are proposed to be assessed via Monte Carlo methods in order to derive a physically plausible estimation of it (and, therefore, an accurate and precise estimation of the clock bias), avoiding the derivation of sparse channel solutions (with few dominant channel components instead of the expected diffuse channel). The proposed estimators can be implemented based on state-of-the-art multi-correlator receiver architectures, which is of interest to optimize their implementation in real applications. Moreover, they can be applied to low-end arrays of antennas, where phase-calibration might not be ensured.

This chapter is organized as follows. Section 4.1 discusses the background and motivation. Section 4.2 presents the system and signal model exploited by the timing solutions proposed. Section 4.3 presents the joint time and composite MIMO channel estimator based on an *a priori* knowledge of the receiver's position and a coarse clock bias estimation to be refined. A first refinement of the coarse clock bias exploiting the spatial diversity introduced by the MIMO-GNSS system based on the MLE is proposed in order to reduce the computational burden. Then, the structure of the diffuse channel is exploited in the estimation problem to obtain the ultimate fine clock bias estimation. Section 4.4 presents the simulation results obtained in light-indoor and indoor conditions based on a realistic indoor channel model. Finally, Section 4.5 presents the conclusions.

The material presented in this chapter has been published by the author in [Gar18a], and [Gar18c].

### 4.1 Background and motivation

GNSS signals are broadly used for precise time synchronization in many different applications, including the telecom, finance and energy sectors [GNS17]. In this context, the exploitation of GNSS signals is typically limited to outdoor applications where there is no GNSS coverage problem. Indeed, the usage of GNSS signals in indoor conditions is very challenging due to the important impact of blockage and multipath [Sec12], [He17], [Hei08], [Bro11b], which highly degrade the accuracy achieved with current GNSS receivers. Tight time synchronization requirements of the order of tens or hundreds of ns may be expected in near-future applications operating in indoor conditions. An example of this is 5G small cells covering indoor areas [Jun14], where time synchronization is expected to be a key enabler of some of the underlying technologies exploited [3GP17]. Although several technical solutions may be considered for meeting future time synchronization requirements (e.g., wire-based solutions like the precise time protocol [IEE07], or commercial solutions based on satellite signals from low-earth orbits [Cor17], [Lau17]), a solution based on free, open access and worldwide available GNSS signals, and not requiring any additional infrastructure to operate, would be of high interest.

The performance of GNSS-based time synchronization solutions in indoor scenarios is driven by the indoor channel propagation conditions, where the impact of effects like blockage, diffraction, scattering and reflection introduces an important degradation with respect to open-sky scenarios. The main reasons are the high attenuation, or complete absence, of the LOS GNSS signals (impacting the SNR conditions in which the estimators are operating) and the presence of dominant NLOS multipath components (introducing biases in the estimation) [Sec12], [Hei08], [Jos14]. Under the assumption that the receiver's position is *a priori* known, the reception of a single satellite's signal can be enough for solving the time synchronization problem (i.e., to obtain the time offset between the receiver's time and the GNSS system time, in the following referred to as the receiver's clock bias) [Kap06]. This is actually the approach followed by some commercial timing receivers designed for operating in static indoor conditions, at the cost of timing accuracies of the order of hundreds of ns with respect to tens of ns achieved in open-sky scenarios [NEO16]. This limits the direct application of current GNSS receivers to meet the tight time synchronization requirements foreseen in future indoor applications.

In order to be able to operate in degraded signal conditions and mitigate the impact of multipath in GNSS receivers, different high-sensitivity architectures and multipath estimation or mitigation techniques have been proposed in the literature [Pan09], [Bro11a], [Sah08], [Won12], [Clo08], including direct position and time estimators (DPE/DTE) [Clo07], [Axe11], [Bha17], and array-based mitigation techniques [Sec05], [Fer16], [Clo09], [Gar18a], [Gar18c]. Nevertheless, these techniques still present limitations in indoor conditions. On the one hand, the techniques based on the estimation of the multipath components for mitigating their impact are typically considering the presence of a LOS signal component and one or few multiple multipath components. Nevertheless, the low  $C/N_0$  conditions in which the signals are received indoors make difficult, or unfeasible, to distinguish between LOS, NLOS and noise components [Sec12], [Hei08], [Jos14]. Moreover, the diffuse (i.e., non-sparse or unresolvable) multipath expected in indoor propagation conditions [Sec12] makes even more complex the identification and estimation of the multipath components (due to the large number of e.g., diffracted and scattered contributions received in very close time-delays). On the other hand, high-sensitivity techniques enable the exploitation of GNSS signals in harsh propagation environments like indoor conditions [Pan09], [Bro11a], but typically at the cost of an important degradation of the accuracy achieved. Therefore, a combination of both high-sensitivity and multipath estimation approaches may be required for achieving an accurate and precise time synchronization in indoor conditions. Based on this, a joint time and composite MIMO channel estimation approach is presented in this chapter for static indoor GNSS receivers, as originally proposed in [Gar18a].

## 4.2 System and signal model

Let us consider a system consisting of a static receiver featuring an array of  $N$  antennas (with  $N \geq 1$ ) and receiving  $M$  navigation signals with equivalent correlation properties (with  $M \geq 1$ ) from a given GNSS constellation in indoor propagation conditions. The signals received by all the antennas are referenced to the same receiver clock. The receiver's position and the baseline between each of the antennas and the receiver's phase center is considered to be known *a priori*, as well as the coarse clock bias and drift estimations  $\hat{\delta t}_c$  and  $\hat{\delta \dot{t}}_c$  (e.g., estimated by the receiver based on state-of-the-art techniques [Kap06]). The navigation data required for the derivation of the GNSS satellites' state vectors is also considered to be known by the receiver (e.g., via assistance data [Dig09]). The target now is to perform a fine estimation of the receiver's clock bias based on the defined MIMO-GNSS system.

In general, in indoor propagation conditions the complex baseband signal received by the  $n$ -th GNSS antenna from the LOS and NLOS multipath contributions of the  $M$  GNSS satellites above the horizon can be modeled as

$$\begin{aligned}
 x_n(t) = & \sum_{m=1}^M a_{m,n,0}(t) g_m(t - \tau_{m,n,0}(t)) \exp\{j2\pi f_{m,n,0}(t)t\} \\
 & + \sum_{m=1}^M \sum_{d=1}^{D_{m,n}} a_{m,n,d}(t) g_m(t - \tau_{m,n,d}(t)) \exp\{j2\pi f_{m,n,d}(t)t\} + e_n(t),
 \end{aligned} \tag{4.1}$$

where a LOS signal and  $D_{m,n}$  NLOS multipath rays received by the  $n$ -th antenna from the  $m$ -th satellite are considered;  $a_{m,n,d}$ ,  $\tau_{m,n,d}$  and  $f_{m,n,d}$  are the complex amplitude, time-delay and frequency-shift, respectively, for the  $d$ -th signal propagation ray (with  $d = 0$  for the LOS signal) of the  $m$ -th satellite received by the  $n$ -th antenna;  $e_n$  is the noise component for the  $n$ -th antenna, which is modeled as a complex, circularly-symmetric, zero-mean and temporally and spatially white Gaussian process; and  $g_m$  is the complex baseband model of the modulated DSSS signal transmitted by the  $m$ -th GNSS satellite. It is to be noticed that the complex amplitudes  $a_{m,n,d}$  model both the changes introduced by the data modulated onto the GNSS signal and any change introduced in the complex amplitude by the propagation channel. Additionally, the NLOS multipath rays received by the different antennas are expected to be spatially correlated (depending on the separation between antennas and on the geometry with respect to each of the satellites).

The time-delay  $\tau_{m,n,d}(t)$  and frequency-shift  $f_{m,n,d}(t)$  parameters of each of the signal components (LOS and NLOS rays) received by the  $n$ -th antenna for each satellite at time  $t$  are dependent on a state vector  $\Phi_n$  for each antenna, i.e.,  $\tau_{m,n,d}(t) \triangleq \tau_{m,n,d}(t, \Phi_n)$  and  $f_{m,n,d}(t) \triangleq f_{m,n,d}(t, \Phi_n)$ . The state vector per antenna can be defined as  $\Phi_n \triangleq \Phi_n(t) \triangleq$

$[\delta t(t), \delta \dot{t}(t), \mathbf{p}_n^T]^T$ , where  $\delta t$  and  $\delta \dot{t}$  are the receiver's clock bias and clock drift, respectively, which are common to all the antennas, and  $\mathbf{p}_n$  is a vector containing the position of the  $n$ -th antenna in the ECEF coordinate system [Kap06]. The position of the  $n$ -th antenna and of the receiver's phase center  $\mathbf{p}_0$  are related as  $\mathbf{p}_n = \mathbf{p}_0 - \Delta \mathbf{p}_n$ , with  $\Delta \mathbf{p}_n$  the relative vector between them, which is fixed for the static receiver considered herein. Therefore, we can define  $\Phi_n(t) \triangleq [\delta t(t), \delta \dot{t}(t), \mathbf{p}_0^T, \Delta \mathbf{p}_n^T]^T$ .

For the static indoor conditions considered herein, the frequency shift of the LOS and NLOS multipath components are expected to be in practice equivalent or very similar [Sat12], such that  $f_{m,n,d} \approx f_{m,n,0}, \forall d$ . In order to simplify the signal model, and taking into account the diffuse structure of the indoor multipath components, let us approximate the LOS and NLOS multipath signal components as  $D$  components at  $D$  discrete time-delays uniformly distributed (with a time-delay resolution  $T_\delta$ , typically in the order of several ns), covering the channel delay spread for all the signals received by all the antennas. Therefore, in the following  $D_{m,n} = D - 1, \forall m, n$ , such that we can define the multipath rays' time-delays based on the LOS signal's time-delay as  $\tau_{m,n,d}(t) = \tau_{m,n,0}(t, \Phi_n) + dT_\delta$ . Based on the previous assumptions, let us now define the basis function  $b_m(t, \Phi_n, d)$  for the  $m$ -th satellite, the  $n$ -th antenna and the  $d$ -th ray as

$$\begin{aligned}
 b_m(t, \Phi_n, d) = \\
 g_m(t - \tau_{m,n,0}(t, \Phi_n) - dT_\delta) \exp\{j2\pi f_{m,n,0}(t, \Phi_n)t\},
 \end{aligned} \tag{4.2}$$

such that the signal model in (4.1) can be redefined as

$$\begin{aligned}
 x_n(t) = & \sum_{m=1}^M a_{m,n,0}(t) b_m(t, \Phi_n, 0) \\
 & + \sum_{m=1}^M \sum_{d=1}^{D-1} a_{m,n,d}(t) b_m(t, \Phi_n, d) + e_n(t).
 \end{aligned} \tag{4.3}$$

As mentioned earlier, the target herein is the fine estimation of the clock bias  $\delta t$  when considering the receiver's position is known *a priori* and a coarse estimation of  $\delta t$  and  $\delta \dot{t}$  is available. Based on this, the dependence of the signal model with  $\delta \dot{t}$ ,  $\mathbf{p}_0$  and  $\Delta \mathbf{p}_n$  is omitted from now on for simplicity (i.e.,  $b_m(t, \Phi_n, d) \triangleq b_m(t, \delta t, d) = b_m(t, \delta t - dT_\delta)$ ). The

dependence of all the received signals with the clock bias will be exploited later on for jointly estimating a fine version of  $\delta t$  in the clock bias domain.

Let us define now the vector  $\mathbf{x}_n = [x_n(t_0) \dots x_n(t_{K-1})]^T \in \mathbb{C}^{K \times 1}$  containing a signal snapshot of  $K$  samples received by the  $n$ -th antenna with a sampling period  $T_s = t_K - t_{K-1}$ . Assuming that  $a_{m,n,d}$ ,  $\tau_{m,n,d}$  and  $f_{m,n,0}$  parameters are constant during the observation time  $T_s K$  (note that, in practice, variations of  $\tau_{m,n,d}$  and  $f_{m,n,0}$  can be compensated based on the *a priori* known or estimated receiver's position and clock drift), the vector  $\mathbf{x}_n$  can be modeled as

$$\mathbf{x}_n \approx \mathbf{B}(\delta t) \mathbf{a}_{n,0} + \sum_{d=1}^{D-1} \mathbf{B}(\delta t - dT_\delta) \mathbf{a}_{n,d} + \mathbf{e}_n, \quad (4.4)$$

where the dependence with  $t$  has been omitted for simplicity,  $\mathbf{a}_{n,0} = [a_{1,n,0} \dots a_{M,n,0}]^T \in \mathbb{C}^{M \times 1}$  gathers the complex amplitudes for the  $M$  LOS contributions,  $\mathbf{a}_{n,d} = [a_{1,n,d} \dots a_{M,n,d}]^T \in \mathbb{C}^{M \times 1}$  gathers the complex amplitudes for the  $M$  NLOS contributions for the  $d$ -th discrete time-delay,  $\mathbf{e}_n \in \mathbb{C}^{K \times 1}$  is the complex noise vector (with  $\mathbf{e}_n \sim \mathcal{CN}(\mathbf{0}, \sigma^2 \mathbf{I})$ ), and  $\mathbf{B}(\delta t - dT_\delta) = [\mathbf{b}_1(\delta t - dT_\delta) \dots \mathbf{b}_M(\delta t - dT_\delta)] \in \mathbb{C}^{K \times M}$  is the basis function matrix for the  $d$ -th discrete time-delay, which is composed by the basis function vectors for each satellite  $\mathbf{b}_m(\delta t - dT_\delta) = [b_m(t_0, \delta t - dT_\delta) \dots b_m(t_{0+K-1}, \delta t - dT_\delta)]^T \in \mathbb{C}^{K \times 1}$ .

Keeping now in mind the later exploitation of the structure of the diffuse channel in the clock bias estimation (an exponential PDP of the diffuse multipath components is in general expected [Jos14]), let us define the vector  $\mathbf{h} \in \mathbb{R}^{D \times 1}$  containing the coefficients of the composite MIMO channel gathering the aggregated power contribution of the  $MN$  propagation channels for the  $D$  discrete time-delays of interest, such that  $[\mathbf{h}]_d \triangleq h_d \triangleq \sum_{n=1}^N \mathbf{a}_{n,d}^H \mathbf{a}_{n,d}$  is the  $d$ -th coefficient of the composite MIMO channel vector (with the coefficient  $h_0$  corresponding to the LOS contributions, which mark the actual receiver's clock bias to be estimated). Therefore, the composite MIMO channel gives a measure of the aggregated PDP for the MIMO channel. Each of the coefficients of the composite MIMO channel (one per time-delay) can be considered to follow an arbitrary and unknown PDF which in practice is going to be highly dependent on the indoor environment surrounding the receiver. It is to be noticed that the PDF per coefficient depends on the  $MN$  signal contributions received for the corresponding time-delay, with e.g., potentially different exponential PDPs for the  $MN$  indoor channels, and different attenuations of the LOS components.

### 4.3 Exploiting the spatial diversity

Several aspects need to be considered in the receiver's clock bias and channel estimation if targeting an accurate time synchronization in indoor conditions. First, GNSS signals received indoors are very weak [Sec12], so the estimation of the multipath components received for each of the GNSS signals is very challenging or unfeasible (indeed, both LOS and NLOS components are buried in noise). Therefore, a channel estimation per satellite is discarded. Second, the channel is expected to be spatially correlated. Thus, arrays of antennas may be exploited to obtain spatially correlated versions of the GNSS signals received indoors. Third, the indoor multipath channel is diffuse, with unresolvable multipath components, and is expected to follow an exponential PDP model highly dependent on the indoor environment [Jos14]. And, last but not least, the LOS signals expected to be received for each GNSS satellite are aligned in the clock bias domain (marking the time reference), while diffuse NLOS multipath components are received with a delay with respect to this reference to be estimated. Based on these aspects, the signals received by an array of antennas are proposed to be exploited for the estimation of a composite MIMO channel (as referred to in the text) embedding the aggregated contribution of  $MN$  propagation channels (with  $M$  satellites and  $N$  antennas) as a function of the time-delay with respect to the actual receiver's clock bias, as originally presented in [Gar18a]. Both transmission and reception diversities available in the MIMO-GNSS system are jointly exploited in order to improve the SNR conditions in which the estimator works. It is to be noticed that the composite MIMO channel gives a measure of the total aggregated power of all the received signal contributions as a function of the time-delay. Therefore, based on the estimation of the composite MIMO channel, an estimation of the receiver's clock bias can be derived (i.e., a joint estimation process can be performed).

Taking advantage of the relatively slow temporal decorrelation of the indoor channel (of the order of tens of seconds [Sat12]), a snapshot estimation of the composite MIMO channel is considered herein. The snapshot estimation approach will enable the straightforward application of the concept either continuously or with a certain duty cycle, allowing the adaptation of the computational burden of the implementation. Given the diffuse nature of the channel, the snapshot estimation is proposed to be performed based on a multi-hypothesis optimization problem in which different PDP models are evaluated based on Monte Carlo methods. Two different estimators are presented. The first one targets the direct fitting of the observed composite MIMO channel. The second estimator exploits the spatial correlation between the NLOS multipath components received by the different antennas as a way to reduce the spatially correlated miss-modeling errors.

### 4.3.1 Intermediate clock bias estimation

Let us consider the *a priori* coarse clock bias estimation  $\hat{\delta t}_c$  derived by the GNSS receiver with an arbitrary state-of-the-art estimator. This coarse estimation is to be refined in the following by the estimators proposed herein. In AWGN conditions and under the assumption of only LOS

signal components being received (i.e., no multipath present), we can use the MLE to start exploiting all the signals of the MIMO-GNSS system, defining an “intermediate” estimation of the clock bias as the optimization problem

$$\begin{aligned} \hat{\delta t}_{int} &= \arg \max_{\delta t} \hat{\Lambda}(\delta t) \\ s.t. \quad &|\delta t - \hat{\delta t}_c| < \varsigma, \end{aligned} \quad (4.5)$$

where  $\hat{\Lambda}(\delta t)$  is referred to as the estimated composite MIMO cross-correlation function evaluated for the receiver’s discrete clock bias  $\delta t$ , and  $\varsigma$  is a threshold defining the search space around  $\hat{\delta t}_c$  (being  $\varsigma$  dependent on the quality of  $\hat{\delta t}_c$ , expected to be of the order of tens or hundreds of ns). Based on the MIMO-GNSS system considered, the composite MIMO cross-correlation function can be derived as [Gar19a]

$$\hat{\Lambda}(\delta t) = \sum_{n=1}^N \hat{\theta}_n(\delta t), \quad (4.6)$$

where  $\hat{\theta}_n(\delta t)$  is the estimated composite MISO cross-correlation function for the  $n$ -th antenna defined as [Gar19a]

$$\hat{\theta}_n(\delta t) = \hat{\mathbf{r}}_{x_nb}^H(\delta t) \hat{\mathbf{R}}_{bb}^{-1}(\delta t) \hat{\mathbf{r}}_{x_nb}(\delta t), \quad (4.7)$$

with the cross-correlations for each of the receiver’s antennas defined as

$$\hat{\mathbf{r}}_{x_nb}(\delta t) \triangleq \mathbf{B}^H(\delta t) \mathbf{x}_n, \text{ and} \quad (4.8)$$

$$\hat{\mathbf{R}}_{bb}(\delta t) \triangleq \mathbf{B}^H(\delta t) \mathbf{B}(\delta t). \quad (4.9)$$

Therefore, the composite MIMO cross-correlation function can be obtained based on the output of the correlators implementing the matched-filtering operation in GNSS receivers. This will drastically ease the application of the concept based on state-of-the-art multi-correlator architectures. It is to be noticed that the term  $\hat{\mathbf{r}}_{x_nb}^H(\delta t) \hat{\mathbf{R}}_{bb}^{-1}(\delta t)$  in (4.7) corresponds to the

LS estimator of the complex amplitudes for the  $n$ -th antenna (i.e., a different weighting applies for each satellite-antenna pair depending on the corresponding SNR conditions). Moreover, the derivation of the composite MISO cross-correlation function in (4.7) can be simplified by approximating  $\widehat{\mathbf{R}}_{bb}(\delta t)$  as an identity matrix when the cross-correlations between the different GNSS signals can be considered approximately null. This simplification is exploited in the simulations performed in Section 4.4. The estimation  $\widehat{\delta t}_{int}$  obtained in (4.5) is referred to as the intermediate clock bias estimation since an improvement of the accuracy is expected with respect to the coarse estimation  $\widehat{\delta t}_c$  thanks to the joint exploitation of all the received signals in the MIMO-MLE estimator, but the composite MIMO channel estimation is not yet considered in the problem.

### 4.3.2 Exploiting the indoor channel properties

In indoor propagation conditions the estimated composite MIMO cross-correlation function will be distorted by the presence of NLOS multipath components, making the estimator in (4.5) not any more optimum. To deal with that, the receiver's clock bias is proposed to be jointly estimated with the composite MIMO channel, whose first coefficient actually marks the common time-delay of the  $MN$  LOS signals and, therefore, the receiver's clock bias. In the following, the estimation of the composite MIMO channel is proposed to be solved as a multi-hypothesis estimation problem in which different PDF assumptions for each coefficient of the composite MIMO channel are assessed.  $N_l$  hypotheses on the PDF followed by each of the coefficients are exploited in the estimation. Under the  $l$ -th hypothesis, the coefficients of the composite MIMO channel  $\{[\mathbf{h}]_d\}_{d=0}^{D-1}$  are considered to follow the arbitrary set of PDFs  $\{p([\mathbf{h}]_d)\}_{d=0}^{D-1} \triangleq \{p_{l,d}\}_{d=0}^{D-1}$ , with  $p_{l,d}$  the PDF for the  $l$ -th hypothesis and the  $d$ -th coefficient. Let us define the fine clock bias estimation  $\widehat{\delta t}_f$  based on the intermediate clock bias estimation  $\widehat{\delta t}_{int}$  from (4.5) and the integer offset  $\hat{\beta} \in \mathbb{Z}$  (to be estimated) as  $\widehat{\delta t}_f = \widehat{\delta t}_{int} - \hat{\beta}T_\delta$ . Based on this, the joint estimator of  $\mathbf{h}$  and  $\beta$  for the  $l$ -th hypothesis can be defined as the solution to the constrained optimization problem [Gar18a]

$$\begin{aligned} \hat{\mathbf{h}}_l, \hat{\beta}_l &= \arg \min_{\mathbf{h}, \beta} \|\widehat{\mathbf{Y}}(\mathbf{h}, \beta)\|^2 \\ &s. t. [\mathbf{h}]_d \sim p_{l,d}, \forall d \text{ and } |\beta| < W, \end{aligned} \quad (4.10)$$

where the miss-modeling error for the composite MIMO channel  $\widehat{\mathbf{Y}}(\mathbf{h}, \beta)$  is defined as [Gar18a]

$$\hat{\mathbf{Y}} = \hat{\mathbf{\Lambda}} - \kappa(\mathbf{h}) \left( \sum_{d=0}^{D-1} [\mathbf{h}]_d |\mathbf{s}(\hat{\delta t}_{int} - (\beta - d)T_\delta)|^2 \right) - \hat{\mathbf{w}}, \quad (4.11)$$

with  $\hat{\mathbf{\Lambda}} = [\hat{\Lambda}(\delta t_1) \dots \hat{\Lambda}(\delta t_Q)]^T \in \mathbb{R}^{Q \times 1}$  the estimated composite MIMO cross-correlation vector, which is uniformly sampling (with a time-delay resolution  $T_\delta$ ) the composite MIMO cross-correlation function  $\Lambda(\delta t)$  at  $Q$  clock bias values, being centered at the intermediate clock bias estimation  $\hat{\delta t}_{int}$ , such that  $\delta t_{(Q+1)/2} = \hat{\delta t}_{int}$ ;  $W \in \mathbb{N}$  constrains the values evaluated for the integer offset  $\beta$  (in total,  $N_w = 2W - 1$  values evaluated) based on the expected error of the intermediate clock bias  $\hat{\delta t}_{int}$ ;  $|\mathbf{s}(\hat{\delta t}_{int} - (\beta - d)T_\delta)|^2 \in \mathbb{R}^{Q \times 1}$  is a vector with the absolute square values of the samples of the reference correlation function (for the GNSS signal of interest) centered at the clock bias  $\hat{\delta t}_{int} - (\beta - d)T_\delta$ ; the factor  $\kappa(\mathbf{h})$ , defined as [Gar18a]

$$\kappa(\mathbf{h}) = \frac{\|\hat{\mathbf{\Lambda}} - \hat{\mathbf{w}}\|}{\left\| \sum_{d=0}^{D-1} [\mathbf{h}]_d |\mathbf{s}(\hat{\delta t}_{int} + dT_\delta)|^2 \right\|}, \quad (4.12)$$

is normalizing the composite MIMO channel contribution to the MIMO cross-correlation vector (which allows to define  $p_{l,0}$  normalized to 1, as discussed later on); and  $\hat{\mathbf{w}} = \hat{w}\mathbf{1} \in \mathbb{R}^{Q \times 1}$ , where  $\hat{w}$  is an estimation of the noise floor of the composite MIMO cross-correlation function (which can be derived e.g., as  $\hat{w} = \hat{\Lambda}(\hat{\delta t}_c + \vartheta)$ , with  $\vartheta > 2/T_c$  and  $T_c$  the chip period of the GNSS signals being considered).  $\hat{w}$  is introduced in the problem to compensate the squaring loss [Kap06] introduced in the estimation of the composite MIMO cross-correlation vector.

Taking into account that the optimization problem in (4.10) has no analytical solution, it is proposed to be solved via the application of Monte Carlo methods, being the coefficients of the composite MIMO channel vector  $\mathbf{h}$  treated as random variables drawn from the corresponding PDFs (with  $N_l$  PDF hypotheses for each of the coefficients of the composite MIMO channel, and  $N_c$  Monte Carlo runs assessed for each coefficient in each hypothesis). This way, the derivation of a physically plausible channel estimation (with diffuse multipath components with a certain PDP) is enforced, avoiding sparse channel solutions with few dominant components (as may be obtained when applying e.g., iterative approaches like SAGE-based algorithms [Fes94]). Additionally, the application of Monte Carlo methods allows a much more efficient implementation than grid-search methods [Kay13] (which is considered a non-practical approach in the diffuse channel estimation problem treated herein due to the large number of possible combinations to be evaluated). Algorithm 4.1 summarizes the proposed composite MIMO channel and fine clock bias estimation (in the following, this estimator is referred to as the MIMO-JTC estimator). Note that in step 3 the composite MIMO cross-correlation vector is

derived based on (4.6) to (4.9), such that the MIMO-JTC estimator is based on the cross-correlation estimations for each satellite-antenna pair. Therefore, the MIMO-JTC is naturally operating with the output correlation samples of multi-correlator receiver architectures. For the definition of the PDFs  $\{p_{l,d}\}_{d=0}^{D-1}$  the exponential PDP expected to be in general followed by the diffuse multipath channel for each pair satellite-antenna [Jos14] is proposed to be exploited. In practice, each of the  $MN$  indoor channels may be modeled by different exponential PDPs, with different relative powers and decay rates, as well as different delay spreads, depending on the geometry between each pair satellite-antenna [Jos14]. Moreover, in some cases attenuated LOS components may be received (e.g., via apertures in the walls in the case of light-indoor conditions), while in other cases only NLOS components can be received. In any case, in general a power decay as a function of the time-delay can be fairly expected for the composite MIMO channel. Based on this, a simplified PDF model is proposed herein in order to deal with different indoor scenarios and propagation conditions between the  $MN$  indoor channels. In particular, it is considered that, under the  $l$ -th hypothesis,  $p_{l,d} = U(0, \wp_l(d))$ , where  $\wp_l(d) = e^{-\eta_l d}$ ,  $d = 0, \dots, D - 1$ , with  $\eta_l \geq 0$  the decay rate (i.e.,  $p_{l,0}$  is normalized to 1 and a certain power decay vs. the time-delay is considered). With this approach the constraint in the optimization problem in (4.10) is in practice bounding the set of values that can be considered for each discrete time-delay, targeting to ensure that the estimated composite MIMO channel is in general physically plausible in indoor conditions (note that  $\kappa(\mathbf{h})$  is then normalizing the drawn samples to the composite MIMO cross-correlation vector). Despite the simplicity of this model, it will be shown that this approach allows to substantially improve the clock bias estimation accuracy with respect to the MIMO-MLE estimator in (4.5). Moreover, the approach can be made applicable to different indoor conditions by evaluating different hypotheses on the decay rate and delay spread.

### 4.3.3 Alternative exploitation of the spatial correlation of the NLOS multipath components

An alternative joint estimator of  $\mathbf{h}$  and  $\beta$  is defined in the following for directly exploiting the spatial correlation of the NLOS multipath components. This estimator is referred to as the MIMO-JTCC estimator. In this case, the composite MIMO channel is derived by minimizing the correlated miss-modeling errors between all the antennas (i.e., the errors introduced by the correlated NLOS multipath components between antennas). Let us first define the multipath miss-modeling errors  $\boldsymbol{\varepsilon}_n$  per antenna for the candidate composite MIMO channel vector being assessed as [Gar18a]

$$\hat{\boldsymbol{\varepsilon}}_n(\mathbf{h}, \beta) = \hat{\boldsymbol{\theta}}_n - \kappa_n(\mathbf{h}) \left( \sum_{d=0}^{D-1} [\mathbf{h}]_d |\mathbf{s}(\hat{t}_{int} - (\beta - d)T_\delta)|^2 \right) - \hat{\mathbf{v}}_n, \quad (4.13)$$

---

**Algorithm 4.1** MIMO-JTC estimator [Gar18a].

---

**Require:**  $\{\mathbf{x}_n\}_{n=1}^N$ ,  $\{\{b_m(t, \Phi_n)\}_{n=1}^N\}_{m=1}^M$ ,  $\delta t_c$ ,  $\varsigma$ ,  $N_l$ ,  $N_c$ ,  $W$ ,  $\{\{p_{l,d}\}_{d=0}^{D-1}\}_{l=1}^{N_l}$ ,  $Q$ ,  $D$ ,  $\mathbf{s}$ ,  $T_\delta$

**Output:**  $\hat{\mathbf{h}}$ ,  $\hat{\delta t}_f$

- 1: Initialize the minimum mean square error  $\xi_{min} = \infty$
  - 2: Estimate the intermediate clock bias  $\hat{\delta t}_{int}$  based on (4.5)
  - 3: Compute  $\hat{\Lambda} = [\hat{\Lambda}(\delta t_1) \dots \hat{\Lambda}(\delta t_Q)]^T$  based on (4.6) to (4.9)
  - 4: **for**  $l = 1$  to  $N_l$  **do**
  - 5:   **for**  $c = 1$  to  $N_c$  **do**
  - 6:     Draw the channel coefficients  $[\mathbf{h}_{l,c}]_d \sim p_{l,d}, \forall d$
  - 7:     **for**  $\beta = -W + 1$  to  $W - 1$  **do**
  - 8:        $\xi_{l,c,\beta} = \|\hat{\mathbf{Y}}(\mathbf{h}_{l,c}, \beta)\|^2$ , with  $\hat{\mathbf{Y}}(\mathbf{h}_{l,c}, \beta)$  based on (4.11)
  - 9:       **if**  $\xi_{l,c,\beta} < \xi_{min}$  **then**
  - 10:           $\xi_{min} = \xi_{l,c,\beta}$
  - 11:           $\hat{\mathbf{h}} = \mathbf{h}_{l,c}$
  - 12:           $\hat{\beta} = \beta$
  - 13:       **end if**
  - 14:     **end for**
  - 15:   **end for**
  - 16: **end for**
  - 17:  $\hat{\delta t}_f = \hat{\delta t}_{int} - \hat{\beta}T_\delta$
- 

where the factor  $\kappa_n(\mathbf{h})$ , defined as [Gar18a]

$$\kappa_n(\mathbf{h}) = \frac{\|\hat{\boldsymbol{\theta}}_n - \hat{\mathbf{v}}_n\|}{\left\| \sum_{d=0}^{D-1} [\mathbf{h}]_d |\mathbf{s}(\hat{\delta t}_{int} + dT_\delta)|^2 \right\|}, \quad (4.14)$$

is normalizing the composite MIMO channel contribution to the  $n$ -th antenna;  $\hat{\mathbf{v}}_n = \hat{v}_n \mathbf{1} \in \mathbb{R}^{Q \times 1}$ , where  $\hat{v}_n$  is an estimation of the noise floor of the composite multiple-input single-output (MISO) cross-correlation function for the  $n$ -th antenna (which can be derived as e.g.,  $\hat{v}_n = \hat{\theta}_n(\hat{\delta t}_c + \vartheta)$ , with  $\vartheta > 2/T_c$  and  $T_c$  the chip period of the GNSS signals being considered); and  $\hat{\boldsymbol{\theta}}_n = [\hat{\theta}_n(\delta t_1) \dots \hat{\theta}_n(\delta t_Q)]^T \in \mathbb{R}^{Q \times 1}$  is the estimated composite MISO cross-correlation vector for the  $n$ -th antenna, which is uniformly sampling the composite cross-correlation function  $\theta_n(\delta t)$  at  $Q$  clock bias values, with  $\hat{\theta}_n(\delta t)$  defined in (4.7). Based on the estimated multipath miss-modeling errors  $\hat{\boldsymbol{\epsilon}}_n$  we can derive a spatial covariance matrix  $\hat{\mathbf{C}}_\epsilon(\mathbf{h}, \beta) = \hat{\mathbf{E}}(\mathbf{h}, \beta) \hat{\mathbf{E}}(\mathbf{h}, \beta)^T$ , with  $\hat{\mathbf{E}}(\mathbf{h}, \beta) = [\hat{\boldsymbol{\epsilon}}_1(\mathbf{h}, \beta) \dots \hat{\boldsymbol{\epsilon}}_N(\mathbf{h}, \beta)]^T \in \mathbb{R}^{Q \times N}$  a matrix containing the vectors with  $\hat{\boldsymbol{\epsilon}}_n$  for each antenna. The departure from diagonal of  $\mathbf{C}_\epsilon$  gives a measure of the presence of spatially correlated multipath components not being modeled by the candidate composite MIMO channel model. Based on this, the joint estimator can be defined as the solution to the constrained optimization problem [Gar18a]

$$\begin{aligned} \hat{\mathbf{h}}_l, \hat{\beta}_l &= \arg \min_{\mathbf{h}, \beta} \hat{\gamma}(\mathbf{h}, \beta) \\ \text{s. t. } [\mathbf{h}]_d &\sim p_{l,d}, \forall_d \text{ and } |\beta| < W, \end{aligned} \quad (4.15)$$

where  $\hat{\gamma}$ , in charge of measuring the departure from diagonal of  $\hat{\mathbf{C}}_\epsilon$ , can be defined as [Clo09]

$$\hat{\gamma}(\mathbf{h}, \beta) = \frac{\frac{1}{N} \sum_{n=1}^N \hat{\lambda}_n(\mathbf{h}, \beta)}{(\prod_{n=1}^N \hat{\lambda}_n(\mathbf{h}, \beta))^{1/N}}, \quad (4.16)$$

where  $\hat{\lambda}_n(\mathbf{h}, \beta)$  is the  $n$ -th eigenvalue associated to  $\hat{\mathbf{C}}_\epsilon(\mathbf{h}, \beta)$ . Algorithm 4.2 summarizes the composite MIMO channel and fine clock bias estimation based on the MIMO-JTCC estimator. The definition of the PDFs  $p_{l,d}$  used as input is equivalent to the MIMO-JTC estimator.

#### 4.3.4 Implementation aspects of the proposed indoor timing solutions

As mentioned earlier, the time estimators presented in this chapter (i.e., MIMO-MLE, MIMO-JTC and MIMO-JTCC estimators) are well suited for their implementation at post-correlation level in parallel to state-of-the-art timing receivers, exploiting existing multi-correlator tracking architectures (note that the proposed estimators are derived based on the correlation samples for each satellite-antenna pair). The target of the proposed techniques is the refinement of the

---

**Algorithm 4.2** MIMO-JTCC estimator [Gar18a].

---

**Require:**  $\{\mathbf{x}_n\}_{n=1}^N$ ,  $\{\{b_m(t, \Phi_n)\}_{n=1}^N\}_{m=1}^M$ ,  $\delta t_c$ ,  $\varsigma$ ,  $N_l$ ,  $N_c$ ,  $W$ ,  $\{\{p_{l,d}\}_{d=0}^{D-1}\}_{l=1}^{N_l}$ ,  $Q$ ,  $D$ ,  $\mathbf{s}$ ,  $T_\delta$

**Output:**  $\hat{\mathbf{h}}$ ,  $\hat{\delta t}_f$

- 1: Initialize  $\gamma_{min} = \infty$
  - 2: Estimate the intermediate clock bias  $\hat{\delta t}_{int}$  based on (4.5)
  - 3: Compute  $\hat{\boldsymbol{\theta}}_n = [\hat{\theta}_n(\delta t_1) \dots \hat{\theta}_n(\delta t_Q)]^T$  based on (4.7)  $\forall_n$
  - 4: Compute  $\hat{\boldsymbol{\Lambda}} = [\hat{\Lambda}(\delta t_1) \dots \hat{\Lambda}(\delta t_Q)]^T$  based on (4.6) to (4.9)
  - 5: **for**  $l = 1$  to  $N_l$  **do**
  - 6: **for**  $c = 1$  to  $N_c$  **do**
  - 7: Draw the channel coefficients  $[\mathbf{h}_{l,c}]_d \sim p_{l,d}, \forall_d$
  - 8: **for**  $n = 1$  to  $N$  **do**
  - 9: Compute  $\kappa_n(\mathbf{h}_{l,c})$  based on (4.14)
  - 10: **end for**
  - 11: **for**  $\beta = -W + 1$  to  $W - 1$  **do**
  - 12: **for**  $n = 1$  to  $N$  **do**
  - 13: Compute  $\boldsymbol{\varepsilon}_{l,c,\beta,n} = \boldsymbol{\varepsilon}_n(\mathbf{h}_{l,c}, \beta)$  based on (4.13)
  - 14: **end for**
  - 15: Form  $\mathbf{E}_{l,c,\beta} = [\boldsymbol{\varepsilon}_{l,c,\beta,1} \dots \boldsymbol{\varepsilon}_{l,c,\beta,N}]^T$
  - 16:  $\mathbf{C}_{l,c,\beta} = \mathbf{E}_{l,c,\beta} \mathbf{E}_{l,c,\beta}^T$
  - 17: Estimate the eigenvalues  $\{\lambda_n\}_{n=1}^N$  of  $\mathbf{C}_{l,c,\beta}$
  - 18: Compute  $\gamma_{l,c,\beta} = \gamma(\mathbf{h}_{l,c}, \beta)$  based on (4.16)
  - 19: **if**  $\gamma_{l,c,\beta} < \gamma_{min}$  **then**
  - 20:  $\gamma_{min} = \gamma_{l,c,\beta}$
  - 21:  $\hat{\mathbf{h}} = \mathbf{h}_{l,c}$
  - 22:  $\hat{\beta} = \beta$
  - 23: **end if**
  - 24: **end for**
  - 25: **end for**
  - 26: **end for**
  - 27:  $\hat{\delta t}_f = \hat{\delta t}_{int} - \hat{\beta} T_\delta$
-

clock bias estimation performed by state-of-the-art receivers by mitigating the impact of the indoor multipath channel. The MIMO-MLE can be seen as an intermediate improved solution of state-of-the-art timing solutions, and can be additionally used to reduce the search space of the MIMO-JTC and MIMO-JTCC. Although computationally more demanding than the MIMO-MLE, the MIMO-JTC and MIMO-JTCC will provide the ultimate timing performance by considering the estimation of the composite MIMO channel. Taking advantage of the slow temporal decorrelation of the indoor channel for a static receiver [Sat12], the estimators can be applied per signal snapshot with a certain duty cycle (e.g., snapshots of tens or hundreds of ms processed every several seconds or even tens of seconds), allowing to limit the computational burden of the proposed solutions depending on the available processing resources. Additionally, the slow temporal decorrelation may allow as well the relaxation of the processing time requirements. This may enable the remote processing of the signal snapshots (e.g., in the Cloud [Luc16], [Gar17c]), offloading the local receiver from the processing required by the proposed techniques, and mitigating the impact of the indoor multipath with a certain latency.

## 4.4 Simulation results

The joint time and composite MIMO channel estimators proposed in the previous section (i.e., the MIMO-JTC and MIMO-JTCC estimators) have been simulated via a semi-analytical approach at post-correlation level when considering BPSK(1) signals being transmitted by the GNSS satellites (as e.g., in GPS L1 C/A, which is commonly used as baseline signal in current mass-market receivers). Additionally, the intermediate timing solution based on the MIMO-MLE and a reference solution based on a conventional WLS solution have also been assessed in order to understand the benefit introduced by the proposed methods. A single snapshot estimation is considered in all cases. The realistic wideband satellite-to-indoor channel model in the Recommendation ITU-R P.681 [ITU17] has been used to simulate the propagation conditions in two indoor scenarios: one for light-indoor conditions (in a room with windows), and another one for indoor conditions (in a room without windows, where only NLOS signals can be received). The simulated light-indoor scenario is illustrated in Fig. 4.1, where the location of the receiver antennas is indicated (for the indoor case, the same scenario without windows is simulated). It is to be noticed that the spatial correlations between the signals received for each antenna are considered in this model, such that the actual gain introduced by the exploitation of arrays of antennas in indoor propagation conditions can be assessed in a realistic way. In both scenarios a static receiver with 1, 4 and 8 antennas (with a common receiver clock) following the array configurations depicted in Fig. 4.2 are considered. No phase calibration is considered in the array of antennas. The reference SNR at post-correlation level per satellite LOS signal (when not considering yet the channel) is 35 dB for all the satellites (equivalent to a post-correlation C/No of 45 dB-Hz for a coherent integration period of 100 ms). In both light-indoor and indoor conditions the simulated channel introduces an important

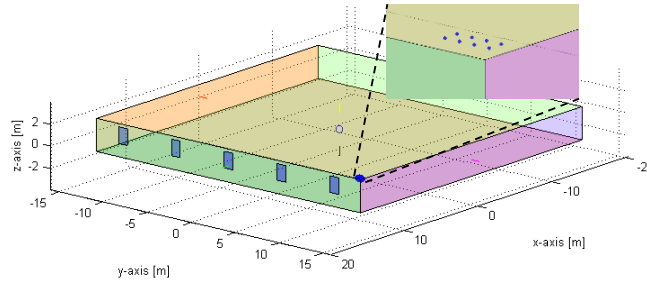


Fig. 4.1. Simulated scenario for the light-indoor conditions (room with windows), with the antenna array place in the ceiling of a corner of the room (see [ITU17], [Jos14]). For the indoor conditions, the same scenario without windows is considered.

degradation of the power of the LOS signal components, if present at all (typically attenuations above 20-30 dB are observed, depending on the scenario, satellite, and antenna). Additionally, an important number of NLOS multipath components are simulated by the channel per satellite and antenna (typically several tens or hundreds of NLOS components), with delay spreads of the order of hundreds or few hundreds of ns, depending on the propagation conditions for each satellite-antenna pair. Eleven satellites above the horizon are simulated in a representative geometric configuration resulting in an HDOP equal to one. Fig. 4.3 illustrates the indoor channel conditions simulated, showing an example of the discrete channel impulse response (CIR) per satellite for one of the receiver antennas. For each satellite, the CIR contains the relative power and delay of all the received multipath rays with respect to the ideal LOS signal that would be obtained in the absence of the channel. As can be observed, the impact of fading

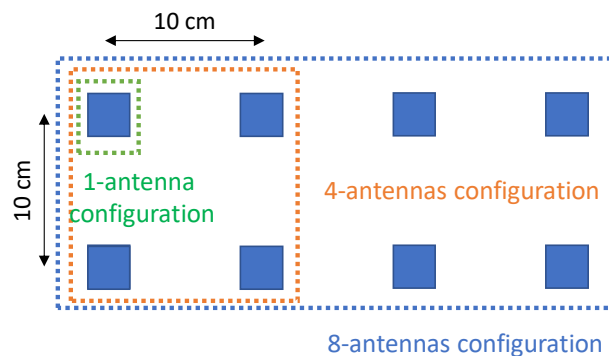


Fig. 4.2. Antenna array configurations considered in the simulations.

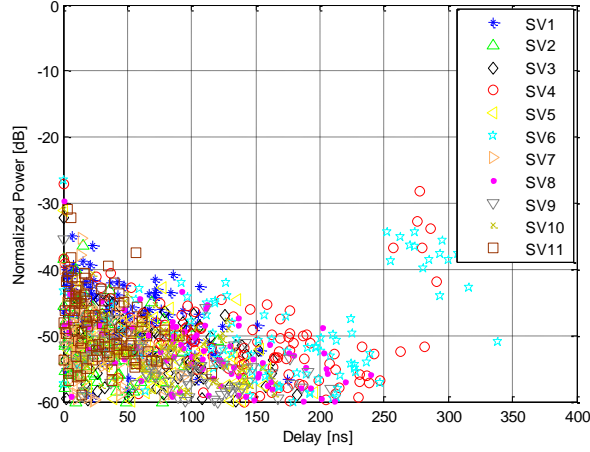


Fig. 4.3. Illustration of the simulated indoor propagation conditions. Example of the relative power and delay of the multipath components per satellite vehicle (SV) received by the antenna considered in the 1-antenna configuration (see Fig. 4.1) in the light-indoor scenario.

on the LOS signal is very important (all the LOS signals are attenuated more than 25 dB in the example), and a very important number of multipath rays are received (which will explain the important impact of the channel on the clock bias estimation). It is to be noticed that the discrete CIR for each satellite-antenna pair obtained are exploited directly at post-correlation level in the simulations. Therefore, the cross-correlation function for each satellite-antenna pair is derived as the sum of the cross-correlation contributions of all the multipath rays (each with a given complex amplitude and delay). This allows the direct generation of the cross-correlation vectors  $\hat{\mathbf{r}}_{x_{nb}}(\delta t)$  for each of the antennas, as defined in (4.8), used then for generating the composite MISO cross-correlation exploited by all the estimators proposed.

System errors (e.g., satellites' clock and orbit errors) and atmospheric errors (e.g., ionospheric and tropospheric errors) are not included in the simulations. The simulation parameters considered in the MIMO-JTC, MIMO-JTCC and MIMO-MLE estimators are summarized in Table 4.1 (same configuration used for comparison). It is to be noticed that only 2 hypotheses are evaluated in the MIMO-JTC and MIMO-JTCC estimators (i.e.,  $N_l = 2$ ). For each of the hypotheses, a different delay spread of the channel is considered: 230 ns and 460 ns. This is defined in Table 4.1 based on the number of discrete time-delays ( $D$ ) and the time-delay resolution ( $T_\delta$ ). The corresponding decay rate ( $\eta_l$ ) considered in the exponential model is also indicated. Note that since only 2 hypotheses are considered, the delay spreads are chosen based on lower and upper values typically expected for the composite MIMO channel. 10 Monte Carlo runs are used for each of the two hypotheses (i.e.,  $N_c = 10$ ) in order to limit the

computational burden of the implemented solutions. Although a larger number of hypotheses and Monte Carlo runs may result in improved performance of the estimators, this configuration will show to be enough to achieve an improved estimation of the receiver clock bias (removing part of the bias introduced by the indoor channel in the MIMO-MLE solution). Regarding the values evaluated for the integer offset  $\beta$ ,  $N_w = 21$  integer offsets are considered by the MIMO-JTC and MIMO-JTCC estimators (i.e., the search area around the intermediate clock bias estimation is constrained to  $\pm 115$  ns in order to limit the computational burden). In the reference WLS solution, the individual pseudorange measurements are derived from the estimation of the maximum of the cross-correlation function of the BPSK signal for each satellite (which corresponds to the MLE of the pseudorange) when considering a correlation span of  $\pm 1$  chip. For each simulated scenario 300 Monte Carlo simulation runs are considered for the derivation of the results presented.

The RMSE of the clock bias estimated with the methods proposed (i.e., the intermediate MIMO-MLE solution, and the MIMO-JTC and MIMO-JTCC estimators) in the light-indoor scenario is shown in Fig. 4.4 with respect to the number of antennas considered in the solutions, together with the results obtained for the conventional WLS-based approach with one antenna.

| Parameter  | Value          |
|--|----------------|
| Modulation   | BPSK(1)        |
| Receiver BW  | 5 MHz          |
| Number of satellites ( $M$ )                                     | 11             |
| Number of antennas ( $N$ )                                       | [1, 4, 8]      |
| Propagation conditions   | (light-)indoor |
| Number of hypotheses ( $N_l$ )                                   | 2              |
| Number of discrete time-delays ( $D$ )                           | [20, 40]       |
| Decay rate ( $\eta_l$ )  | [0.29, 0.14]   |
| Number of Monte Carlo runs ( $N_c$ )                             | 10             |
| Number of integer offsets ( $N_w$ )                              | 21             |
| Time-delay resolution ( $T_\delta$ )                             | 11.5 ns        |
| Number samples of the composite cross-correlation vector ( $Q$ ) | 103            |

Table 4.1. Summary of simulation parameters.

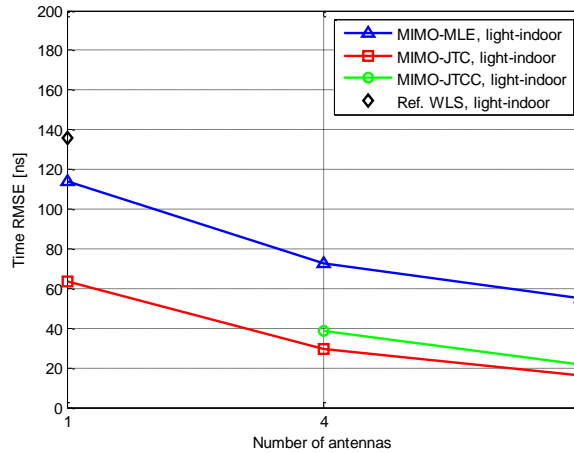


Fig. 4.4. RMSE of the clock bias estimated with the methods proposed for a receiver featuring 1, 4 and 8 antennas in light-indoor propagation conditions.

As can be observed, the usage of the MIMO-MLE estimator in the light-indoor scenario enables already an important improvement of the timing accuracy thanks to the exploitation of the spatial diversity introduced by the array of antennas, with an RMSE below 60 ns for the 8-antennas configuration. The introduction of the composite MIMO channel in the MIMO-JTC and MIMO-JTCC estimators allows to further reduce the timing error with respect to the MIMO-MLE. This shows that the simplified hypotheses considered herein to constrain the estimated composite MIMO channel to physically plausible values are enough to improve the timing accuracy in indoor conditions (even with a relatively low number of Monte Carlo runs considered in the estimation). Looking at the results for the single-antenna configuration, it is observed that the MIMO-MLE solution improves the accuracy with respect to the reference WLS solution, and the application of the MIMO-JTC allows to get even better timing results, with an error around 60 ns thanks, again, to the exploitation of the composite MIMO channel. Indeed, it is observed that the MIMO-JTC results for the single-antenna configuration are approximately in line with the results for the MIMO-MLE in the 8-antennas configuration. In general, it is observed that the introduction of additional antennas in the receiver for all the proposed estimators enables an improvement of the timing accuracy per estimator, at least in the light-indoor scenario simulated. Indeed, the introduction of new antennas to a baseline set of antennas (i.e., the availability of further spatial diversity) is in general expected to be beneficial in the timing estimation so far the signals received through these new antennas are in similar or better propagation conditions than the baseline set (i.e., for clearly worse propagation conditions there might be no benefit). Comparing the MIMO-JTC and MIMO-JTCC estimators, slightly better results are obtained for the first. For the 8-antennas configuration both estimators result in very similar performances, with an RMSE around 20 ns.

This accuracy is substantially better than the almost 140 ns obtained for the reference WLS solution (with 1 antenna).

Fig. 4.5 shows the RMSE results obtained for the indoor scenario. In this case, the degradation introduced by the channel is higher due to the absence of windows in the simulated indoor conditions, resulting in general in worse results for all the estimators. Additionally, the gain introduced by the spatial diversity seems to be lower than for the light-indoor scenario. The exploitation of the composite MIMO channel is shown to be advantageous. Indeed, it is observed that the RMSE for the MIMO-JTC estimator in the single-antenna configuration (around 80 ns) is lower than the one obtained by the MIMO-MLE in the 8-antennas configuration (around 110 ns). The performance differences between the MIMO-JTC and MIMO-JTCC estimators are reduced with respect to the light-indoor scenario, resulting in a similar RMSE slightly below 50 ns for the 8-antennas configuration.

In order to further understand the RMSE results obtained, Fig. 4.6 shows a comparison of the histogram of the clock bias error obtained with the MIMO-MLE, the MIMO-JTC and the MIMO-JTCC estimators for the case of 4 antennas in the light-indoor scenario (equivalent results are shown in Fig. 4.7 for 8 antennas). As can be observed, the MIMO-JTC and MIMO-JTCC estimators reduce the bias introduced by the channel with respect to the MIMO-MLE. This clearly shows the benefit introduced by the estimation of the composite MIMO channel. It can be also observed that the dispersion of the errors is slightly lower for the MIMO-JTC estimator, explaining the lower RMSE errors obtained in Fig. 4.4. A similar conclusion is obtained for the case of 8 antennas in Fig. 4.7, but in this case further reducing the bias thanks to the availability of a higher spatial diversity (since more signals received in slightly different

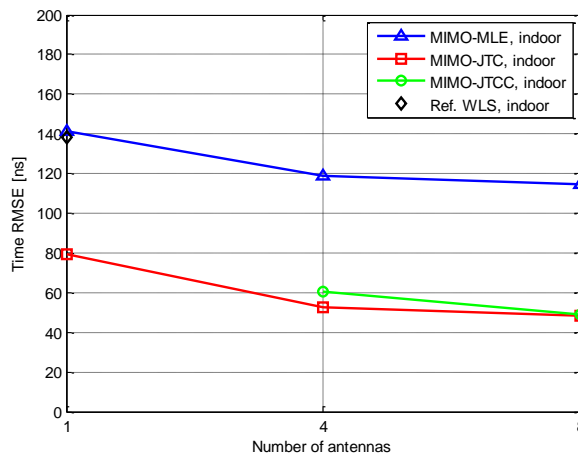


Fig. 4.5. RMSE of the clock bias estimated with the methods proposed for a receiver featuring 1, 4 and 8 antennas in indoor propagation conditions.

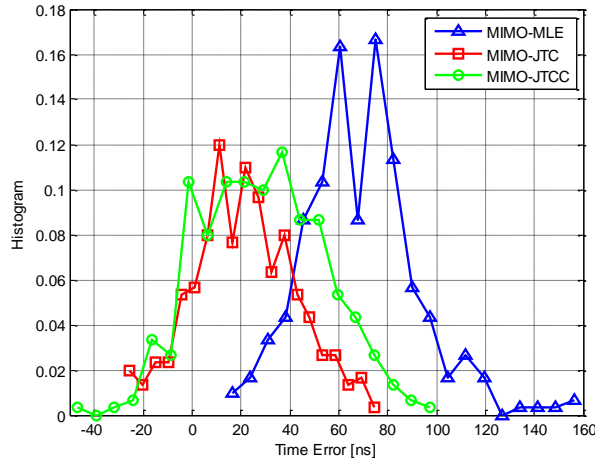


Fig. 4.6. Histogram of the clock bias error obtained with the estimators proposed in the configuration with 4 antennas for the light-indoor scenario.

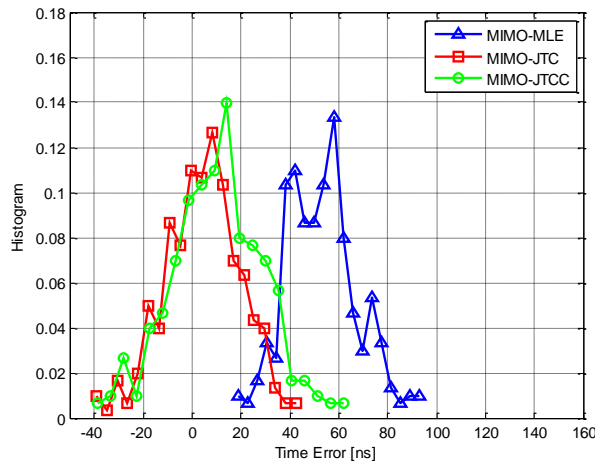


Fig. 4.7. Histogram of the clock bias error obtained with the estimators proposed in the configuration with 8 antennas for the light-indoor scenario.

propagation conditions can be jointly exploited). Fig. 4.8 shows equivalent results for the indoor scenario in a room without windows. In this case, results are also improved with respect to the MIMO-MLE, but it can be observed that the residual bias is bigger than for the light-indoor scenario. This is considered to be a result of the worse propagation conditions, with only NLOS components received and worse SNR conditions in which the estimators need to operate.

To explain the differences observed between the MIMO-JTC and MIMO-JTCC estimators, Fig. 4.9 shows the relative miss-modeling errors of the estimated composite MIMO channel

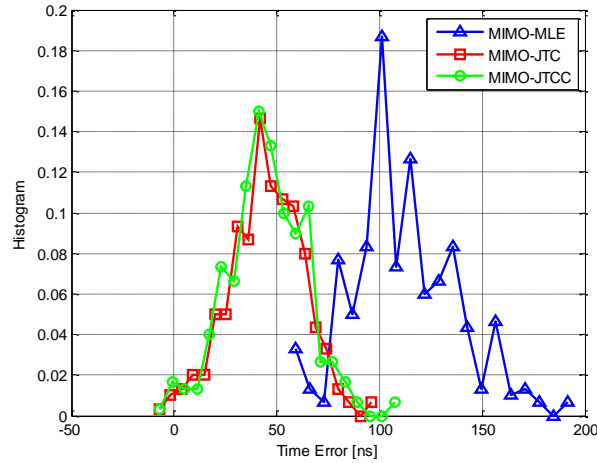


Fig. 4.8. Histogram of the clock bias error obtained with the estimators proposed in the configuration with 8 antennas for the indoor scenario.

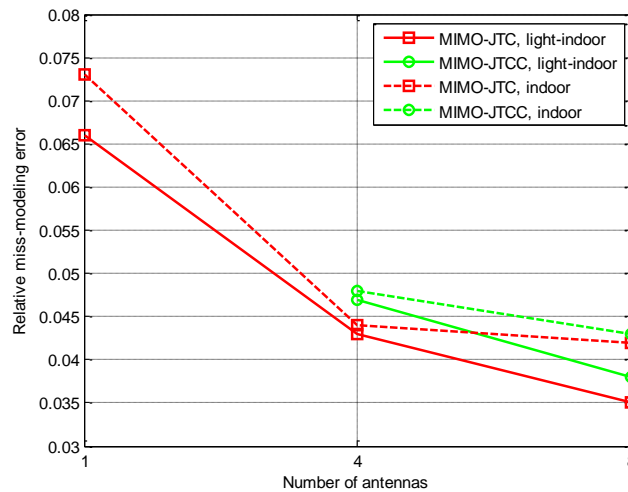


Fig. 4.9. Comparison of the relative miss-modeling error of the estimated composite MIMO channel with the MIMO-JTC and MIMO-JTCC estimators for both light-indoor and indoor scenarios.

obtained in both cases (indicating how well we are estimating the channel). As can be observed, the channel estimation error is lower for the MIMO-JTC than for the MIMO-JTCC in both light-indoor and indoor conditions; and is lower in light-indoor conditions than in the indoor conditions, and when the number of antennas increases (in line with the RMSE results obtained). These results indicate that the contribution of NLOS multipath components spatially not correlated cannot be neglected in the problem. Thus, focusing only on the minimization of

the impact of the correlated NLOS multipath components between antennas does not result in the best performance (at least for the indoor conditions simulated). Therefore, it appears to be more beneficial to exploit the spatial diversity for improving the equivalent SNR conditions in which the joint composite MIMO channel and time estimator operates, as is done in the MIMO-JTC estimator.

Last, but not least, Fig. 4.10 shows an estimation of the computational burden of the MIMO-JTC and MIMO-JTCC estimators as a factor of the computational burden of the MIMO-MLE in a single antenna configuration (i.e., the MISO-MLE). This estimation has been derived based on the processing time of the simulation of each of the estimators. As can be observed, for the 8-antennas configuration the MIMO-JTC is around three times more computationally demanding than the MIMO-MLE for the same number of antennas (and around 22 times with respect to the MISO-MLE). In the case of the MIMO-JTCC this factor is drastically increased. Therefore, the MIMO-JTC is not only outperforming the MIMO-JTCC in terms of timing performance, but also in terms of computational burden. And although the computational burden for the MIMO-JTC is higher than for the MIMO-MLE, the improved timing performance can justify its usage in certain indoor applications.

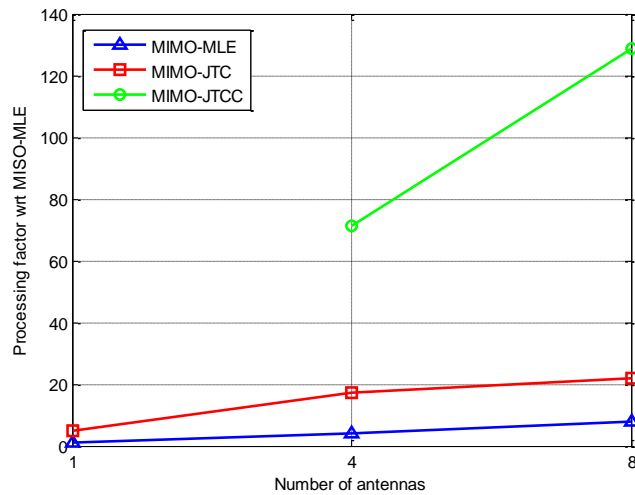


Fig. 4.10. Processing factor for the proposed estimators in different antenna configurations with respect to the MISO-MLE (MIMO-MLE with 1 antenna).

## 4.5 Conclusions

The indoor time synchronization problem based on GNSS signals has been discussed in this chapter. In particular, a novel joint time and composite MIMO channel estimation approach has been proposed in order to mitigate the important degradation introduced by blockage and multipath effects in the timing solution provided by state-of-the-art indoor GNSS receivers. The simulation results obtained with a realistic wideband satellite-to-indoor channel model show that the exploitation of the spatial diversity introduced by arrays of antennas, together with the estimation of the composite MIMO channel in the proposed estimators, allows an important mitigation of the indoor multipath. Timing accuracies below 50 ns are demonstrated to be feasible in both light-indoor and indoor conditions. Therefore, the proposed estimation approach is considered an appealing solution for indoor applications with tight synchronization requirements, as can be the case in indoor small cells for 5G.

# 5

## From Co-located to Distributed Array Solutions

**T**HE exploitation of GNSS signals for positioning applications in harsh propagation conditions like urban or indoor scenarios is still a very challenging topic due to the dominant impact of the propagation conditions. Indeed, the usage of GNSS indoors may result in positioning errors in the order of tens or even hundreds of meters. Thus, other technologies may be exploited together with, or as alternative to, state-of-the-art GNSS receivers to improve the availability and accuracy of the final positioning solution in challenging propagation conditions.

This thesis proposes to exploit the MIMO-GNSS framework for positioning in harsh propagation conditions. First, the MIMO-MLE solution derived in Chapter 3 is exploited in indoor conditions. Then, a novel distributed array processing approach for collaborative GNSS-

based snapshot positioning in harsh propagation conditions is proposed. The spatial diversity introduced by the distributed receivers is proposed to be exploited by jointly processing in the position domain all the GNSS signals received by all the receivers. This is equivalent to derive the collaborative position as the solution of a distributed or collaborative MIMO-GNSS (Co-MIMO-GNSS) problem. In order to significantly reduce the computational burden of this approach (which otherwise would be too high), the positioning problem needs to be constrained by the structure of the distributed array (which defines the spatial distribution of all the receivers). Therefore, the distributed array needs to be first formed based on the peer-to-peer ranges between all the receivers (potentially also aided by the coarse position estimation of some of them). Based on this, taking one of the receivers as anchor (e.g., the receiver with the best estimated accuracy, or a receiver in a fixed known location), the collaborative positioning problem can be transformed into a collaborative angle estimation problem in the horizontal position plane (i.e., a 1D problem).

This chapter is organized as follows. Section 5.1 presents the background and motivation. Section 5.2 briefly discusses the exploitation of co-located antennas for indoor positioning in the MIMO-GNSS framework, and presents the simulation results obtained in this case. Then, Section 5.3 introduces the exploitation of distributed receivers for the formation of distributed arrays of antennas, and simulation results are presented. Finally, Section 5.4 presents the conclusions.

The material presented in this chapter has been partially published by the author in [Gar17b], [Gar17c], [Gar18b], [Gar18c], and [Gar19c].

### 5.1 Background and motivation

GNSS signals are broadly used for positioning in different applications and use cases, including important market segments like LBS [GNS17]. Moreover, GNSS is expected to play a key role in IoT applications where positioning may be required only from time to time. In this context, elements like the energy required to derive a position fix by the receiver, and the achievable accuracy and availability of the position fix when required by the application, independently of the scenario in which the receiver is operating, are expected to be key drivers in the design of the positioning solutions. Indeed, current mass-market receivers may operate either in continuous tracking mode, or applying a certain duty-cycling in order to save power (being the receiver engine active only a portion of the time), targeting a certain position accuracy while maintaining the power consumption as low as possible. Another possible approach to meet some of the IoT requirements is the application of snapshot positioning, targeting the exploitation of limited periods of signal around the time instant in which the position fix is needed [Sec12]. The snapshot positioning may be performed either locally at the receiver, or remotely in the Cloud, offloading the receiver from the position estimation process [Luc16],

[Gar17c]. This latest option can be additionally of interest to exploit advanced assistance information (e.g., 3D or fingerprint maps) in the processing of the received signal; or for the exploitation of the signal snapshots in other applications (e.g., jamming and spoofing localization) when multiple receivers are jointly processed [Gar16b], [Gar17c].

Typically, the exploitation of GNSS signals outdoors is not a problem. Nevertheless, the exploitation of GNSS signals in harsh propagation conditions typical of urban or indoor scenarios is a very challenging topic. Indeed, in these scenarios the observed C/No conditions may be very low, and the impact of NLOS signal propagation conditions can be dominant, highly degrading the position solution or making not possible the derivation of a position fix [Sec12], [Ste03], [Hei08]. Moreover, this may limit the application of power-save modes in mass-market receivers since applying a certain duty-cycling is equivalent to a reduction of the SNR conditions observed by the receiver.

Different techniques and architectures have been proposed in the literature in order to try to improve the exploitation of GNSS signals in harsh propagation conditions. Among those, we can find high-sensitivity and multipath estimation and mitigation techniques operating at satellite signal level [Pan09], [Sah08], [Clo08], [Bro11a]; advanced techniques like vector tracking loops [Las09] and direct position estimators [DiE07], [Clo07], [Clo09a], [Clo09b] operating directly at position level; array-based techniques exploiting the spatial diversity provided by different co-located antennas [Sec05], [Fer09a], [Fer09b], [Fer16]; cooperative and collaborative techniques exploiting the GNSS observables or signals from different receivers in nearby locations, together with the estimated ranges (i.e., distances) between those receivers [Gare12a], [Gare12b], [Sol13], [And18]; or hybrid positioning techniques focusing on the fusion of GNSS estimations with other sensors and/or signals of opportunity in order to try to improve the availability and/or accuracy provided by the GNSS-only solution [Per18].

Among the previous techniques, the exploitation of direct position estimators and array-based techniques may allow to overcome the limitations of high-sensitivity and multipath mitigation techniques working at single-satellite level. This is achieved by not only exploiting the time diversity (e.g., longer coherent and non-coherent integration times can be exploited to improve the acquisition sensitivity; and filtering in the time domain can be exploited both at tracking and positioning levels), but also the spatial diversity introduced by multiple GNSS satellites and/or receiver antennas. This can be implemented via the application of the MIMO-MLE position solution discussed in Chapter 3. Even if computationally demanding, this solution may be applied remotely in the Cloud, offloading the receiver from the MIMO-GNSS processing. The application of the MIMO-GNSS approach in indoor conditions is discussed in Section 5.2 for co-located arrays of antennas, as originally presented in [Gar18b].

Also exploiting the spatial diversity, but in this case from different receivers, cooperative and collaborative positioning is a promising approach to enable the ubiquitous, accurate and precise positioning of receivers in urban and indoor conditions [Gare12a], [Gare12b], [Sol13], [And18]. The basic idea of this approach consists in the exploitation of the GNSS observables or signals from different receivers in nearby locations (e.g., receivers separated by several

meters or tens of meters), together with the estimated ranges between the receivers (i.e., the peer-to-peer ranges). A broad application of the collaborative positioning approach may be feasible in the near future thanks to the fast evolution of 5G standards and V2V/V2X communications [3GP19], [5G16], as well as the availability of UWB-based and Wi-Fi RTT range estimation solutions [Guv18], [Au16]. Section 5.3 proposes a collaborative positioning approach in the MIMO-GNSS framework based on GNSS signal snapshots from distributed receivers in harsh propagation conditions, as presented in [Gar19c].

## 5.2 The MIMO-GNSS solution indoors

Let us consider the MIMO-GNSS system of Fig. 5.1, with a receiver featuring an array of antennas operating in indoor conditions, and the availability of a coarse position solution  $\hat{\mathbf{p}}_c$ . For simplicity, let us reuse the signal model exploited in Section 3.3.2 to reformulate the MIMO-MLE position solution indoors as the optimization problem

$$\begin{aligned} \hat{\mathbf{p}}_0 &= \arg \max_{\mathbf{p}_0} \Lambda(\mathbf{p}_0) \\ \text{s. t. } &\|\mathbf{p}_0 - \hat{\mathbf{p}}_c\| < \psi, \end{aligned} \quad (5.1)$$

where, equivalently to (3.30), the cost function is defined as

$$\Lambda(\mathbf{p}_0) = \sum_{n=1}^N \hat{\mathbf{r}}_{xnb}^H(\mathbf{p}_0 - \Delta\mathbf{p}_n) \hat{\mathbf{R}}_{bb}^{-1}(\mathbf{p}_0 - \Delta\mathbf{p}_n) \hat{\mathbf{r}}_{xnb}(\mathbf{p}_0 - \Delta\mathbf{p}_n), \quad (5.2)$$

$\psi$  defines the search area around the coarse position estimation (in this case, easily in the order of tens or even hundreds of meters), and all the other parameters are defined as in Section 3.3.2.2. In practice,  $\hat{\mathbf{R}}_{bb}(\mathbf{p})$  will be approximated to an identity matrix. Moreover, and as discussed earlier in Section 3.3.2.3, when considering relatively short baselines between antennas (e.g., of the order of tens of cm), the cost function in (5.2) may be also simplified by approximating  $\Delta\mathbf{p}_n$  as a zero vector in the case meter-level (or above) positioning accuracies are expected to be achievable with the MIMO-MLE solution (as can be the case indoors). This simplification removes the need to know the baselines between antennas.

Note that the indoor MIMO-MLE position solution above is analogous to the intermediate timing solution discussed in Chapter 4 for indoor timing. Therefore, this solution is by definition

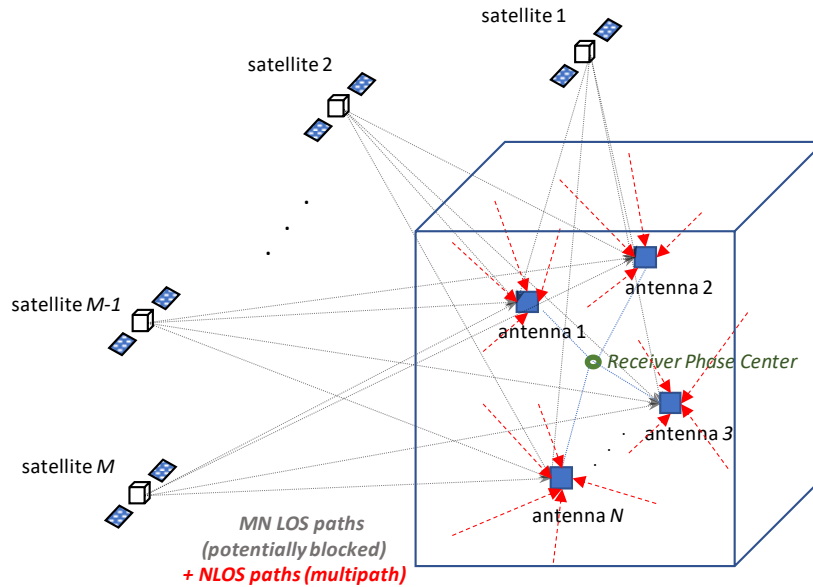


Fig. 5.1. Illustration of the MIMO-GNSS system in indoor conditions for an arbitrary distribution of the array of antennas featured by the GNSS receiver. The LOS components are in general expected to be highly attenuated or fully blocked, while NLOS multipath components can be dominant [Gar18b].

sub-optimum, since does not model the NLOS multipath components. Nevertheless, the exploitation of the spatial diversities available will enable to mitigate, to some extent, the impact of the NLOS multipath components. In contrast to the indoor timing problem, herein the estimation of the indoor channel (or the composite MIMO channel) is not considered in the solution as a way to further improve the MIMO-MLE solution due to the higher complexity to estimate the channel contribution in the position domain. Instead, a collaborative solution will be proposed in the next section to achieve a better positioning performance thanks to the availability of a richer diversity of the propagation conditions per receiver antenna (with some receivers in harsh conditions, while others in milder conditions).

The proposed indoor positioning approach based on the MIMO-MLE has been assessed at post-correlation level for BPSK(1) signals (as e.g., in GPS L1 C/A, which is commonly used as baseline signal in current mass-market receivers) when received with different antenna configurations (1, 4 and 8 antennas distributed as in Fig. 4.2 of Section 4.4), as originally presented in [Gar18b]. Simulations have been performed in realistic indoor (in a room without windows) and light-indoor (in a room with windows) conditions based on the physical-statistical wideband satellite-to-indoor channel model (Recommendation ITU-R P.681 [ITU17], [Jos14]), as in Section 4.4. In all the scenarios, the processing of a single signal

snapshot is considered for a static receiver, 11 satellites are simulated with an HDOP equal to 1, and no phase calibration is considered between the antennas. The search space of the MIMO-MLE is limited to the horizontal 2D position in a square of 400 by 400 m around the truth receiver position (area selected given the important impact of the indoor channel). Other parameters are considered known *a priori*. An open-loop WLS solution has been used as reference for the single-antenna configuration. In this case, the maximum of the cross-correlation function per satellite signal is used for the estimation of the pseudoranges used later on in the WLS solution. 200 independent Monte Carlo runs are considered per receiver configuration.

Fig. 5.2 summarizes the horizontal position RMSE obtained for both light-indoor and indoor scenarios; and Fig. 5.3 and Fig. 5.4 show separately the horizontal position solutions obtained in light-indoor and indoor propagation conditions, respectively. In both cases important attenuations (typically above 20-30 dB) of the LOS signals are observed for all the satellites, with an important presence of NLOS multipath components (dominant in most of the cases). For the single-antenna configuration, important horizontal errors are obtained for both MISO-MLE (equivalent to DPE) and open-loop WLS solutions (in particular for the indoor scenario, with errors above hundred meters, being both approaches not able to provide acceptable or stable solutions). As can be observed, in general the usage of larger arrays of antennas by the MIMO-MLE allows the improvement of the indoor position solution thanks to the spatial diversity introduced by the new antenna elements (going from horizontal errors of several tens or above hundred meters, to few tens of meters). This is in general expected to be the case when the signals received by the new antenna elements are in similar or better conditions than the original antenna elements considered in the solution. Additionally, even for the 8-antenna

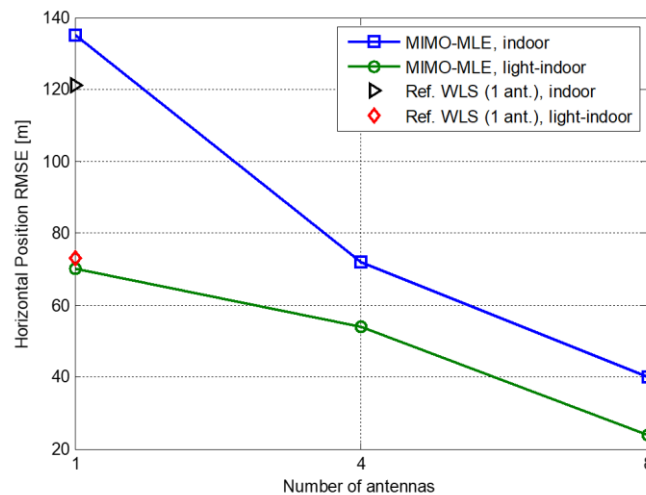


Fig. 5.2. Horizontal positioning RMSE for the light-indoor and indoor scenarios with BPSK(1) signals [Gar18b].

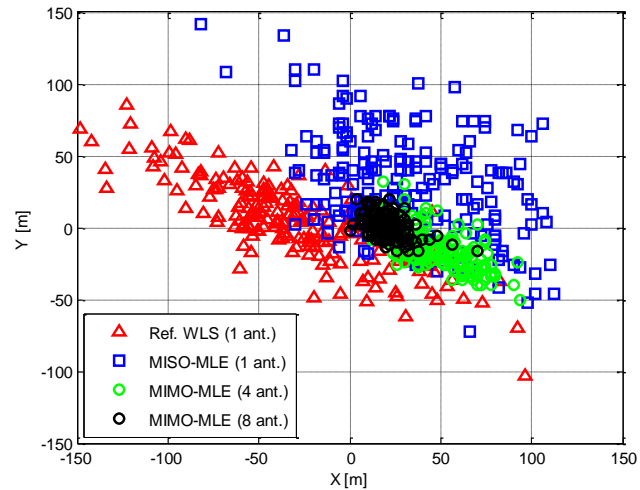


Fig. 5.3. Horizontal positioning results for a light-indoor scenario (static receiver in a room with windows) with BPSK(1) signals [Gar18b].

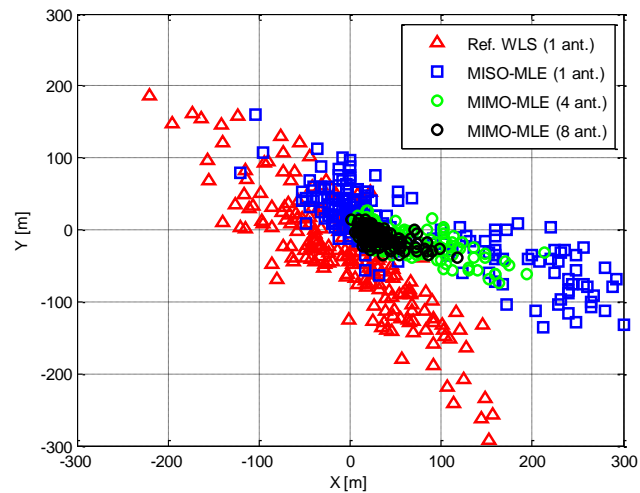


Fig. 5.4. Horizontal positioning results for an indoor scenario (static receiver in a room without windows) with BPSK(1) signals [Gar18b].

configuration, a bias is still observed in the position solution due to the important degradation of the LOS signals and the dominant presence of NLOS multipath components.

In summary, the simulation results show that there is still room for improvement in the MIMO-GNSS framework, in particular for the reduction of residual biases introduced in the position solution by the dominant NLOS propagation conditions. Based on this, a collaborative solution in the MIMO-GNSS framework enabling a further exploitation of the spatial reception diversity is proposed in Section 5.3. Finally, it is to be noticed that when considering high-order BOC signals in the same indoor conditions, better positioning accuracies are achieved thanks to the better code accuracy of these signals with respect to BPSK(1) signals, as shown the simulation results presented in Section 3.3.3.

## **5.3 A collaborative solution in the MIMO-GNSS framework (Co-MIMO-GNSS)**

### **5.3.1 System and signal model**

Let us consider a distributed system consisting of  $N$  independent receivers (with  $N \geq 1$ ), each of them featuring a GNSS antenna and receiving  $M$  navigation signals (with  $M \geq 1$ ) from a certain GNSS constellation and frequency band. Each of the receivers is potentially able to perform an initial coarse estimation of its state vector (containing, among others, the receiver's position, velocity and clock bias and drift). Additionally, a dedicated RF link between each of the receivers is available to estimate the peer-to-peer ranges between any pair of receivers. A subset of the  $N$  receivers is expected to be operating in harsh propagation conditions, such that the independent state vector estimations performed by the corresponding receivers may be highly degraded, or even not available. Out of the  $N$  receivers, at least one of them is considered to operate in mild propagation conditions (i.e., a relatively good estimation of the position, velocity and clock bias and drift can be performed without a dominant impact of the propagation channel), such that it can be used as anchor receiver in the collaborative position solution. It is to be noticed that the joint exploitation of all the GNSS signals received by all the receivers is highly dependent on the proper synchronization of the receivers to a common system time (e.g., the GNSS system time). This is going to be an important factor in collaborative positioning since, in practice, the time and frequency synchronization of each receiver will be achieved only with a certain accuracy (with potential important degradations in the harsh conditions where collaborative processing is actually expected to provide benefits). Therefore, time and frequency synchronization will in practice play an important role in the final performance of the collaborative processing [Gar17c].

In the following, the collaborative positioning problem discussed herein focuses on the derivation of an improved horizontal 2D position estimation for all the receivers (except the

one used as anchor), being the position of the  $n$ -th receiver at a certain time instant denoted as  $\mathbf{p}_n \triangleq \mathbf{p}_n(t) \in \mathbb{R}^{2 \times 1}$  (for simplicity, the dependence with time will be omitted in the following unless necessary). Therefore, the receivers are assumed to be operating at the same altitude (or the altitude for each receiver can be estimated and compensated by other means, e.g., based on barometric estimations [Li13]). Multipath is not considered in the signal model exploited by the proposed collaborative estimator. The reason is threefold. First, including the NLOS multipath components in the signal model would drastically increase the complexity of the resulting estimator. Second, diffuse multipath is expected in indoor conditions, being the components unresolvable and completely buried in noise, thus making very difficult their practical estimation and separation from the LOS contributions (if available at all) [Sec12], [Hei08], [Jos14]. And, last but not least, it is proposed to deal with the NLOS multipath components by jointly exploiting all the available received signals from spatially distributed receivers in different propagation conditions. Based on this, the complex baseband signal received by the  $n$ -th receiver from the potentially attenuated (or even missing) LOS contributions of the  $M$  GNSS satellites above the horizon are modeled in the following as

$$x_n(t) = \sum_{m=1}^M a_{m,n}(t) g_m(t - \tau_{m,n}(t)) \exp\{j2\pi f_{m,n}(t)t\} + e_n(t), \quad (5.3)$$

where the complex amplitude, time-delay and frequency-shift of the modeled LOS signals are denoted as  $a_{m,n}$ ,  $\tau_{m,n}$  and  $f_{m,n}$ , respectively. Taking now advantage of the DPE approach, as done in the previous chapters, we can define the time-delay and frequency shift for the LOS signal of each satellite-receiver pair as  $\tau_{m,n}(t) \triangleq \tau_{m,n}(t, \mathbf{p}_n)$  and  $f_{m,n}(t) \triangleq f_{m,n}(t, \mathbf{p}_n)$ , where the dependence with the 2D position vector  $\mathbf{p}_n \triangleq \mathbf{p}_n(t)$  for the  $n$ -th receiver is defined. Note that the dependence with other parameters of the receiver's state vector is omitted for simplicity. Exploiting the dependence with  $\mathbf{p}_n$ , we can now define a basis function  $b_{m,n}$  for the modeled LOS signal of each satellite-receiver pair as [Gar19a]

$$b_{m,n}(t, \mathbf{p}_n) = g_m(t - \tau_{m,n}(t, \mathbf{p}_n)) \exp\{j2\pi f_{m,n}(t, \mathbf{p}_n)t\}. \quad (5.4)$$

Note that (5.4) does not rely on the narrowband signal assumption since  $\mathbf{p}_n \triangleq \mathbf{p}_n(t)$ . Using the basis function in (5.4), and considering only a snapshot of  $K$  samples of  $x_n(t)$  for which  $a_{m,n}$ ,  $\tau_{m,n}$  and  $f_{m,n}$  are approximately constant during the observation time (or for which the variations of  $\tau_{m,n}$  and  $f_{m,n}$  can be compensated), the vector  $\mathbf{x}_n = [x_n(t_0) \dots x_n(t_{K-1})]^T \in \mathbb{C}^{K \times 1}$  gathering these samples can be modeled as

$$\mathbf{x}_n \approx \mathbf{B}(\mathbf{p}_n)\mathbf{a}_n + \mathbf{e}_n, \quad (5.5)$$

where  $\mathbf{B}(\mathbf{p}_n) = [\mathbf{b}_{1,n}(\mathbf{p}_n) \dots \mathbf{b}_{M,n}(\mathbf{p}_n)] \in \mathbb{C}^{K \times M}$  is the basis function matrix for the  $n$ -th receiver, composed by the basis function vectors for each satellite  $\mathbf{b}_{m,n}$ , defined based on (5.4) as  $\mathbf{b}_{m,n} = [b_{m,n}(t_0, \mathbf{p}_n) \dots b_{m,n}(t_{K-1}, \mathbf{p}_n)]^T \in \mathbb{C}^{K \times 1}$ ;  $\mathbf{a}_n = [a_{1,n} \dots a_{M,n}]^T \in \mathbb{C}^{M \times 1}$  is the complex amplitudes vector; and  $\mathbf{e}_n \in \mathbb{C}^{K \times 1}$  is the complex noise vector, with  $\mathbf{e}_n \sim \mathcal{CN}(\mathbf{0}, \sigma^2 \mathbf{I})$ .

### 5.3.2 Formation of the distributed array rigid body

In order to define the distributed array signal model based on the signal snapshots of all the receivers at a given time instant, the formation of a distributed array “rigid body” defining the relative spatial distribution between all the receivers for that time instant needs to be performed. As illustrated in Fig. 5.5, the orientation and position of the distributed array rigid body in the horizontal 2D plane is defined by two parameters: its angle  $\alpha_{RB} \triangleq \alpha_{RB}(t)$  with respect to the local 2D reference coordinates, and the position of one of the receivers (used as anchor). This basically means that by estimating  $\alpha_{RB}$  we obtain a collaborative 2D position of all the receivers (except the anchor). Without loss of generality, in the following the receiver 1 (with position  $\mathbf{p}_1$ ) is considered to be the anchor; and  $\alpha_{RB}$  is defined as the angle of the vector  $\mathbf{p}_2 - \mathbf{p}_1$  in the local 2D coordinates system used (with the receiver 2 any of the remaining receivers). Assuming that the correct rigid body solution is available, the position of the  $n$ -th receiver  $\mathbf{p}_n$  can be defined as a function of  $\alpha_{RB}$  based on the position of the anchor receiver  $\mathbf{p}_1$  as [Gar19c]

$$\hat{\mathbf{p}}_n(\alpha_{RB}) = \mathbf{p}_1 + \Delta \mathbf{p}_n(\alpha_{RB}), \quad (5.6)$$

where the offset vector  $\Delta \mathbf{p}_n(\alpha_{RB})$  is defined as [Gar19c]

$$\Delta \mathbf{p}_n(\alpha_{RB}) = [\hat{\rho}_{n,1} \cos(\alpha_{RB} + \widehat{\Delta \alpha}_n), \hat{\rho}_{n,1} \sin(\alpha_{RB} + \widehat{\Delta \alpha}_n)]^T, \quad (5.7)$$

with  $\widehat{\Delta \alpha}_n$  the offset angle between the vectors  $\hat{\mathbf{p}}_n(\alpha_{RB} = 0) - \mathbf{p}_1$  and  $\hat{\mathbf{p}}_2(\alpha_{RB} = 0) - \mathbf{p}_1$  (note that  $\widehat{\Delta \alpha}_n$  is easily estimated once the array rigid body is formed). The derivation of the array rigid body is possible thanks to the available estimated peer-to-peer ranges  $\hat{\rho}_{a,b} \triangleq \hat{\rho}_{a,b}(t) = \hat{\rho}_{b,a}(t)$  between all the receivers. Different estimation approaches exploited in standard cooperative positioning may be applied to form the rigid body, from LS based solutions to other more advanced approaches [Gare12a], [Gare12b], [Sol13], [Mon14]. It is to be noticed that a detailed discussion of this topic is considered out of the scope of this thesis.

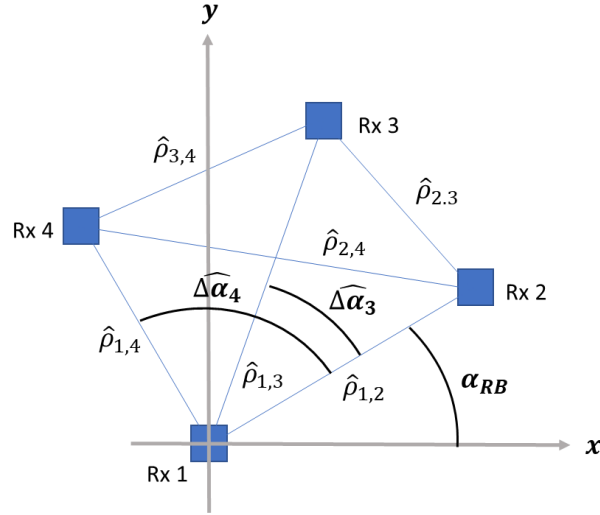


Fig. 5.5. Illustration of the distributed array rigid body [Gar19c].

A sequential LS based solution will be considered in the following to form the rigid body. The basic idea of this sequential approach is to build, step by step, the rigid body by adding in each step a new receiver. In each step, an LS position estimator is used to derive the position of the next receiver based on the previously derived receiver positions and the estimated ranges between these receivers and the next receiver. In general, to ensure the convergence of the LS estimator, this should be initialised with a coarse 2D position (since linearization may be an issue for short peer-to-peer ranges). A coarse 2D position  $\hat{\mathbf{p}}_c$  can be derived based on a grid-search approach as the solution to the minimization problem

$$\hat{\mathbf{p}}_c = \arg \min_{\mathbf{p}} \|\mathbf{v} - \mathbf{d}(\mathbf{p})\|^2, \quad (5.8)$$

where the vector  $\mathbf{v}$  contains the peer-to-peer ranges from the receivers previously derived and the next receiver, and the vector  $\mathbf{d}(\mathbf{p})$  contains the ranges between the evaluated position and the previous receivers. Note that the search-space applied in (5.8) should be constrained to the area of interest, with an accuracy just enough to ensure the later convergence of the LS estimator. Given the position  $\mathbf{p}_1$  of the anchor receiver and the range  $\hat{\rho}_{1,2}$  between receivers 1 and 2, we can define  $\mathbf{p}_2(\alpha_{RB} = 0)$  as any arbitrary position satisfying  $\|\mathbf{p}_2 - \mathbf{p}_1\| = \hat{\rho}_{1,2}$  (i.e., any point in the circle with radius  $\hat{\rho}_{1,2}$  centered in  $\mathbf{p}_1$ ). Note that the selection of  $\mathbf{p}_2(\alpha_{RB} = 0)$  defines the local 2D coordinates system of the array rigid body. Based on  $\mathbf{p}_1$ ,  $\mathbf{p}_2(\alpha_{RB} = 0)$ ,  $\hat{\rho}_{1,3}$ , and  $\hat{\rho}_{2,3}$ , we can now derive two possible 2D position solutions for receiver 3 by applying

an LS estimator initialised based on (5.8). For each of the two solutions derived for receiver 3, we can repeat the process to derive in each new iteration the position of a new receiver (from then on, a single position solution is obtained for each of the two solutions for receiver 3), until the positions of all the receivers are obtained. Under the assumption of decimeter-level peer-to-peer range estimation accuracies and peer-to-peer ranges of the order of several meters or tens of meters, the application of this approach (with the LS estimator being initialized based on the optimization problem in (5.8), or equivalent approaches) should converge to a plausible formation of the rigid body (within a certain error). It is to be noticed that two possible symmetric solutions for the array rigid body will be derived out of this process unless the individual estimation of the receivers' positions or previous collaborative estimations are used to discard the non-correct rigid body solution (in particular, in the derivation of the position for receiver 3). Otherwise, both rigid body solutions should be evaluated in the collaborative solution.

### 5.3.3 Distributed array signal model

Based on the formation of the distributed array rigid body and the signal model for each of the receivers in (5.5), a generalist unstructured array signal model (i.e., not relying on the narrowband array assumption) is considered in the following. Let us define a distributed basis function matrix  $\Psi$  modeling the relation between the signals gathered by all the receivers and the anchor receiver; based on the basis function matrices  $\{\mathbf{B}(\mathbf{p}_n(\alpha_{RB}))\}_{n=2}^N$ ,  $\Psi$  can be defined as a function of  $\alpha_{RB}$  as [Gar19c]

$$\Psi(\alpha_{RB}) = \begin{bmatrix} \mathbf{B}(\mathbf{p}_2(\alpha_{RB})) & \mathbf{0} & \dots & \mathbf{0} \\ \mathbf{0} & \mathbf{B}(\mathbf{p}_3(\alpha_{RB})) & \dots & \mathbf{0} \\ \vdots & \vdots & \ddots & \vdots \\ \mathbf{0} & \mathbf{0} & \dots & \mathbf{B}(\mathbf{p}_N(\alpha_{RB})) \end{bmatrix}. \quad (5.9)$$

Based on (5.9), the signal vector  $\mathbf{y}$  gathering the signals from  $N - 1$  receivers of the distributed array (all except the anchor receiver) can be modeled as [Gar19c]

$$\mathbf{y} \approx \Psi(\alpha_{RB})\mathbf{c} + \mathbf{i}, \quad (5.10)$$

where  $\mathbf{y} = [\mathbf{x}_2^T \dots \mathbf{x}_N^T]^T \in \mathbb{C}^{(N-1)K \times 1}$ ,  $\mathbf{c} = [\mathbf{a}_2^T \dots \mathbf{a}_N^T]^T \in \mathbb{C}^{M(N-1) \times 1}$  contains the complex amplitudes for the  $M(N - 1)$  paths, and  $\mathbf{i} = [\mathbf{e}_2^T \dots \mathbf{e}_N^T]^T \in \mathbb{C}^{(N-1)K \times 1}$  gathers the corresponding noise components (with  $\mathbf{i} \sim \mathcal{CN}(\mathbf{0}, \sigma^2 \mathbf{I})$ , such that the noise components of the different receivers are considered to be normalized between them).

### 5.3.4 MLE of the angle of the distributed array rigid body

Based on the signal model in (5.10), and following a similar approach as in [Gar19a] for the case of the direct position estimation, the maximum likelihood estimation of the angle  $\alpha_{RB}$  of the distributed array rigid body can be found as the maximization problem [Gar19c]

$$\hat{\alpha}_{RB} = \arg \max_{\alpha_{RB}} \left\{ \hat{\mathbf{r}}_{y\psi}^H(\alpha_{RB}) \hat{\mathbf{R}}_{\psi\psi}^{-1}(\alpha_{RB}) \hat{\mathbf{r}}_{y\psi}(\alpha_{RB}) \right\}, \quad (5.11)$$

with the estimated correlation vectors defined as [Gar19c]

$$\hat{\mathbf{r}}_{y\psi}(\alpha_{RB}) = \mathbf{\Psi}^H(\alpha_{RB}) \mathbf{y}, \text{ and} \quad (5.12)$$

$$\hat{\mathbf{R}}_{\psi\psi}(\alpha_{RB}) = \mathbf{\Psi}^H(\alpha_{RB}) \mathbf{\Psi}(\alpha_{RB}). \quad (5.13)$$

The direct application of a 1D grid search approach [Kay13] may be considered to solve (5.11), with tens or hundreds of grid points expected to be enough for achieving reasonable accuracies. The collaborative 2D position solution for all the receivers (except the anchor) can then be derived based on  $\hat{\alpha}_{RB}$  as [Gar19c]

$$\{\hat{\mathbf{p}}_n\}_{n=2}^N = \mathbf{p}_1 + \{\Delta \mathbf{p}_n(\hat{\alpha}_{RB})\}_{n=2}^N. \quad (5.14)$$

The reduction of the collaborative position problem to an angle estimation problem (i.e., to a 1D estimation problem) based on (5.11) and (5.14) allows an important reduction of the computational burden with respect to the direct 2D position estimation. The computational burden may be further reduced by approximating  $\hat{\mathbf{R}}_{\psi\psi}$  by an identity matrix (assuming good cross-correlation properties of the GNSS signals exploited), such that only the generation of the correlation vectors in (5.12) is required. This simplification is exploited in the simulations presented in Section 5.3.7.

### 5.3.5 Hybrid position solution

A hybrid DPE (H-DPE) solution (equivalent to a hybrid MISO-MLE solution) can be obtained as an intermediate solution to the collaborative position by exploiting the signal snapshot for

each receiver together with the estimated range to the anchor (this is equivalent to the DPE or MISO-MLE solution constrained by a circle around the anchor in the horizontal position domain). The H-DPE solution can be defined as

$$\begin{aligned} \hat{\mathbf{p}}_n^{hyb} &= \arg \max_{\mathbf{p}} \{ \hat{\mathbf{r}}_{x_nb}^H(\mathbf{p}) \hat{\mathbf{r}}_{x_nb}(\mathbf{p}) \} \\ &s. t. \|\mathbf{p} - \mathbf{p}_1\| = \hat{\rho}_{1,n}. \end{aligned} \quad (5.15)$$

where the correlation vectors  $\hat{\mathbf{r}}_{x_nb}(\mathbf{p})$  for each receiver are defined as in Section 3.3.2.2.

### 5.3.6 Implementation aspects of the collaborative solution

The collaborative position solution proposed herein requires the joint processing of signal snapshots from the multiple receivers considered (together with the estimated ranges between them, and the individual estimations of the receivers' state vectors). Therefore, the application of the concept requires a centralized processing. This may be performed by one of the receivers (e.g., the anchor receiver). Alternatively, and taking advantage of the high data rates and very low latencies expected to be provided by 5G [3GP19], it may be performed in the Cloud [Luc16], [Gar17c]. This second approach allows to offload the receivers from the processing required by the proposed collaborative solution.

Depending on the target application, the collaborative processing of the signal snapshots may need to be performed with a higher or lower duty cycle. In some cases the collaborative solution could be used as a back-up to verify or correct the individual position solution of the receivers, such that low duty cycles may be applicable. In other cases, a continuous collaborative position may be of interest. In any case, the exploitation of information from previous epochs and assistance data is considered of high interest in the collaborative positioning process to reduce the computational burden and improve the positioning performance.

### 5.3.7 Simulation results

The collaborative position estimator proposed in this chapter has been simulated via a semi-analytical approach at post-correlation level. A grid search approach with a resolution of 1 degree is used. A scenario with 5 receivers in which all the peer-to-peer ranges are available with an accuracy of 0.1 m (1-sigma) is considered. “Rx 1” is the anchor receiver, whose position is considered to be known, and the rest of receivers are operating in different (light-)indoor conditions, as shown in Fig. 5.6. In order to simulate the indoor conditions, the realistic wideband satellite-to-indoor channel model in Recommendation ITU-R P.681 [ITU17], [Jos14] has been used. A sequential LS-based solution is exploited for the formation of the distributed array rigid body, accounting in this way for the impact of peer-to-peer range errors in the collaborative estimation. Synchronization errors between the receivers are simulated, being dependent on the simulated channel conditions. Eleven satellites are simulated in a geometric configuration with an HDOP equal to one. System and atmospheric errors are not included in the simulations. Assistance data is considered to be available. BPSK(1) signals (as e.g., in GPS L1 C/A) are transmitted by the simulated GNSS satellites. A single signal snapshot is considered and the reference SNR at post-correlation level per satellite LOS signal (when not considering yet the channel) is 35 dB for all the satellites (equivalent to a post-correlation C/No of 45 dB-Hz for a coherent integration period of 100 ms; note that C/No values below 15-25 dB-Hz are observed in the simulated indoor conditions). A conventional snapshot-based WLS solution has been used as reference for each of the receivers in order to assess the benefit introduced by the collaborative approach (note this is considered a representative processing approach when a single snapshot is available, e.g., in the case of Cloud-GNSS processing [Luc16], [Gar17c]). Additionally, the H-DPE solution is also used in the comparison. In order to show the benefit introduced when an additional receiver in better propagation conditions (i.e., considering AWGN conditions) is exploited in the collaborative solution (on top of the

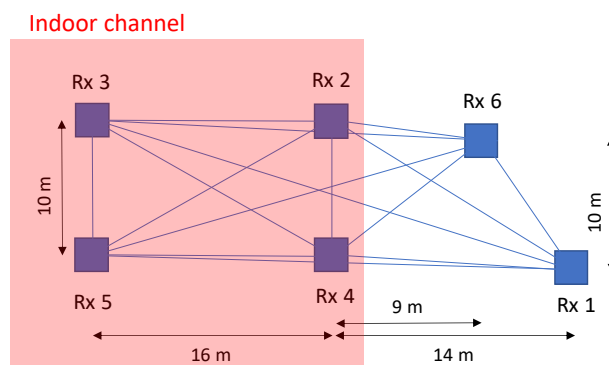


Fig. 5.6. Illustration of the simulated scenario for collaborative positioning [Gar19c].

anchor), “Rx 6” is included in the simulations. 300 Monte Carlo simulation runs are used in the results presented.

The RMSE of the horizontal 2D position obtained for each of the receivers (and the aggregate statistics) based on the WLS, H-DPE and collaborative solutions are shown in Fig. 5.7 (Rx 1, used as anchor, not included since not impacted by the collaborative solution). Note that the x-axis in Fig. 5.7 indicates the processing approach used. As can be observed for the WLS results, the impact of the propagation channel varies from receiver to receiver (as expected in reality), with a RMSE between around 30 and 80 m (and aggregate RMSE of around 50 m). These errors may be considered not acceptable in some applications. The positioning results are substantially improved when exploiting the peer-to-peer ranges between each of the receivers and the anchor receiver in the H-DPE solution, resulting in an aggregate RMSE of around 25 m. This improvement is introduced by the exploitation of the signals in the position domain and by constraining the solution to the positions at a certain distance from the anchor. The situation is further improved when the collaborative solution is taking advantage of the spatial reception diversity by jointly exploiting all the received signals from Rx2 to Rx5, resulting in an aggregate RMSE of around 16 m. It is to be noticed that Rx2 to Rx5 are highly degraded by the indoor propagation conditions, explaining the limited improvement introduced by the spatial diversity in this case. Indeed, when Rx6 (operating in mild conditions) is included in the scenario, the collaborative position solution is drastically improved, resulting in an aggregate RMSE of around 2 m. Therefore, the proposed collaborative solution allows to improve the positioning accuracy even if all the receivers, except the anchor, are operating in

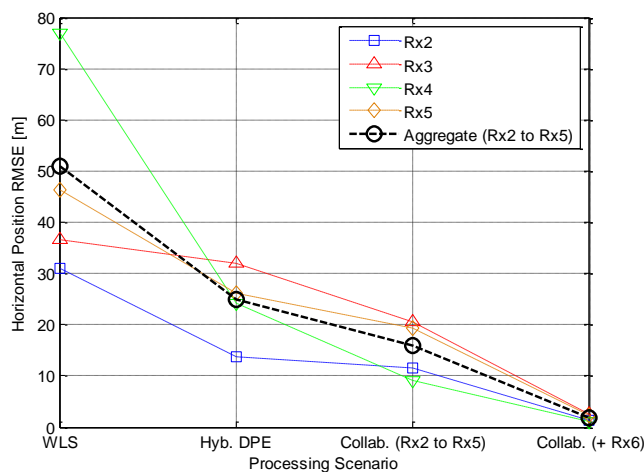


Fig. 5.7. RMSE of the horizontal position estimated in indoor propagation conditions [Gar19c].

harsh conditions, while enables a drastic improvement of the positioning accuracy when some of the receivers are operating in milder conditions. This is of particular interest in indoor-outdoor scenarios with some receivers operating indoors (with highly degraded or even not available position solution) and others operating outdoors (potentially impacted by a milder channel).

### 5.3.8 Trusted distributed array rigid body

As has been shown in the previous section, the collaborative solution relies on the availability of a subset of receivers in good enough propagation conditions such that the rest of the receivers in degraded or highly degraded propagation conditions can obtain a position solution with improved performance (even when a position fix was not possible). The ML-based solution derived in (5.11) is weighting the contribution of each of the signals received from the different receivers based on the observed SNR conditions. This may be enough in many situations since, in general, better SNR (or C/No) conditions are expected for signals (and receivers) in better propagation conditions. Nevertheless, there might be certain situations in which signals (and receivers) with apparently good SNR conditions may introduce a degradation in the collaborative position solution (e.g., in the form of a bias). This can be the case in the presence of strong multipath reflections in open-sky like conditions (for very specific situations) or under a spoofing attack.

In order to be able to deal with this potential problem in collaborative positioning, the concept of “trusted” distributed array rigid body is introduced in the following. The concept is rather simple, and is based on the definition of the rigid body based on the subset of receivers expected to have a positive contribution to the collaborative position solution. Thus, the estimation of  $\hat{\alpha}_{RB}$  in (5.11) is to be derived considering only the subset of receivers that form by the trusted rigid body. Based on the estimated  $\hat{\alpha}_{RB}$  in this case, the position of all the receivers can then be derived based on (5.14). This will allow not only to ensure that the collaborative position solution is robust to the impact of position biases introduced by one or some of the receivers, but also to solve the position bias of those receivers.

The definition of the subset of receivers that form the trusted rigid body can be considered a binary classification problem. There are definitely different ways in which this classification problem can be tackled, so the detailed assessment of this research line is considered out of the scope of this thesis. Nevertheless, an initial discussion on this topic is presented in the next paragraphs. In the following, we will consider as basic measurements the individual position solutions obtained by each receiver,  $\hat{\mathbf{p}}_n^{ind}$  (e.g., obtained based on a WLS solution or any other GNSS-based solution), and the H-DPE solution of each receiver,  $\hat{\mathbf{p}}_n^{hyb}$  (exploiting the position

of the anchor receiver and the peer-to-peer range estimation). Note that receivers for which an individual position solution is not available can be already discarded from the trusted rigid body. These are in general not expected to have a positive contribution to the collaborative solution, since will make in practice difficult the time and frequency synchronization of the signals from those receivers (although estimations from previous fixes may be exploited). Based on this, for each receiver for which a position fix is available we can generate the residual

$$\hat{\varepsilon}_n = \|\hat{\mathbf{p}}_n^{ind} - \hat{\mathbf{p}}_n^{hyb}\|. \quad (5.16)$$

This residual provides information about the consistency between the individual and hybrid solutions. It is to be noticed that the H-DPE solution in the horizontal 2D plane is constrained to a circle around the anchor (which position is considered to be known with a good accuracy). Therefore, in general this residual can be used to understand how much we can rely on the GNSS signals from this receiver. Additionally to the residual, we may also want to exploit the information regarding the relative SNR conditions for each for the receivers. For doing so, we can define the factor

$$\hat{\eta}_n = \frac{\hat{\mathbf{r}}_{x_nb}^H(\hat{\mathbf{p}}_n^{hyb})\hat{\mathbf{r}}_{x_nb}(\hat{\mathbf{p}}_n^{hyb})}{\sum_{n=2}^N \hat{\mathbf{r}}_{x_nb}^H(\hat{\mathbf{p}}_n^{hyb})\hat{\mathbf{r}}_{x_nb}(\hat{\mathbf{p}}_n^{hyb})}, \quad (5.17)$$

where the correlation vectors  $\hat{\mathbf{r}}_{x_nb}(\hat{\mathbf{p}}_n^{hyb})$  for each receiver are obtained for the hybrid position estimation, and are defined as in Section 3.3.2.2 (note that the noise components of the different receivers are considered to be normalized between them). Note that (5.17) assumes a position fix is available for all the receivers.

Exploiting now (5.16) and (5.17) together, Fig. 5.8 illustrates the classification of the subset of receivers with positive (and negative) contribution to the collaborative solution. In general, “desired” receivers are expected to show a relatively low  $\hat{\varepsilon}_n$  and a relatively high  $\hat{\eta}_n$ . Based on this, two subsets containing the desired and undesired receivers can be defined, targeting to filter out receivers with negative contribution, or just not useful. This is the case in particular for receivers with relatively high  $\hat{\varepsilon}_n$  and  $\hat{\eta}_n$ , since their potentially negative contribution won’t be properly weighted down by the ML-based collaborative position solution proposed in Section 5.3.4.

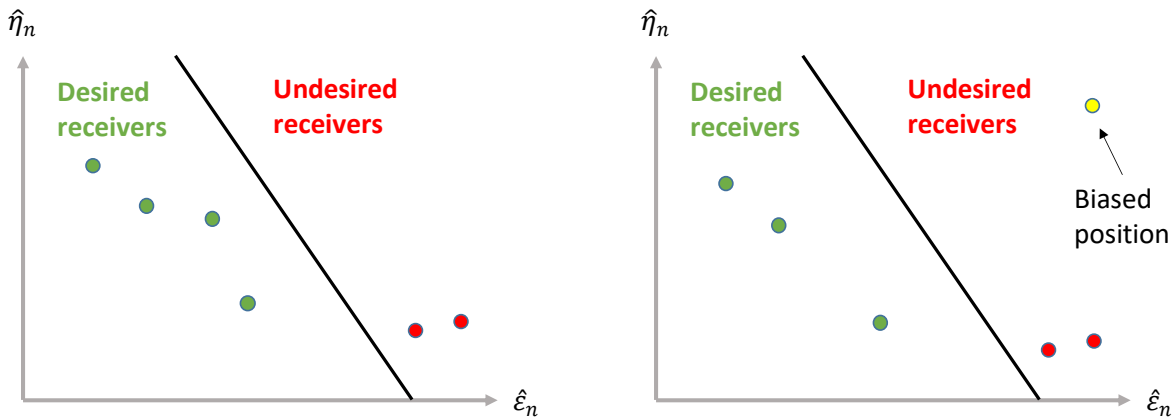


Fig. 5.8. Illustration of the classification of receivers as desired receivers (to be used in the trusted rigid body for deriving the collaborative solution) and undesired receivers. On the left, typical expected distribution, with lower  $\hat{\eta}_n$  for higher  $\hat{\epsilon}_n$ , and possible definition of the hyperplane used in the classification. On the right, a receiver with a relative high  $\hat{\eta}_n$  and  $\hat{\epsilon}_n$  is additionally introduced.

Fig. 5.9 and 5.10 illustrate an example of collaborative positioning with one of the receivers (Rx4) under a spoofing attack (resulting in a biased position obtained by the individual GNSS-based solution). In particular, for this example  $\hat{\eta}_4$  is relatively high with respect to  $\hat{\eta}_1$ ,  $\hat{\eta}_2$  and  $\hat{\eta}_3$  (such that the collaborative position with all the receivers is impacted, not being able to deal by itself with the spoofing attack). In Fig. 5.9, all the receivers are exploited in the collaborative solution, showing the bias introduced in the collaborative position solution. The estimated angle of the distributed rigid body is biased due to the impact of Rx4. Note that for the non-spoofed receivers (Rx1, Rx2, and Rx3) the H-DPE solutions are aligned with the truth positions, while for Rx4 the H-DPE and collaborative solution are biased, and aligned between them (due to the high  $\hat{\eta}_4$ ). In Fig. 5.10, Rx4 is filtered out, being the collaborative position solution based only on the trusted rigid body (with Rx1, Rx2 and Rx3). This allows the derivation of unbiased collaborative position solutions for all the receivers.

## 5.4 Conclusions

The positioning in harsh propagation conditions with multiple antennas, from co-located to distributed array solutions, has been discussed in this chapter. In the case of co-located antennas in indoor conditions, simulation results have shown that achieving accurate positioning results

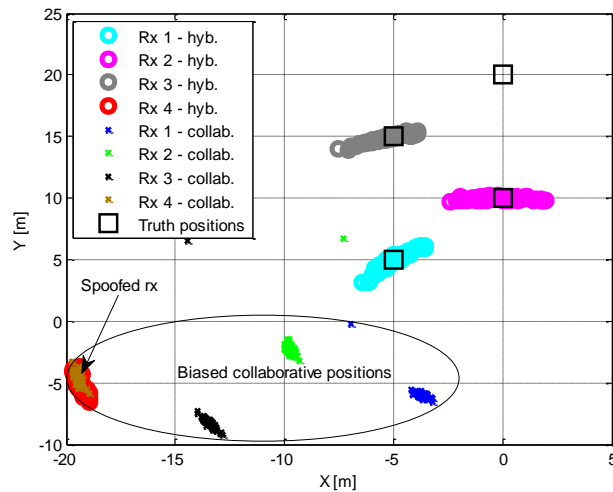


Fig. 5.9. Illustration of the H-DPE and collaborative position solution under the presence of a spoofing attack (for Rx4) and a relatively high  $\hat{\eta}_4$ . The concept of trusted rigid body is not applied.

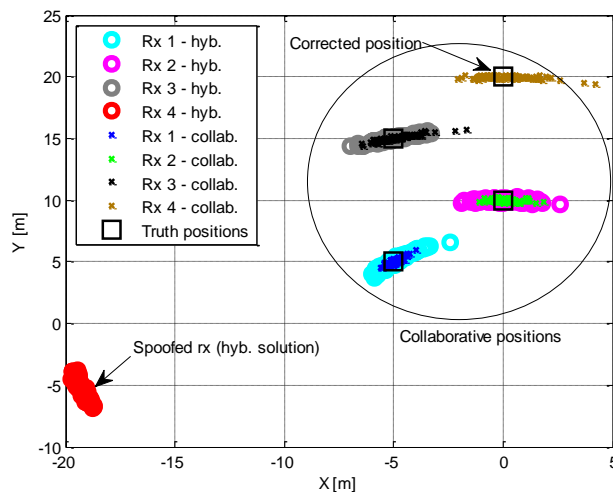


Fig. 5.10. Illustration of the H-DPE and collaborative position solution under the presence of a spoofing attack (for Rx4) and a relatively high  $\hat{\eta}_4$ . The concept of trusted rigid body is applied.

remains a challenging problem. In order to overcome this limitation, a novel distributed array processing approach jointly exploiting the GNSS signals from multiple receivers in the position domain as an angle estimation problem has been proposed. The proposed solution, which relies on the usage of one receiver as anchor and the formation of a distributed array rigid body, allows an important reduction of the computational burden. The simulation results in realistic indoor propagation conditions show that the exploitation of the spatial diversity introduced by the usage of multiple receivers enables the derivation of an improved position solution for receivers in degraded propagation conditions, taking in particular advantage of those in better propagation conditions. Moreover, the proposed approach allows to derive a position solution for receivers that originally may not be able to fix their position. Finally, the concept of trusted rigid body has been introduced as a way to deal in the collaborative solution with receivers impacted by strong multipath reflections or spoofing attacks.



# 6

## Conclusions and Future Research

**T**HIS thesis has dealt with the processing of GNSS signals for positioning and timing in harsh propagation conditions, focusing on the exploitation of the spatial diversities present when multiple GNSS satellites are in view by multiple receiver antennas. In particular, position and time estimators in the MIMO-GNSS framework have been proposed to deal with the impact introduced by realistic fading and multipath conditions in which it is very challenging to achieve accurate and precise solutions. This is the case in environments in which LOS signals are highly attenuated (or not present) and NLOS multipath components are dominant, as happens in indoor scenarios. The availability of spatial diversity allows in general to improve the equivalent SNR conditions of the proposed estimators, in particular when both transmission and reception diversities are jointly exploited in the position or time domain. Moreover, exploiting the spatial diversity allows to take advantage of the GNSS signals received in better channel conditions to improve the derived solution.

The robust unambiguous positioning with high-order BOC signals in harsh propagation conditions has been tackled in **Chapter 3**. First, the DOME approach has been presented to deal with the ambiguity problem at single-satellite level. The results obtained show that the DOME approach fully exploits the BOC signal accuracy while being robust at low C/No conditions and in the presence of fading and multipath. The exploitation of several integration periods is considered by the DOME approach in order to improve the observed SNR conditions in which the estimations are performed. Nevertheless, since the integration periods that can be applied in practice are limited by receiver, user and environment constraints, for very low C/No conditions the equivalent SNR observed by the estimator remains also low and the probability of false lock is still important. In order to overcome this limitation, the unambiguous estimation has been proposed to be tackled in the position domain, enabling the joint exploitation of all the BOC signals received by the GNSS receiver. For this purpose, the ML-based estimators in the MISO- and MIMO-GNSS systems resulting from the exploitation of one or multiple antennas, respectively, have been derived. The processing gain introduced in the unambiguous estimation problem by the spatial transmission and reception diversities allows to improve the equivalent SNR conditions in which the estimator operates and, thus, a reduction of the impact of false locks. Simulation results with  $\text{BOC}_{\cos}(15, 2.5)$  signals show the robustness introduced with respect to solutions operating at single-satellite level. Moreover, when several receiver antennas are available, the proposed estimator allows the exploitation of high-order BOC signals even in indoor conditions, achieving accuracies of few meters (which is far better than what can be achieved with BPSK(1) signals in the same conditions). Therefore, the proposed estimators in the MIMO-GNSS framework are a promising approach to enable the unambiguous positioning with high-order BOC signals in harsh propagation conditions, while being implementable based on state-of-the-art multi-correlator receiver architectures.

As potential future research, the estimators proposed for high-order BOC signals may be also exploited with the so-called meta-signals, as preliminary discussed in [Gar19b]. In this case, a pair of signals are jointly exploited to create a meta-signal, showing similar advantages (narrower main peak) and drawbacks (multiple correlation peaks) than high-order BOC signals. Therefore, the exploitation of meta-signals in the MIMO-GNSS framework is a research area that might be worth exploring. Indeed, this may allow to achieve meter-level accuracies in indoor conditions based on the joint exploitation of multiple BPSK signals.

**Chapter 4** has dealt with indoor timing based on GNSS signals, introducing the concept of composite MIMO channel for mitigating the impact of the propagation channel. Two estimators operating in the time domain, each following a different approach to exploit the spatial diversity, have been proposed. Simulation results with a realistic wideband satellite-to-indoor channel model have shown that the exploitation of the spatial diversity introduced by arrays of antennas, together with the estimation of the composite MIMO channel, allows an important mitigation of the indoor multipath. Indeed, timing accuracies below 50 ns are demonstrated to be feasible in both light-indoor and indoor conditions. Therefore, the proposed estimation approach is considered an appealing solution for indoor applications with tight synchronization requirements, as can be the case in indoor small cells for 5G.

As potential future research work in the timing area, it may be worth investigating the definition of the PDFs assessed for each of the coefficients of the composite MIMO channel based on the composite MIMO channel estimated in previous epochs, as introduced in [Gar18a]. This may allow to enhance the achieved performance and to reduce to computational burden of the joint time and composite MIMO channel estimator.

**Chapter 5** has dealt with positioning in harsh propagation conditions with multiple antennas, from co-located to distributed array solutions. In the case of co-located antennas in indoor conditions, simulation results have shown that achieving accurate positioning results remains a challenging problem. In order to overcome this limitation, a distributed array processing approach jointly exploiting the GNSS signals from multiple receivers in the position domain as an angle estimation problem has been proposed. Simulation results with a realistic wideband satellite-to-indoor channel model show that the exploitation of the spatial diversity introduced by the usage of multiple receivers enables the derivation of an improved position solution for receivers in degraded propagation conditions, taking in particular advantage of those in better propagation conditions. Moreover, the proposed approach allows to derive a position solution for receivers that originally may not be able to fix their position.

As potential future research work in the collaborative positioning area, it may be worth further investigating the concept of trusted distributed array rigid body presented in this thesis to deal with the exclusion of receivers impacted by the propagation channel or spoofing attacks.

Last, but not least, as potential additional future research work in the MIMO-GNSS framework, the positioning and timing estimators discussed in this thesis may be extended to the case of multi-constellation and multi-frequency receivers, with different signal modulations in different frequencies being jointly exploited. This is expected to allow a further improvement of positioning and timing accuracies in harsh propagation conditions.



# List of Publications

This thesis is based on the material of the following journal articles, patents and conference papers:

## Journal Articles

- [Gar19a] J. A. Garcia-Molina, and J. A. Fernandez-Rubio, “Collective Unambiguous Positioning with High-Order BOC Signals,” *IEEE Transactions on Aerospace and Electronic Systems*, vol. 55, no. 3, pp. 1461-1473, June 2019. © 2018 IEEE. <https://ieeexplore.ieee.org/document/8477092>
- [Gar16a] J. A. Garcia-Molina, M. Navarro-Gallardo, G. Lopez-Risueño, and M. Crisci, “Robust unambiguous Estimation of High-Order BOC Signals: The DOME approach,” *NAVIGATION, Journal of the Institute of Navigation*, vol. 63, no. 4, pp. 509–518, Winter 2016. © 2016 Institute of Navigation <https://doi.org/10.1002/navi.162>

## Patents

- [Gar18a] J. A. Garcia-Molina, “Method and Apparatus for Performing Joint Channel and Time Estimation in a GNSS Receiver,” International Patent Application No. PCT/EP2018/063660, 2018.
- [Gar15a] J. A. Garcia-Molina, “Method and Apparatus for Tracking a Binary Offset Carrier Navigation Signal,” European Patent Application No. EP3104195A1, 10 Jun. 2015.

## Conference Papers

## List of Publications

---

- [Gar19c] J. A. Garcia-Molina, and J. A. Fernandez-Rubio, “Collaborative Snapshot Positioning via Distributed Array Processing,” *ION GNSS+ 2019*, Miami, Florida, Sep. 2019. <https://doi.org/10.33012/2019.16876>
- [Gar19b] J. A. Garcia-Molina, and J. A. Fernandez-Rubio, “Array Processing and Unambiguous Positioning of Signals with Multi-Peak Correlations,” *ION GNSS+ 2019*, Miami, Florida, Sep. 2019. <https://doi.org/10.33012/2019.17024>
- [Gar18c] J. A. Garcia-Molina, and J. A. Fernandez-Rubio, “Positioning and Timing in the MIMO-GNSS Framework,” *NAVITEC 2018*, Noordwijk, The Netherlands, Dec. 2018. <https://ieeexplore.ieee.org/document/8642703>
- [Gar18b] J. A. Garcia-Molina, J. A. Fernandez-Rubio, and J. M. Parro, “Exploiting Spatial Diversity for NLOS Indoor Positioning,” *ION GNSS+ 2018*, Miami, Florida, Sep. 2018. <https://doi.org/10.33012/2018.15865>
- [Gar17c] J. A. Garcia-Molina, and J. M. Parro, “Cloud-based GNSS Processing of Distributed Receivers of Opportunity: Techniques, Applications and Data-collection Strategies,” *6th International Colloquium on Scientific and Fundamental Aspects of GNSS/Galileo*, Valencia, Spain, Oct. 2017.
- [Gar17b] J. A. Garcia-Molina, and J. A. Fernandez-Rubio, “Exploiting Spatial Diversity in Low-cost SDR Platforms: the MIMO-GNSS approach,” *6th International Colloquium on Scientific and Fundamental Aspects of GNSS/Galileo*, Valencia, Spain, Oct. 2017.
- [Gar17a] J. A. Garcia-Molina, J. A. Fernandez-Rubio, R. Weiler, and M. Crisci, “Snapshot Processing of High-Order BOC Signals in the Cloud: on Sensitivity and Distortion Effects,” *ION GNSS+ 2017*, Portland, Oregon, Sep. 2017. <https://doi.org/10.33012/2017.15245>
- [Gar15b] J. A. Garcia-Molina, M. Navarro-Gallardo, G. Lopez-Risueño, and M. Crisci, “Robust Unambiguous Tracking of High-Order BOC Signals: a Multi-Correlator Approach,” *ION GNSS+ 2015*, Tampa, Florida, Sep. 2015. <https://www.ion.org/publications/abstract.cfm?articleID=13049>

# Bibliography

- [3GP19] 3GPP Release 15, <http://www.3gpp.org/release-15>
- [3GP17] “LTE; Evolved Universal Terrestrial Radio Access (E-UTRA); Base Station (BS) radio transmission and reception (3GPP TS 36.104 version 13.7.0 Release 13),” ETSI TS 136 104 v13.7.0 (2017-04). Accessed on: May 19th, 2018. Available: <http://www.etsi.org>.
- [5G16] 5G Automotive Association, “The case for cellular V2X for safety and cooperative driving”, White Paper, November 2016.URL: <http://5gaa.org/wp-content/uploads/2017/10/5GAA-whitepaper-23-Nov-2016.pdf>.
- [And18] M. Andrianarison, M. Sahmoudi, and R. Landry, “New Strategy of Collaborative Acquisition for Connected GNSS Receivers in Deep Urban Environments,” *Positioning*, 2018, 9, 23-46.
- [Au16] E. Au, “The Latest Progress on IEEE 802.11mc and IEEE 802.11ai,” *IEEE Vehicular Technology Magazine*, vol. 11, issue 3, pp. 19-21, Sep. 2016.
- [Axe09] P. Axelrad, J. Donna, and M. Mitchell, “Enhancing GNSS Acquisition by Combining Signals from Multiple Channels and Satellites”, *Proceedings of the 22nd International Technical Meeting of The Satellite Division of the Institute of Navigation (ION GNSS 2009)*, Savannah, GA, September 2009, pp. 2617-2628.
- [Axe11] P. Axelrad, B. K. Bradley, J. Donna, M. Mitchell, and S. Mohiuddin, “Collective Detection and Direct Positioning Using Multiple GNSS Satellites,” in *NAVIGATION: Journal of the Institute of Navigation*, vol. 58, no. 4, pp. 305-321, Winter 2011.
- [Bha17] S. Bhamidipati, and G. X. Gao, “GPS Multi-Receiver Joint Direct Time Estimation and Spoofer Localization,” *IEEE Transactions on Aerospace and Electronic Systems*, DOI: 10.1109/TAES.2018.2879532, Nov. 2018.
- [Bra10] B. K. Bradley, P. Axelrad, J. Donna, “Performance Analysis of Collective Detection of Weak GPS Signals”, *Proceedings of the 23rd International Technical Meeting of The Satellite Division of the Institute of Navigation (ION GNSS 2010)*, Portland, OR, September 2010, pp. 3041-3053.

## Bibliography

---

- [Bro11a] A. Broumandan, J. Nielsen, and G. Lachapelle, "Coherent Integration Time Limits for Mobile GNSS Receivers in Multipath Fading Environments", *Inside GNSS*, pp. 62-65, March/April 2011.
- [Bro11b] A. Broumandan, J. Nielsen, G. Lachapelle, "Indoor GNSS Signal Acquisition Performance using a Synthetic Antenna Array," *IEEE Transactions on Aerospace and Electronic Systems*, Vol. 47, No. 2, Apr. 2011.
- [Clo07] P. Closas, C. Fernández-Prades, and J. A. Fernández-Rubio, "Maximum Likelihood Estimation of Position in GNSS," *IEEE Signal Processing Lett.*, vol. 14, no. 5, pp. 359-362, May 2007.
- [Clo09a] P. Closas, "Bayesian Signal Processing Techniques for GNSS Receivers: From Multipath Mitigation to Positioning", Ph.D. Thesis, Barcelona, June 2009.
- [Clo09b] P. Closas, C. Fernández-Prades, and J. A. Fernández-Rubio, "Direct Position Estimation approach outperforms conventional two-steps positioning", in *Proc. XVII European Signal Processing Conference, EUSIPCO*, Glasgow, Scotland, August 2009.
- [Clo08] P. Closas, C. Fernandez-Prades, and J. A. Fernandez-Rubio, "A Bayesian Approach to Multipath Mitigation in GNSS Receivers," *IEEE J. Select. Topics in Signal Processing*, vol. 3, no. 4, August 2009.
- [Clo09] P. Closas, and C. Fernandez-Prades, "A Statistical Multipath Detector for Antenna Array Based GNSS Receivers," *IEEE Transactions on Wireless Communications*, vol. 10, no. 3, pp. 916-929, Mar 2011.
- [Cor17] J.V. Cordaro, D. Shull, G. Gutt, and M. O'Connor, "An Alternative Source of Timing and Location using the Low Earth Orbit Iridium Satellite Constellation," *Joint Navigation Conference*, Dayton, Ohio, June 2017.
- [Die92] A. J. Van Dierendonck, P. Fenton, and T. Ford, "Theory and Performance of Narrow Correlator Spacing in a GPS Receiver," *NAVIGATION: Journal of the Institute of Navigation*, Fall 1992, pp. 265-283.
- [DiE07] R. DiEsposti, "GPS PRN Code Signal Processing and Receiver Design for Simultaneous All-in-View Coherent Signal Acquisition and Navigation Solution Determination", *Proceedings of the 2007 National Technical Meeting of The Institute of Navigation*, San Diego, CA, pp. 91-103, January 2007.
- [Dig09] F. van Diggelen, "A-GPS: Assited GPS, GNSS, and SBAS," Artech House, 2009.

## Bibliography

---

- [Enn12] C. Enneking, M. Stein, M. Castenada, F. Antreich, and J. A. Nossek, “Multi-Satellite Time-Delay Estimation for Reliable High-Resolution GNSS Receivers,” in *Proc. IEEE/ION Position Location and Navigation Symposium (PLANS)*, South Carolina, U.S., April 2012.
- [Est14] P. Esteves, M. Sahmoudi, and L. Ries, “Collective Detection of Multi-GNSS Signals,” *Inside GNSS*, pp. 54-65, May/June 2014.
- [Fer06] C. Fernandez-Prades, “Advanced Signal Processing Techniques for GNSS Receivers,” PhD Thesis, Dept. of Signal Theory and Communications, Universitat Politecnica de Catalunya (UPC), Barcelona, Spain, May 2006.
- [Fer09a] C. Fernandez-Prades, and P. Closas, “Synchronization of GNSS Signals with Unstructured Antenna Arrays by a Multivariate Minimization of the Generalized Variance”, *16th International Conference on Digital Signal Processing (DSP 2009)*, Santorini, Greece, July 2009.
- [Fer09b] C. Fernandez-Prades, J. Arribas, and P. Closas, “The Decoupling of DOA/Synchronization Parameters in Colored Noise Environments”, *NEW-COM++/ACoRN Joint Workshop*, Barcelona, Spain, March 2009.
- [Fer16] C. Fernández-Prades, J. Arribas, P. Closas, “Robust GNSS Receivers by Array Signal Processing: Theory and Implementation,” *Proceedings of the IEEE*, vol. 104, issue 6, pp. 1207-1220, June 2016.
- [Fes94] A. Fessler, and A. O. Hero, “Space-alternating generalized expectation-maximization algorithm”, *IEEE Trans. on Signal Processing*, Vol. 42, No. 10, pp. 2664–2677, Oct. 1994.
- [Fin99] P. Fine, and W. Wilson, “Tracking Algorithm for GPS Offset Carrier Signals”, *Proceedings of the 1999 National Technical Meeting of The Institute of Navigation*, San Diego, CA, January 25 - 27, 1999.
- [Gar14] J. A. Garcia-Molina, M. Navarro-Gallardo, G. Lopez-Risueño, and M. Crisci, “Unambiguous Tracking of High-Order BOC Signals in Urban Environments: Channel Considerations”, *NAVITEC 2014*, Noordwijk, The Netherlands, December 2014.
- [Gar15a] J. A. Garcia-Molina, “Method and Apparatus for Tracking a Binary Offset Carrier Navigation Signal,” European Patent Application No. EP3104195A1, 10 Jun. 2015.
- [Gar15b] J. A. Garcia-Molina, M. Navarro-Gallardo, G. Lopez-Risueño, and M. Crisci, “Robust Unambiguous Tracking of High-Order BOC Signals: a Multi-Correlator

## Bibliography

---

- Approach,” *ION GNSS+ 2015*, Tampa, Florida, Sep. 2015. <https://www.ion.org/publications/abstract.cfm?articleID=13049>
- [Gar16a] J. A. Garcia-Molina, M. Navarro-Gallardo, G. Lopez-Risueño, and M. Crisci, “Robust unambiguous Estimation of High-Order BOC Signals: The DOME approach,” *NAVIGATION, Journal of the Institute of Navigation*, vol. 63, no. 4, pp. 509–518, Winter 2016. © 2016 Institute of Navigation. <https://doi.org/10.1002/navi.162>
- [Gar16b] J. A. Garcia-Molina, and M. Crisci, “Snapshot Localisation of Multiple Jammers based on Receivers of Opportunity”, *NAVITEC 2016*, Noordwijk, The Netherlands, December 2016.
- [Gar17a] J. A. Garcia-Molina, J. A. Fernandez-Rubio, R. Weiler, and M. Crisci, “Snapshot Processing of High-Order BOC Signals in the Cloud: on Sensitivity and Distortion Effects,” *ION GNSS+ 2017*, Portland, Oregon, Sep. 2017. <https://doi.org/10.33012/2017.15245>
- [Gar17b] J. A. Garcia-Molina, and J. A. Fernandez-Rubio, “Exploiting Spatial Diversity in Low-cost SDR Platforms: the MIMO-GNSS approach,” *6th International Colloquium on Scientific and Fundamental Aspects of GNSS/Galileo*, Valencia, Spain, Oct. 2017.
- [Gar17c] J. A. Garcia-Molina, and J. M. Parro, “Cloud-based GNSS Processing of Distributed Receivers of Opportunity: Techniques, Applications and Data-collection Strategies,” *6th International Colloquium on Scientific and Fundamental Aspects of GNSS/Galileo*, Valencia, Spain, Oct. 2017.
- [Gar18a] J. A. Garcia-Molina, “Method and Apparatus for Performing Joint Channel and Time Estimation in a GNSS Receiver,” International Patent Application No. PCT/EP2018/063660, 2018.
- [Gar18b] J. A. Garcia-Molina, J. A. Fernandez-Rubio, and J. M. Parro, “Exploiting Spatial Diversity for NLOS Indoor Positioning,” *ION GNSS+ 2018*, Miami, Florida, Sep. 2018. <https://doi.org/10.33012/2018.15865>
- [Gar18c] J. A. Garcia-Molina, and J. A. Fernandez-Rubio, “Positioning and Timing in the MIMO-GNSS Framework,” *NAVITEC 2018*, Noordwijk, The Netherlands, Dec. 2018. <https://ieeexplore.ieee.org/document/8642703>
- [Gar19a] J. A. Garcia-Molina, and J. A. Fernandez-Rubio, “Collective Unambiguous Positioning with High-Order BOC Signals,” *IEEE Transactions on Aerospace and*

## Bibliography

---

- Electronic Systems*, vol. 55, no. 3, pp. 1461-1473, June 2019. © 2018 IEEE.  
<https://ieeexplore.ieee.org/document/8477092>
- [Gar19b] J. A. Garcia-Molina, and J. A. Fernandez-Rubio, “Array Processing and Unambiguous Positioning of Signals with Multi-Peak Correlations,” *ION GNSS+ 2019*, Miami, Florida, Sep. 2019. <https://doi.org/10.33012/2019.17024>
- [Gar19c] J. A. Garcia-Molina, and J. A. Fernandez-Rubio, “Collaborative Snapshot Positioning via Distributed Array Processing,” *ION GNSS+ 2019*, Miami, Florida, Sep. 2019. <https://doi.org/10.33012/2019.16876>
- [Gare12a] R. Garello, L. Presti, G. E. Corazza, and J. Samson, “Peer-to-Peer Cooperative Positioning. Part I: GNSS-Aided Acquisition,” *Inside GNSS*, pp. 56-64, July/August 2012.
- [Gare12b] R. Garello, J. Samson, M. Spiritio, H. Wymeersch, “Peer-to-Peer Cooperative Positioning. Part II: Hybrid Devices with GNSS & Terrestrial Ranging Capability,” *Inside GNSS*, pp. 55-63, March/April 2012.
- [Gra09] F. Graas, A. Soloviev, M. U. Haag, S. Gunawardena, “Closed-Loop Sequential Signal Processing and Open-Loop Batch Processing Approaches for GNSS Receiver Design,” *IEEE Journal of Selected Topics in Signal Processing*, vol. 3, no. 4, pp. 571-586, August 2009.
- [Gus16a] A. Gusi, P. Closas, and J. A. Garcia-Molina, “False Lock Probability in BOC Signals,” *ION ITM 2016*, California, USA, January 2016.
- [Gus16b] A. Gusi, P. Closas, and J. A. Garcia-Molina, “Sampling Frequency Impact on False Lock of High Order BOC Signals in Open-Loop Processing,” *NAVITEC 2016*, Noordwijk, The Netherlands, December 2016.
- [Guv18] I. Guvenc, S. Gezici, and Z. Sahinoglu, “Ultra-wideband range estimation: Theoretical limits and practical algorithms,” in *2018 IEEE International Conference on Ultra-Wideband*, Hannover, Germany, 10-12 Sep. 2018.
- [GNS17] “GNSS Market Report,” Issue 5, 2017. doi:10.2878/0426.
- [He17] Z. He, M. G. Petovello, L. Pei, and D. Olesen, “Evaluation of GPS/BDS Indoor Positioning Performance and Enhancement,” *Advances in Space Research*, vol. 59, no. 3, pp. 870-876, 2017.

## Bibliography

---

- [Hei08] G. Hein, and A. Teuber, “GNSS Indoors. Fighting the Fading. Part 3,” *Inside GNSS*, pp. 45-53, July/August 2008.
- [Hod07] M. Hodgart, P. Blunt, and M. Unwin, “The Optimal Dual Estimate Solution for Robust Tracking of Binary Offset Carrier (BOC) Modulation”, *ION GNSS 2007*, Fort Worth, TX, 2007.
- [IEE07] “1588-2008 - IEEE Standard for a Precision Clock Synchronization Protocol for Networked Measurement and Control Systems,” Jul. 2008. doi: 10.1109/IEEESTD.2008.4579760.
- [ITU09] ITU Recommendation ITU-R P.681-7, “Propagation data required for the design of earth-space land mobile telecommunication systems”, (10/2009).
- [ITU17] “Model Parameters for the Physical-Statistical Wideband Model in Recommendation ITU-R P.681,” Report ITU-R P.2145-2, Sep 2017. Accessed on: May 19th, 2018. Available: <https://www.itu.int>.
- [Jos14] T. Jost, W. Wang, U. Fiebig, F. Perez-Fontan, “A Wideband Satellite-to-Indoor Channel Model for Navigation Applications,” *IEEE Transactions on Antennas and Propagation*, vol. 62, no. 10, October 2014, pp. 5307-5320.
- [Jun14] V. Jungnickel et al., “The Role of Small Cells, Coordinated Multipoint, and Massive MIMO in 5G,” *IEEE Communications Magazine*, vol. 52, issue 5, pp. 44-51, May 2014.
- [Kap06] E. D. Kaplan, C. J. Hegarty, “Understanding GPS, Principles and Applications,” 2nd edition, Artech House, 2006.
- [Kay13] S. M. Kay, “Fundamentals of Statistical Signal Processing. Estimation Theory”, Prentice Hall, 2013.
- [Kim07] S. Kim, S. Yoo, S. Yoon, and S. Y. Kim, “A Novel Unambiguous Multipath Mitigation Scheme for BOC(kn,n) Tracking in GNSS”, *Proceedings of the 2007 International Symposium on Applications and the Internet Workshops (SAINTW'07)*, 2007.
- [Las09] M. Lashley, D. M. Bevly, J. Y. Hung, “Performance Analysis of Vector Tracking Algorithms for Weak GNSS Signals in High Dynamics,” *IEEE Journal of Selected Topics in Signal Processing*, vol. 3, no. 4, Aug. 2009.

## Bibliography

---

- [Lau17] D. Lawrence et al., “Innovation: Navigation from LEO,” *GPS World*, June 2017. Available: <http://gpsworld.com/innovation-navigation-from-leo>.
- [Li13] B. Li, B. Harvey, and T. Gallagher, “Using Barometers to Determine the Height for Indoor Positioning,” International Conference on Indoor Positioning and Indoor Navigation, Montbeliard-Belfort, France, Oct. 2013.
- [Loh17] E. S. Lohan, D. A. de Diego, J. A. Lopez-Salcedo, G. Seco-Granados, P. Boto, P. Fernandes, “Unambiguous Tehniques Modernized GNSS Signals: Surveying the Solutions,” *IEEE Signal Processing Magazine*, vol. 34, no. 5, pp. 38 - 52, Sept. 2017.
- [Luc16] V. Lucas-Sabola, G. Seco-Granados, J. A. Lopez-Salcedo, J. A. Garcia-Molina, M. Crisci, “Cloud GNSS receivers: New Advanced Applications Made Possible,” *2016 International Conference on Localization and GNSS (ICL-GNSS 2016)*, Barcelona, Spain, June 2016.
- [Mar03] N. Martin, V. Leblond, G. Guillotel, and V. Heiries, “BOC(x,y) Signal Acquisition Techniques and Performances”, *ION GPS/GNSS 2003*, Portland, OR, Sep. 2003.
- [Mon14] S. Z. Monir Veghefi, “Cooperative Positioning in Wireless Sensor Networks Using Semidefinite Programming,” PhD Thesis, December 8, 2014.
- [Nar14] L. Narula, K. P. Singh, M. G. Petovello, “Accelerated Collective Detection Technique for Weak GNSS Signal Environment,” *Ubiquitous Positioning Indoor Navigation and Location Based Service (UPINLBS)*, Corpus Christ, TX, USA, November 2014.
- [Nav12] M. Navarro-Gallardo, G. López-Risueño, M. Crisci, and G. Seco-Granados, “Analysis of Side Lobes Cancellation Methods for BOCcos(n,m) Signals”, *NAVITEC 2012*, Dec 5-7, 2012.
- [Nav13] M. Navarro-Gallardo, G. Seco-Granados, G. López-Risueño, and M. Crisci, “Code Smoothing for BOC Ambiguity Mitigation”, *ICL-GNSS 2013*, Florence, Italy, Oct. 2013.
- [Nav14] M. Navarro-Gallardo, G. López-Risueño, J. A. Garcia-Molina, M. Crisci, and G. Seco-Granados, “Subcarrier Slip Detection for High-Order BOC Signals”, *NAVITEC 2014*, Noordwijk, The Netherlands, December 2014.
- [NEO16] “NEO/LEA-M8T: u-blox M8 concurrent GNSS timing modules. Data Sheet,” 21 Jun. 2016. Accessed on: May 19th, 2018. Available: <https://www.u-blox.com>.

## Bibliography

---

- [ODr16] C. O’Driscoll, J.A. Avila-Rodriguez, R. Ioannides, “Band-limiting and Dispersive Effects on High Order BOC Signals”, *ION GNSS+ 2016*, Portland, Oregon, Sep 2016.
- [Pan09] T. Pany, D. Riedl, J. Winkel, T. Worz, R. Schweikert, H. Niedermeir, S. Lagrasta, G. Lopez-Risueño, and D. Jimenez-Banos, “Coherent Integration Time: The Longer, the Better”, *Inside GNSS*, pp. 52-61, November/December 2009.
- [Per18] J. A. Del Peral-Rosado, et al., “Performance Analysis of Hybrid GNSS and LTE Localization in Urban Scenarios,” in *NAVITEC 2016*, Noordwijk, The Netherlands, 14-16 Dec. 2016.
- [Phe01] R. E. Phelts, “Multicorrelator Techniques for Robust Mitigation of Threats to GPS Signal Quality,” Ph.D. Thesis, Standford, June 2001.
- [Rub08] D. Rubin, and T. Young, “Femtocells: Bringing Reliable Location and Timing Indoors,” *Inside GNSS*, Fall 2008.
- [Sah08] M. Sahmoudi, M. G. Amin, “Fast Iterative Maximum-Likelihood Algorithm (FIMLA) for Multipath Mitigation in the Next Generation of GNSS Receivers”, *IEEE Transactions on Wireless Communications*, Vol. 7, No. 11, Nov. 2008.
- [San13] J. Sanz-Subirana, J. M. Juan-Zornoza, M. Hernandez-Pajares, “GNSS Data Processing. Volume I: Fundamentals and Algorithms,” ESA Communications (ESA TM-23/1), May 2013.
- [Sat12] S. Satyanarayana, D. Borio, G. Lachapelle, “A Composite Channel Model for Indoor GNSS Signals: Characterization, Experimentation Validation and Simulation,” *NAVIGATION: Journal of the Institute of Navigation*, vol. 59, issue 2, pp. 77-92, Summer 2012.
- [Sch13] F. M. Schubert, and J. Wendel, “BOC Tracking Using Phase and Subcarrier Locked Loops”, *6th European Workshop on GNSS Signals and Signal Processing*, Dec 5-6, 2013, Neubiberg, Germany.
- [Sec05] G. Seco-Granados, J. A. Fernandez-Rubio, and C. Fernandez-Prades, “ML Estimator and Hybrid Beamformer for Multipath and Interference Mitigation in GNSS Receivers,” *IEEE Transactions on Signal Processing*, vol. 53, no. 3, pp. 1194 - 1208, March 2005.
- [Sec12] G. Seco-Granados, J. A. Lopez-Salcedo, D. Jimenez-Banos, and G. Lopez-Risueño, “Challenges in Indoor Global Navigation Satellite Systems: Unveiling its core

## Bibliography

---

- features in signal processing,” *IEEE Signal Processing Magazine*, vol. 29, no. 2, pp. 108 -131, 2012.
- [Ste03] A. Steingass, and A. Lehner, “Land Mobile Satellite Navigation. Characteristics of the Multipath Channel,” in *Proc. Institute of Navigation (ION GPS/GNSS)*, Portland, U.S., Sep. 2003.
- [Sol13] A. Soloviev, and J. Dickman, “Collaborative GNSS Signal Processing,” in *Proceedings of the 26th International Technical Meeting of The Satellite Division of the Institute of Navigation (ION GNSS+ 2013)*, Nashville, TN, September 2013, pp. 135-143.
- [Teu17] P. J. G. Teunissen, O. Montenbruck, “Springer Handbook of Global Navigation Satellite Systems,” Springer, 2017.
- [Wei03] L. R. Weill, “Multipath mitigation. How good can it get with new signals?,” *GPS World*, pp. 106–113, June 2003.
- [Won12] J-H Won, T. Pany, B. Eissfeller, “Iterative Maximum Likelihood Estimators for High-Dynamic GNSS Signal Tracking”, *IEEE Transactions on Aerospace and Electronic Systems*, Vol. 48, No. 4, Oct. 2012.
- [Wen14] J. Wendel, F. M. Schubert, and S. Hager, “A Robust Technique for Unambiguous BOC Tracking,” *NAVIGATION: Journal of The Institute of Navigation*, vol. 61, no. 3, pp. 179-190, Fall 2014.